SKIN DOSIMETRY USING THERMOLUMINESCENT DOSIMETERS

by

Timothy Miles DeBey

B.S., Kansas State University, 1981

A MASTER'S THESIS

submitted in partial fulfillment of the
requirements for the degree

MASTER OF SCIENCE

Department of Nuclear Engineering

KANSAS STATE UNIVERSITY

Manhattan, Kansas

1983

Approved by:

Major Professor

TABLE OF CONTENTS

LIST OF FIGURES

Figure | Page

APPENDICES FIGURES

LIST OF TABLES

APPENDICES TABLES

THIS BOOK
CONTAINS
NUMEROUS PAGES
WITH THE ORIGINAL
PRINTING BEING
SKEWED
DIFFERENTLY FROM
THE TOP OF THE
PAGE TO THE
BOTTOM.

THIS IS AS RECEIVED
FROM THE
CUSTOMER.

I. INTRODUCTION

Experimental and theoretical research was performed on the use of thermoluminescent dosimeters (TLDs) to measure radiation doses to skin, with the majority of the work concentrating on exposure from beta particles.

Beta dosimetry studies included the investigation of TLDs from two commercial suppliers and two locally developed TL type dosimeters, with emphasis on one of the locally developed dosimeter types.

It has long been recognized that exposure to radiation can lead to biological damage, and great efforts have been made to develop means to measure personnel radiation exposure and restrict it to safe levels. The current International Commission on Radiological Protection (ICRP) skin dose limit recommendation is 50 Rem/yr over the skin depth region of 5 to 10 mg/cm^2.[1] In the USA, the Code of Federal Regulations (10CFR20) specifies a maximum permissible skin dose of 7½ Rem per calendar quarter.[2] In this report it is assumed that radiation dose equivalent (Rem), dose (Rad), and exposure (Roentgen) are all equivalent units and are therefore interchangeable.

Typically the skin dose is considered to be the same as the beta dose since beta particles have a very short penetration ability when compared to gamma rays. The "beta" skin exposure will most likely consist of two types of radiation; the electrons emitted during the beta decay of radioisotopes and the electrons produced from photon interactions in materials. Most of the work in this project was performed using radioisotopes which decayed by beta emission only; however photon and electron-photon mixed field investigations were also performed.

Investigators have previously researched the effects of shallow penetrating charged particle radiation upon skin. These results showed that there is a very thin layer of outer skin that will not produce cancerous tumors even when exposed to very high radiation levels. This can be explained by examining the composition of skin, as detailed in the ICRP Publication 23 on the reference man.[3]

Skin actually consists of four layers, which together comprise the epidermis. The outer layer is made of dead cells and is called the stratum corneum. Below this layer is a layer of dying cells called the stratum lucidium. Then a layer of living (but not reproducing) cells follows, called the stratum spinosum, and lastly a layer of reproducing cells called the stratum basale completes the epidermis layer. It is generally considered that only the reproducing cells are capable of forming tumors after high radiation exposure. This is why the ICRP dose limit recommendations apply to the skin layer from 5 to 10 mg/cm^2. The skin layers and typical beta penetration curves are shown in Fig. 1.1. This figure also indicates the beta penetration of a commonly used TLD ribbon which has a thickness of 280 mg/cm^2. It can be seen that many low energy beta emitters would not penetrate this thickness and so it provides a poor representation of the 5 to 10 mg/cm^2 region.

The mean density of skin has been found to be 1.145 g/cm^3, so the ICRP recommendations would apply to an average skin depth range of 43.7 μm to 87.3 μm.[4]

The goal for this project was to develop a method for accurately measuring the radiation dose to skin.

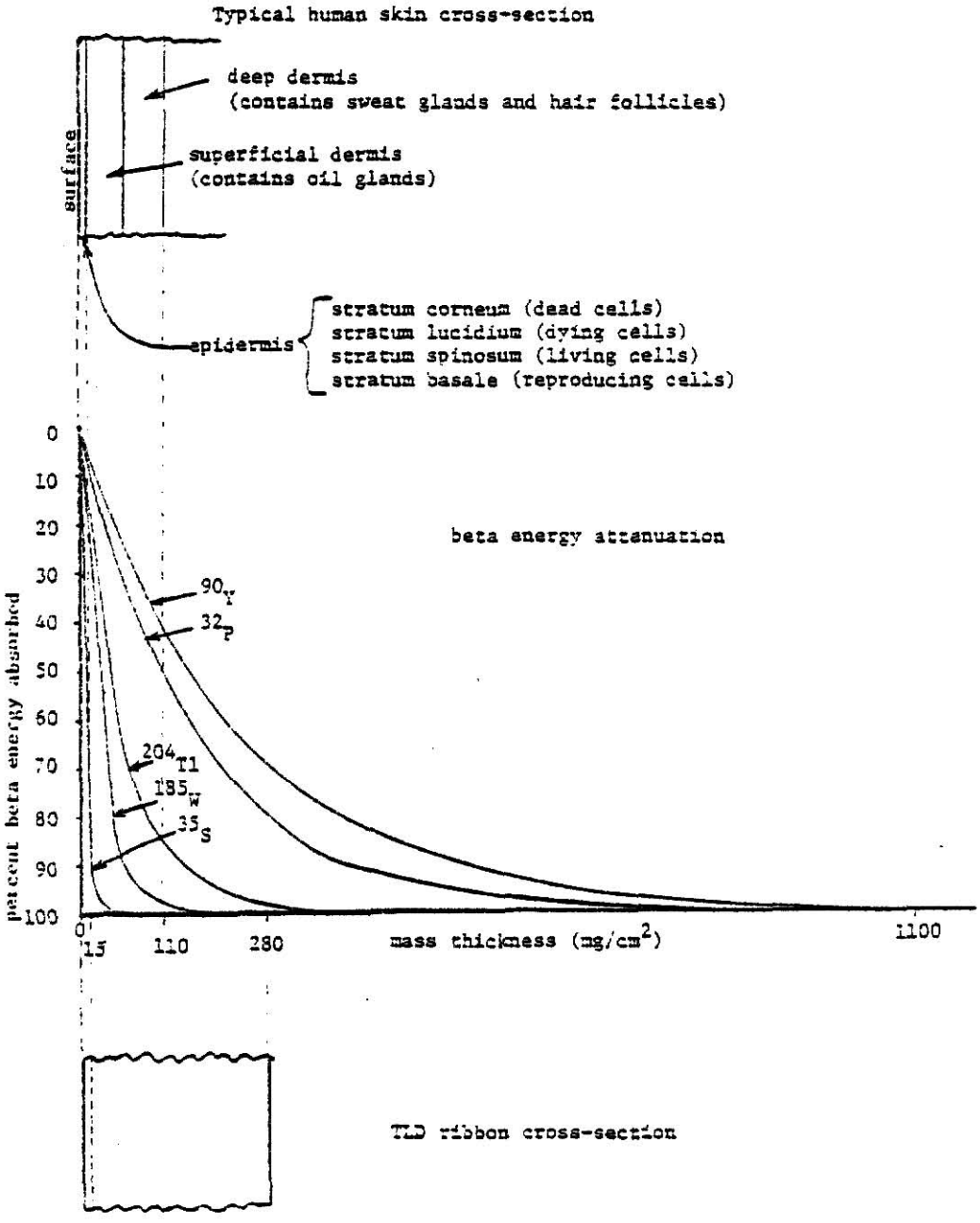

FIG.1.1. Beta penetration curves and typical skin and TLD mass thickness cross-sections.

II. BETA DOSIMETRY THEORY

A. Introduction to thin-layer requirements

In the past, most β-dosimetry methods have been designed to simulate the epidermal layer of the skin, which has the dead epidermis layer above it. Experimentalists, therefore, attempted to use a sensitive layer of approximately 5 mg/cm^2 thickness with a cover of approximately 7 mg/cm^2 to represent the epidermis dead skin layer. The ICRP and the Commission of European Communities recommend that the skin dose be averaged between 5 to 10 mg/cm^2.[1,5] The Idaho National Engineering Laboratory (INEL) indicated that the thicknesses of both the epidermis layer and the epidermal layer vary widely in different areas of the human body.[6] They also suggested that the assumption of the basal cells of the epithelium being the critical tumor-forming cells is unwarranted and gave evidence to suggest that beta radiation with a range of less than 15 mg/cm^2 would not cause tumors. This evidence throws doubt on the need to have an active dosimeter thickness of the small value initially stated, although the ANSI 13.11 standard, approved in 1983, specifies a 7 mg/cm^2 depth for skin dose evaluation.[7]

There is, however, a more important reason for having a thin active dosimeter layer than simply the attempt to simulate the epidermal layer--the beta energy response. The active dosimeter layer must be thin enough so that its thickness is less than the range of all of the beta emitters of interest. If this condition is not met, then the active dosimeter volume changes with variations in the energies of the beta particles striking the dosimeter. Since many beta dosimeters are calibrated with high energy beta particles or gamma rays, the calibration

inherently assumes the entire dosimeter volume is actively absorbing the radiation energy. Again, this will not be a valid assumption if the dosimeter thickness exceeds the beta range and it would result in a very severe underestimation of the beta dose. Thus, a thin-layer dosimeter is required in order to achieve the desired energy response.

Two typical types of thin dosimeters currently in use are the National Radiological Protection Board (NRPB) dosimeters and the Panasonic commercial TLD badges.

The NRPB in England has developed a dosimeter badge which uses disks of LiF embedded in teflon. These disks are of two thicknesses, 0.2 mm (42 mg/cm^2) and 0.4 mm (84 mg/cm^2), with the thin disk being used for measuring the skin dose.[8] A black plastic cover is used to minimize the effects of light and dirt on the teflon discs. The NRPB uses a pre-dose annealing of 300°C for 30 hours and a post-dose anneal of 80°C for 16 hours. They found that the thin disks had a minimum detectable dose of 26 mrem and a standard deviation of approximately 14 mrem. The skin dose energy response was found to be measured within ±30% for photons from 9.9 keV to 2 MeV and for β-rays with an endpoint energy above 0.7 MeV. An angular response check indicated that dose measurements with the radiation at 60° incidence is within 30% of the measurements with normal incidence.[9] It should also be noted that the 0.2 mm disk gave a dose response to 0.76 MeV ^{204}Tl β-rays that was ∿78% of the response to 2.3 MeV ^{90}Sr/^{90}Y β-rays of the same total exposure, and a dose response to 0.22 MeV β-rays that was ∿ 20% of the response to the same exposure of the 2.3 MeV ^{90}Sr/^{90}Y β-rays. This indicates that the NRPB skin dosimeter (with cover) is too thick to give a constant energy response over a very wide range of beta energies.

The Matsushita Electrical Industrial Co., Ltd. (Panasonic) has also developed a thin dosimeter for skin dose measurements.[10] It uses a 15 mg/cm^2 layer of $Li_2B_4O_7$:Cu powder, which has a front cover of 14 mg/cm^2, and therefore provides a dose estimate at a depth from 14 mg/cm^2 to 29 mg/cm^2. This dosimeter provides a minimum detectable level of 3 mR and a standard deviation of 19%. A significant error in β-dose estimates for β-rays below 190 keV is expected with this dosimeter, although it comes much closer to meeting the ICRP requirements than most of the other types of skin dosimeters currently in use. No experimental beta particle energy response data are currently available for this dosimeter.

B. Dosimeter thickness-dependent energy response theory

Two theoretical models were investigated to determine the predicted energy response of beta dosimeters. The basis for these studies involved prediction of the absorbed dose in TLD materials with a wide range of thicknesses, similar to those TLDs studied experimentally. Calculations are presented for many thicknesses of LiF, $CaSO_4$, and CaF_2 materials.

1.0 Exponential attenuation model

If it is assumed that beta particle energy absorption occurs exponentially, then the fraction of the energy absorbed F_1 after traversing a distance ρt is given by

$$F_1 = (1 - e^{-\beta\rho t}) \qquad (2.1)$$

where β is an effective attenuation coefficient. Coefficients which describe the attenuation of beta particles in the subject TLD materials need to be measured. Since specific coefficients were not available, a consistent procedure was selected by assigning a 1% transmission to the range R (mg/cm^2) where

$$\beta = \frac{-\ell n(0.01)}{R} \quad . \tag{2.2}$$

Values of R were calculated from[11]

$$R = 412\ E_o^n \quad \text{for} \quad 0.01 < E_o < 3\ \text{MeV} \quad , \tag{2.3}$$

where

$$n = 1.265 - 0.0954\ \ell n E_o \quad . \tag{2.4}$$

Since the expression for R pertains to monoenergetic electrons, E_o was selected because it corresponds to the maximum electron energy in the beta spectrum in units of MeV.

Equation (2.1) was used to estimate the percentage ($100F_1$) of the beta energy absorbed in TLDs and other materials of interest (see Table 2.1). A quantity of equal importance to radiation dosimetry is the energy absorbed E_a by a given TLD when exposed to a specific beta emitter. Values of E_a were calculated using

$$E_a = F_1\ E_o \tag{2.5}$$

where E_o was selected since this model was based upon the maximum beta energy. E_a would also be proportional to the TL emitted during heating. Therefore, the energy dependence of E_a, as a function of dosimeter thickness, provides information on the energy response of TLDs. Results obtained from this study are shown in Figs. 2.1 - 2.3. Hence, this model indicates that the energy response of a thick TLD varies by nearly a factor of 9 over a beta particle energy range of 0.167 to 2.29 MeV. Conversely, the variation is less than 30% for a thin TLD.

2.0 Multiple-scattering model

Theory which appropriately describes the relationship between the energy of beta particles and the absorbed dose within a given medium has been reported by Martin J. Berger.[12] That report presents state-of-the-art theoretical results of absorbed dose distributions around a point

Table 2.1. Media percentile distances calculated with the exponential attenuation model.

Absorber Material	Density (g/cm^3)	Thickness (t) (cm)	Thickness (t) (mils)	Percent Beta Energy Absorbed for Each Radioisotope ^{35}S	^{204}Tl	^{36}Cl	^{90}Sr	^{32}P	^{90}Y
LiF	2.64	0.089	35	100.0	97.6	98.4	99.7	74.5	62.6
LiF	2.64	0.00762	3	94.6	27.3	29.6	39.4	11.1	8.1
LiF	2.64	0.00508	2	85.8	19.1	20.9	28.4	7.5	5.5
CaF_2	3.18	0.089	35	100.0	98.9	99.3	99.9	80.8	69.4
CaF_2	3.18	0.00762	3	97.1	31.9	34.5	45.3	13.2	9.7
CaF_2	3.18	0.00508	2	90.5	22.6	24.6	33.1	9.0	6.5
$CaSO_4$	2.61	0.089	35	100.0	97.5	98.3	99.7	74.2	62.2
$CaSO_4$	2.61	0.00762	3	94.5	27.0	29.4	39.0	10.9	8.0
$CaSO_4$	2.61	0.00508	2	85.5	18.9	20.7	28.1	7.4	5.4
Polyester	1.40	0.00254	1	40.4	5.5	6.0	8.5	2.0	1.5
Polyester	1.40	0.00508	2	64.5	10.7	11.7	16.2	4.1	2.9
Polyester	1.40	0.0178	7	97.3	32.6	35.3	46.2	13.5	9.9
Air	0.001293	10		84.7	18.5	20.2	27.5	7.3	5.3
Air	0.001293	20		97.7	33.6	36.4	47.5	14.0	10.3
Air	0.001293	90		100.0	84.2	86.9	94.5	49.2	38.6
Beryllium	1.848	0.0127	5	96.7	31.0	33.6	44.2	12.8	9.4
Titanium	4.54	0.0127	5	100.0	59.9	63.5	76.2	28.5	21.5
Graphite	1.7	0.089	35	100.0	90.9	92.9	97.7	58.6	46.9
Polyethylene	0.962	0.1524	60	100.0	90.2	92.3	97.4	57.4	45.9
Styrene	1.108	0.1524	60	100.0	93.1	94.8	98.5	62.6	50.7

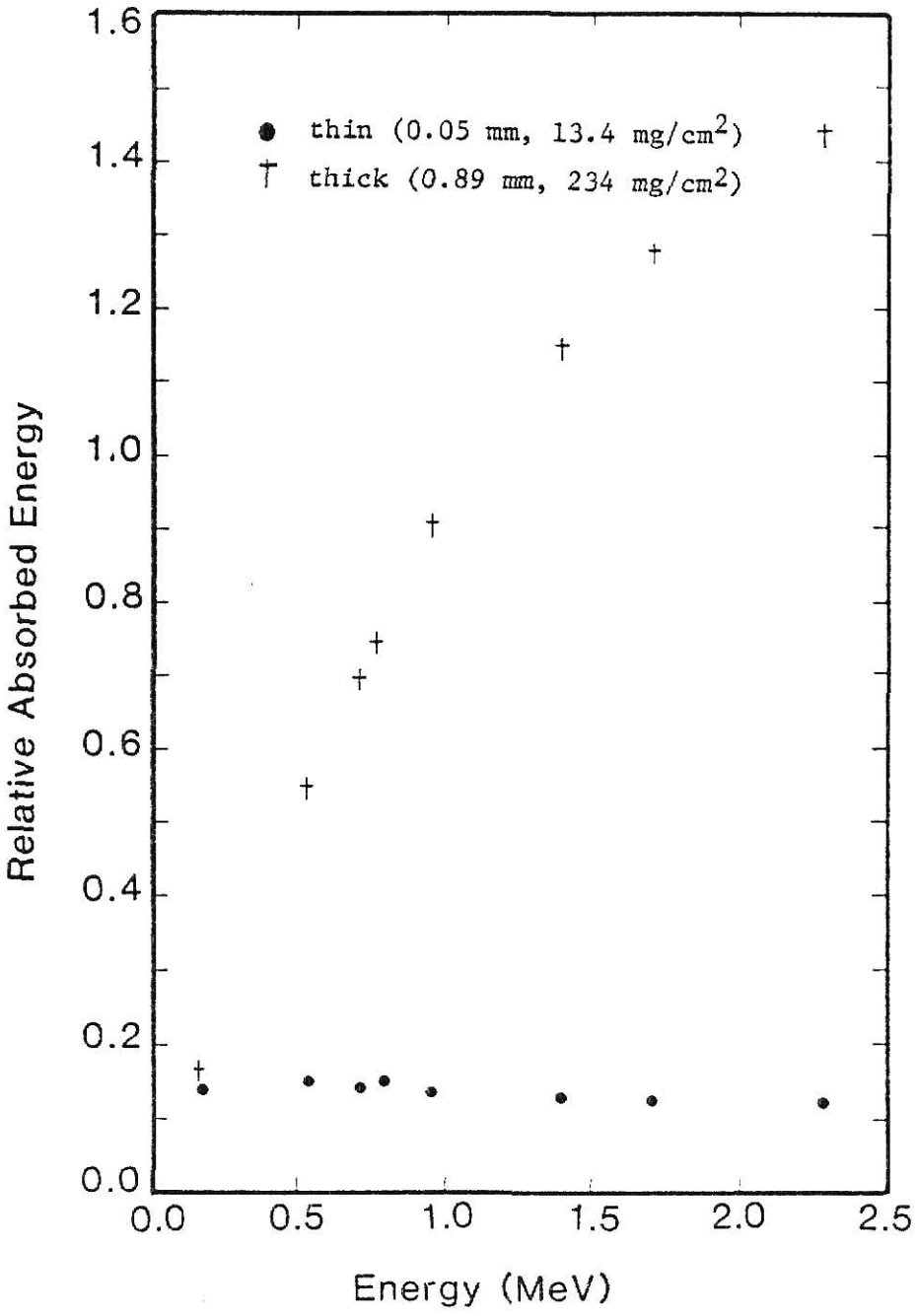

FIG. 2.1. Exponential attenuation model energy response calculations for LiF at 8 beta-emitter energies.

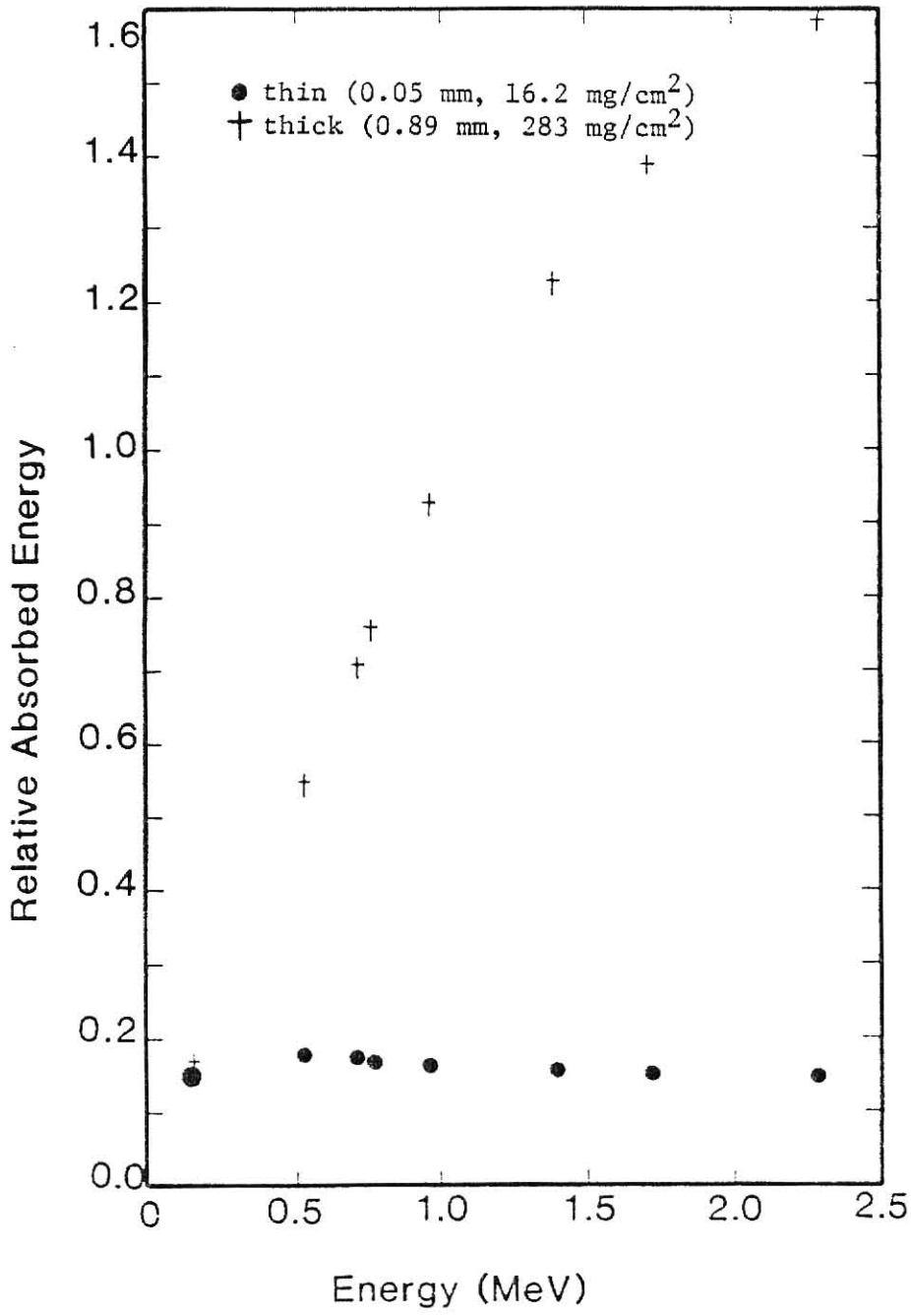

FIG. 2.2. Exponential attenuation model energy response calculations for CaF_2 at 8 beta-emitter energies.

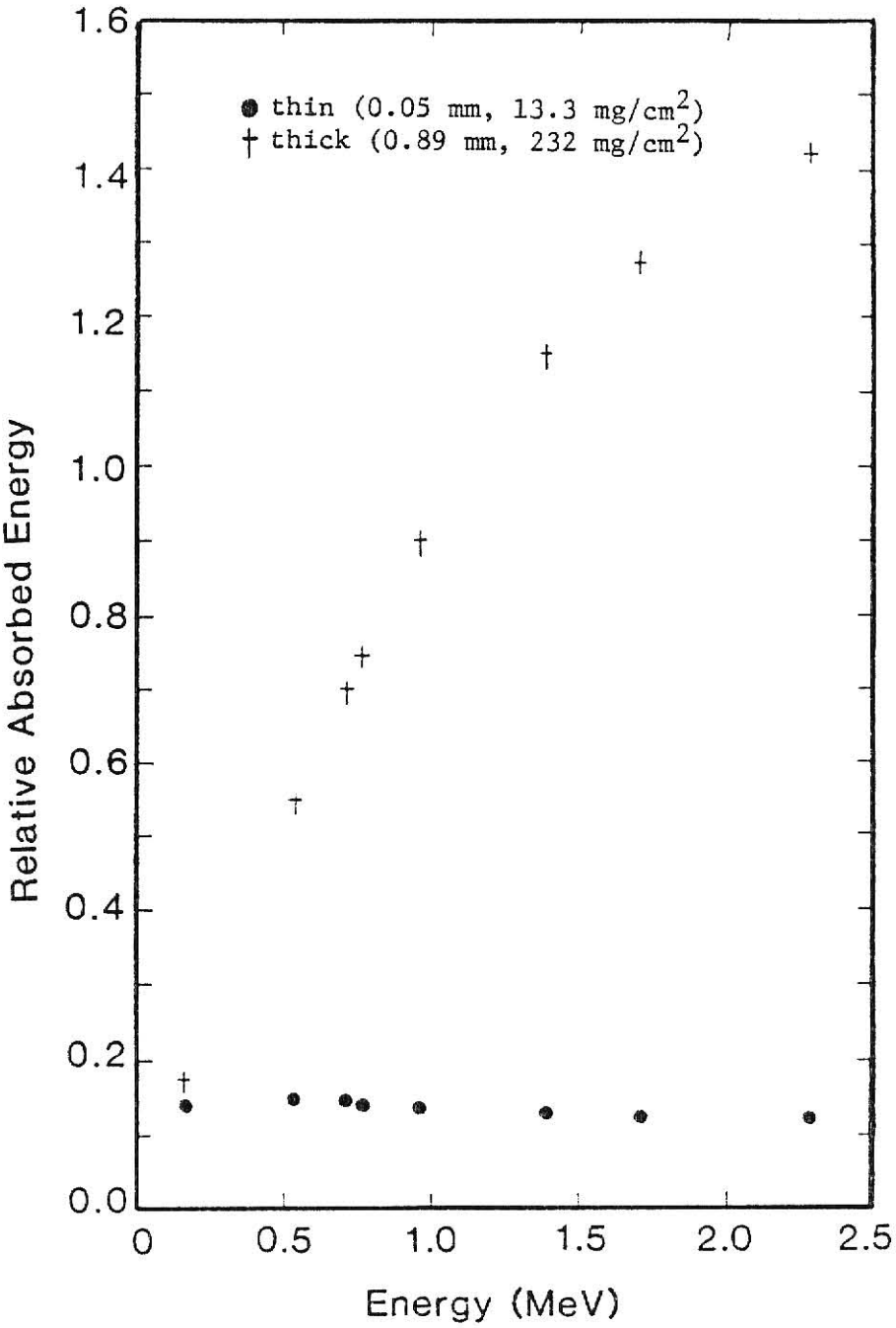

FIG. 2.3. Exponential attenuation model energy response calculations for $CaSO_4$ at 8 beta-emitter energies.

source of electrons and beta particles. Tabulated results, calculated using electron multiple-scattering theory allow accurate determinations of the absorbed dose rate $R_\beta(x)$ in water for beta particles with an average energy $\bar{E}$ at a distance x from a point isotropic source,

$$R_\beta(x) = A\, n_\beta\, k\, \bar{E}\, \phi_\beta\,(x) \tag{2.6}$$

where A is the source activity, n_β the number of beta particles per disintegration, $\phi_\beta(x)$ the specific absorbed dose fraction and $k = 1.6 \times 10^{-8}$ g-rad/MeV.

Results are tabulated in terms of radii X_p, called percentile distances, therefore,

$$\phi_\beta(X_p) \equiv p/100 \quad \text{for} \quad p = 5,10,\ldots,95. \tag{2.7}$$

where p is defined as the fraction of the beta particle energy absorbed in water. The fraction of beta particle energy which is absorbed in media other than water require application of a correction factor a_{21}, as follows:

$$\rho_2\, X_p^{(2)}\, a_{21} = \rho_1\, X_p^{(1)} \tag{2.8}$$

where X_p is the percentile distance (cm) in media 1 (water) or 2 (the desired medium) and ρ is the density (g/cm^3). To determine p for any absorber, values of $X_p^{(2)}$ and ρ_2 for the absorber are substituted into Eq. (2.8) and the corresponding value of $X_p^{(1)}$ for water is calculated. The percent of the beta energy absorbed in a sphere of radius r is then determined by interpolation between the percentile distances $X_p^{(1)}$ given in tabular form for the specified beta particle emitter.

The a_{21} conversion factor can be determined for any material by using the empirical formula

$$a_{21} = (L_c^{(2)}/L_c^{(1)})[1 + 0.02252(\bar{Z}-6.60)], \tag{2.9}$$

where $\bar{Z}$ is the effective atomic number for mixtures or compounds

$$\bar{Z} = \frac{\sum_i w_i Z_i^2 A_i}{\sum_i w_i Z_i A_i} \tag{2.10}$$

where Z_i is the atomic number, A_i the atomic weight and w_i the proportion by weight of the i^{th} constituent. The ratio $L_c^{(2)}/L_c^{(1)}$ is defined as the ratio of the mean collision loss in the medium to water evaluated at 200 keV. Values for L_c can be calculated using the expression[13]

$$L_c = \frac{2\pi e^4}{m_o v^2} NZ \left[\ln \frac{E\, m_o v^2}{1.217\, I^2} - 1.274\right] \tag{2.11}$$

where e = the charge of an electron,

N = the number density of atoms,

Z = the atomic number,

v = the electron velocity (at 200 keV),

m_o = the electron rest mass,

and I = the average excitation energy of the material.

Values of I have been tabulated for many elements and mixtures, e.g. see Ref. (14). For other elements, the approximation

$$I = 13.5Z \text{ (eV)} \tag{2.12}$$

has been suggested. The value of I is often subject to large errors, however the final value of the mean collision loss ratio is reasonably insensitive to variations in I since the logarithm is taken of the term in which I appears.

The method described above was used to determine beta energy absorption percentages for six radioisotopes used in this project. The media of interest were the thermoluminescent dosimeter materials,

detector backing materials, detector cover materials, source window materials, and air. Table 2.2 shows the compositions of these materials, the $L_c^{(2)}/L_c^{(1)}$ ratios, the $\bar{Z}$ values, and the a_{21} correction factors. Table 2.3 gives the effective $X_p^{(2)}$ values for the media of interest and their energy absorption percentages for the six radioisotopes of interest. It should be noted that Berger gave values only at intervals of 5 percentage points, so values above 95% or below 5% are indicated accordingly. Intermediate values were linearly interpolated between the nearest tabulated values.

A second energy response analysis was performed using the percent energy absorption values reported in Table 2.3. However, in this case, the fraction of the energy absorbed $\phi_\beta(x)$ in the TLD was multiplied by the average energy of the beta emitter,

$$E_b = \phi_\beta(x)\bar{E} \tag{2.13}$$

to obtain the relative absorbed energy E_b. The average energy is used in this case to account for spectral shape effects. As shown in Figs. 2.4 - 2.6, the shapes of the energy absorption curves are similar to those obtained from the exponential attenuation model. However, the E_b values become approximately constant for endpoint energies above 1.5 MeV. This energy closely corresponds to the minimum endpoint energy required to have a beta range greater than the thickness of the thick TLD. These figures also show the approximately constant energy response of the thin TLDs for the endpoint energy range of 0.167 MeV to 2.29 MeV. It should be noted that the thin TLD response would not be constant for betas with endpoint energies below approximately 150 keV. However, if desired, better low energy response could be achieved by using a thinner TLD.

Table 2.2. Summary of the parameters used to calculate the percentile distance $X_p^{(2)}$

Absorber Material	Element Composition	f_i	Z	A	I(ev)	L_c ratio	$\bar{Z}$	a_{21}	Density (g/cm^3)
Graphite	C	1.0	6	12.011	78	0.880	6.0	0.8678	1.7
Beryllium	Be	1.0	4	9.012	64	0.801	4	0.7543	1.848
Titanium	Ti	1.0	22	47.90	297	0.672	22	0.9045	4.54
Air	N	0.755	7	14.0067	78	0.8715	8.2	0.9023	0.001293
	O	0.232	8	15.9994	100				
	Ar	0.013	18	39.948	184				
High density Polyethylene	C	0.856	6	12.011	78	1.0502	6.0	1.0357	0.962
	H	0.144	1	1.00797	18.7				
Styrene	C	0.923	6	12.011	78	0.9708	6.0	0.9576	1.108
	H	0.077	1	1.00797	18.7				
Polyester	C	0.625	6	12.011	78	0.9248	7.0	0.9325	1.40
	H	0.042	1	1.00797	18.7				
	O	0.333	8	15.9994	89				
LiF	Li	0.2675	3	6.939	38	0.7989	8.7	0.8375	2.64
	F	0.7325	9	18.9984	121.5				
CaF_2	Ca	0.5133	20	40.08	270	0.7632	16.1	0.9616	3.18
	F	0.4867	9	18.9984	121.5				
$CaSO_4$	Ca	0.2944	20	40.08	270	0.8051	17.1	0.9957	2.61
	S	0.2355	16	32.064	216				
	O	0.4701	8	15.9994	89				
$Li_2B_4O_7$	Li	0.0821	3	6.939	38	0.8536	7.5	0.8709	2.4
	B	0.2557	5	10.811	67.5				
	O	0.6622	8	15.9994	89				

Table 2.3. Media percentile distances for selected radioisotopes derived from the multiple-scattering model.

Absorber Material	Density (g/cm^3)	X_p[2] Thickness (cm)	(mils)	Percent Beta Energy Absorbed for Each Radioisotope ^{35}S	^{204}Tl	^{36}Cl	^{90}Sr	^{32}P	^{90}Y
LiF	2.64	0.089	35	>95	>95	>95	>95	61.7	43.9
LiF	2.64	0.00762	3	>95	24.0	23.0	31.2	5.8	<5
LiF	2.64	0.00508	2	91.5	17.4	16.1	22.2	<5	<5
CaF_2	3.18	0.089	35	>95	>95	>95	>95	78.3	58.3
CaF_2	3.18	0.00762	3	>95	31.0	30.7	40.5	8.0	5.6
CaF_2	3.18	0.00508	2	>95	22.5	16.5	29.2	5.4	<5
$CaSO_4$	2.61	0.089	35	>95	>95	>95	>95	70.1	50.6
$CaSO_4$	2.61	0.00762	3	>95	27.3	26.6	35.6	6.8	<5
$CaSO_4$	2.61	0.00508	2	>95	19.9	18.6	25.5	<5	<5
Polyester	1.40	0.00254	1	50.6	6.4	5.4	8.0	<5	<5
Polyester	1.40	0.00508	2	75.1	11.5	10.1	14.4	<5	<5
Polyester	1.40	0.0178	7	>95	30.9	30.6	40.4	8.0	5.6
Air	0.001293	10		92.5	18.0	16.8	23.0	<5	<5
Air	0.001293	20		>95	31.0	30.7	40.5	8.0	5.6
Air	0.001293	90		>95	85.0	88.9	>95	35.3	24.3
Beryllium	1.848	0.0127	5	>95	25.0	24.1	32.5	6.1	<5
Titanium	4.54	0.0127	5	>95	56.4	59.0	72.8	17.8	12.2
Graphite	1.7	0.089	35	>95	92.2	>95	>95	43.5	30.1
Polyethylene	0.962	0.1524	60	>95	>95	>95	>95	49.6	34.5
Styrene	1.108	0.1524	60	>95	>95	>95	>95	52.4	36.6

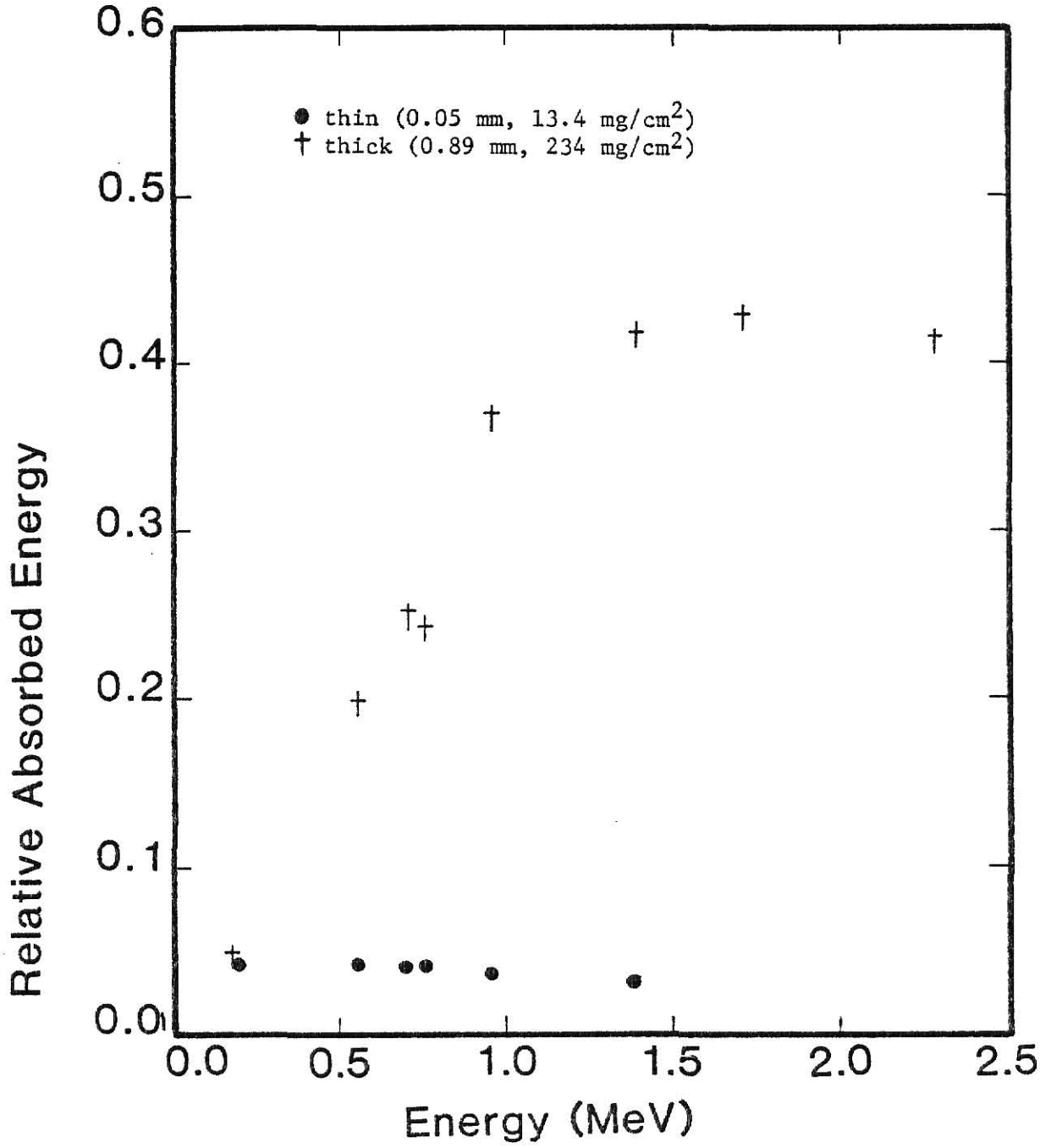

FIG. 2.4. Multiple-scattering model energy response calculations for LiF at 8 beta-emitter energies.

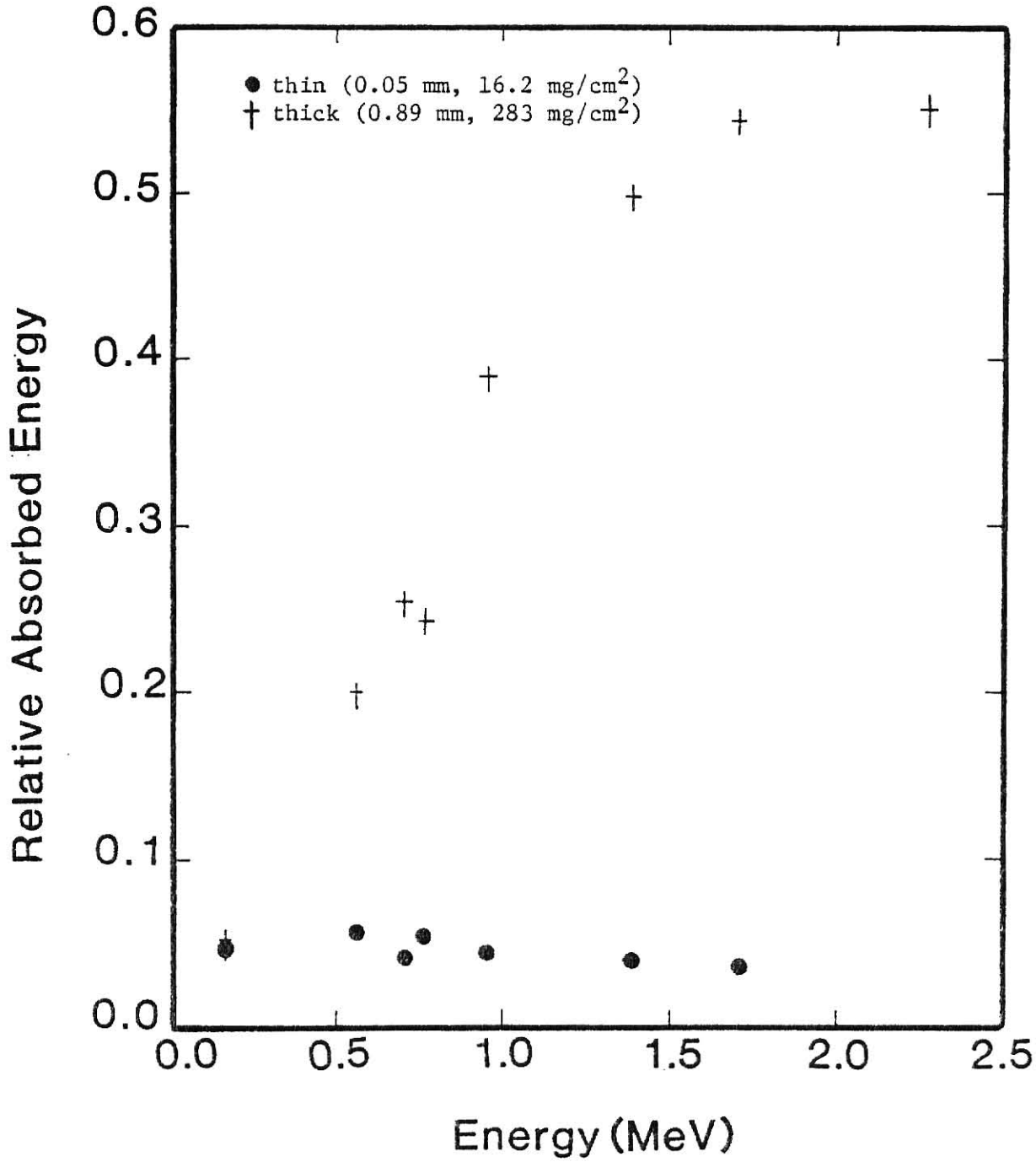

FIG. 2.5. Multiple-scattering model energy response calculations for CaF_2 at 8 beta-emitter energies.

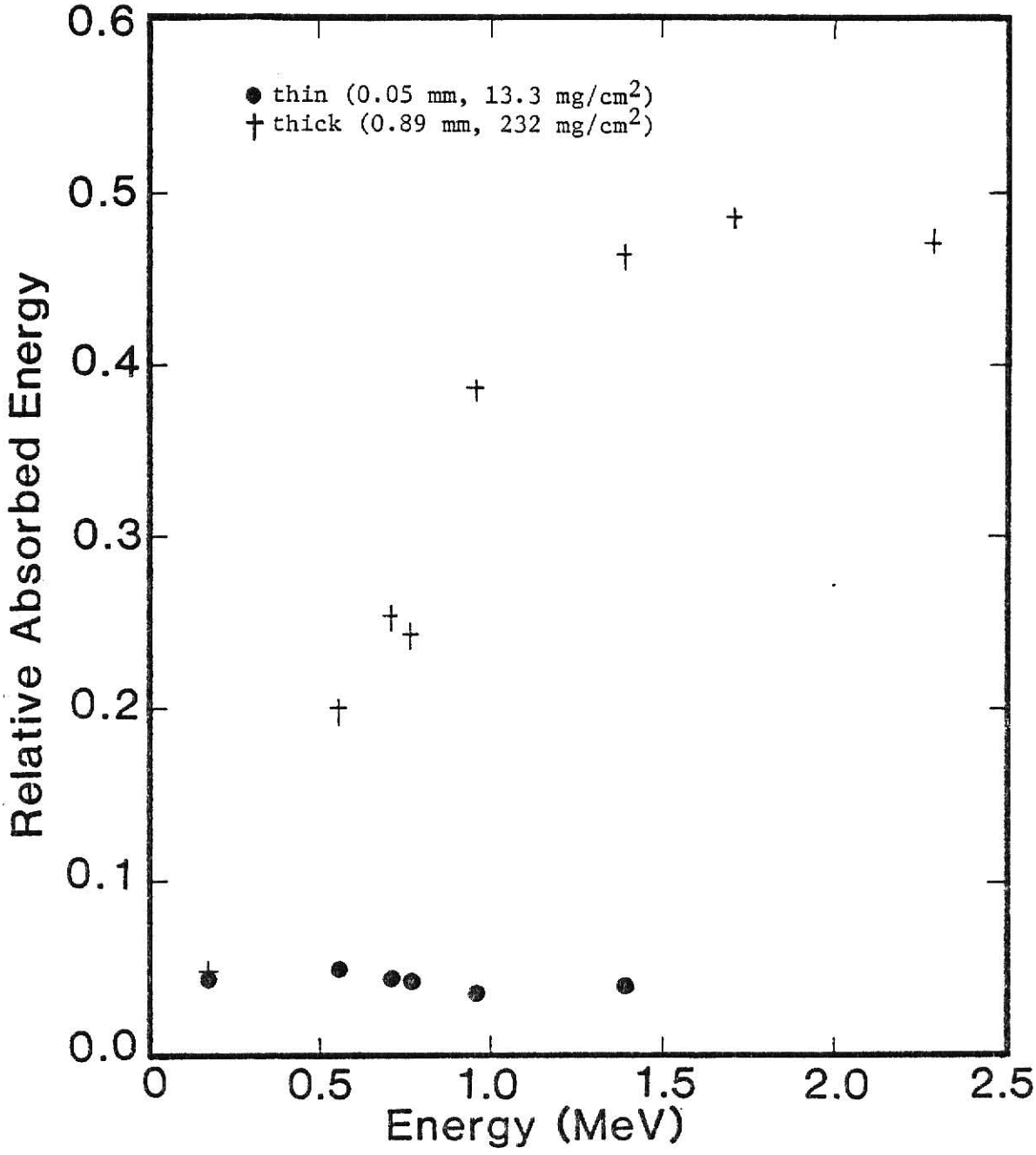

FIG. 2.6. Multiple-scattering model energy response calculations for $CaSO_4$ at 8 beta-emitter energies.

3.0 Theoretical response variations with TLD thickness

The two theoretical models were applied to LiF and CaF_2 TLDs of six thicknesses to show more detail in the effect of changes in thickness. These results were normalized to the response of the 0.051 mm thick (13.4 mg/cm^2 and 16.2 mg/cm^2) TLDs when exposed to ^{35}S betas. The numerical results are provided in Tables 2.4 - 2.5 and the graphical results are given in Figures 2.7 - 2.10. It can be seen that the 0.051 mm thick TLDs should give a constant energy response, within 15%, from 0.125 MeV to 3 MeV according to the exponential theory and a constant energy response, within 20%, from 0.125 MeV to > 1.16 MeV according to the multiple-scattering theory.

The exponential model was applied to seven theoretical thin dosimeters of various mass thicknesses and various cover thicknesses. The responses for the covered dosimeters were calculated by determining the response of the cover plus TLD and then subtracting the response of the cover. The resulting TLD responses are shown in Fig. 2.11, with the TLD mass thickness depth ranges indicated on the curves. The cover mass thicknesses ranged from 0 (no cover) to 14 mg/cm^2.

If the theoretical responses of the dosimeters at 0.76 MeV (^{104}Tl endpoint) are taken as the reference values, then -15% lower energy response cutoff values may be determined. These lower cutoff values have been determined and indicated by the x's on the response curves in Fig. 2.11. It can be seen that increasing TLD thickness and increasing cover thickness both cause the low energy cutoff value to increase. The theoretical response for the 5 to 10 mg/cm^2 TLD (ICRP recommended thickness) has a low energy cutoff of 200 keV. This same low energy

Table 2.4 Theoretical response calculations for 6 thicknesses of LiF using (1) the exponential-attenuation model and (2) the multiple-scattering model.

Isotope	E_o (MeV)	$\bar{E}$ (MeV)	Range (mg/cm^2)	LiF Relative Absorbed Energy											
				13.4 mg/cm^2		26.8 mg/cm^2		67.1 mg/cm^2		134 mg/cm^2		201 mg/cm^2		234 mg/cm^2	
				(1)	(2)	(1)	(2)	(1)	(2)	(1)	(2)	(1)	(2)	(1)	(2)
^{63}Ni	0.06587	0.0172	6.52	0.46	0.38	0.46	0.38	0.46	0.38	0.46	0.38	0.46	0.38	0.46	0.38
^{35}S	0.1674	0.0488	31.7	1.00	1.00	1.14	1.09	1.17	1.09	1.17	1.09	1.17	1.09	1.17	1.09
^{141}Co	0.444	0.1459	138.5	1.11	1.08	1.82	1.77	2.76	2.86	3.06	3.26	3.09	3.26	3.09	3.26
^{204}Tl	0.7635	0.2433	290.8	1.02	0.95	1.84	1.64	3.48	3.23	4.68	4.75	5.10	5.44	5.19	5.44
^{210}Bi	1.161	0.3945	496.6	0.95	0.81	1.78	1.49	3.74	3.29	5.75	5.68	6.83	7.26	7.17	7.80
^{32}P	1.711	0.6950	790.7	0.90	---	1.72	1.20	3.85	2.98	6.46	5.85	8.22	8.44	8.88	9.58
^{90}Y	2.288	0.9367	1099.6	0.87	---	1.69	1.14	3.90	2.76	6,85	5.44	9.07	7.97	9.97	9.19
^{28}Al	2.865	1.2397	1403.6	0.86	---	1.68	---	3.94	2.11	7.10	5.32	9.64	8.01	10.71	9.35

Table 2.5 Theoretical response calculations for 6 thicknesses of CaF_2 using (1) the exponential-attenuation model and (2) the multiple-scattering model.

Isotope	E_o(MeV)	$\bar{E}$(MeV)	Range (mg/cm^2)	CaF_2 Relative Absorbed Energy											
				16.2 mg/cm^2		32.3 mg/cm^2		80.8 mg/cm^2		162 mg/cm^2		242 mg/cm^2		283 mg/cm^2	
				(1)	(2)	(1)	(2)	(1)	(2)	(1)	(2)	(1)	(2)	(1)	(2)
^{63}Ni	0.06587	0.0172	6.52	0.44	0.35	0.44	0.35	0.44	0.35	0.44	0.35	0.44	0.35	0.44	0.35
^{35}S	0.1674	0.0488	31.7	1.00	1.00	1.10	1.00	1.11	1.00	1.11	1.00	1.11	1.00	1.11	1.00
^{141}Ce	0.444	0.1459	138.5	1.22	1.25	1.93	1.98	2.73	2.87	2.92	2.99	2.93	2.99	2.93	2.99
^{204}Tl	0.7635	0.2433	290.8	1.14	1.12	2.02	1.93	3.64	3.62	4.65	4.86	4.93	4.99	4.99	4.99
^{210}Bi	1.161	0.3945	496.6	1.07	0.98	1.99	1.81	4.04	3.93	5.95	6.38	6.86	7.58	7.11	8.01
^{32}P	1.711	0.6950	790.7	1.01	0.77	1.94	1.52	4.24	3.75	6.89	7.21	8.55	10.03	9.12	11.14
^{90}Y	2.288	0.9367	1099.6	0.99	---	1.91	1.42	4.34	3.47	7.43	6.77	9.63	9.78	10.49	11.17
^{28}Al	2.865	1.2397	1403.6	0.98	---	1.90	1.32	4.40	3.34	7.78	6.76	10.38	10.12	11.44	11.75

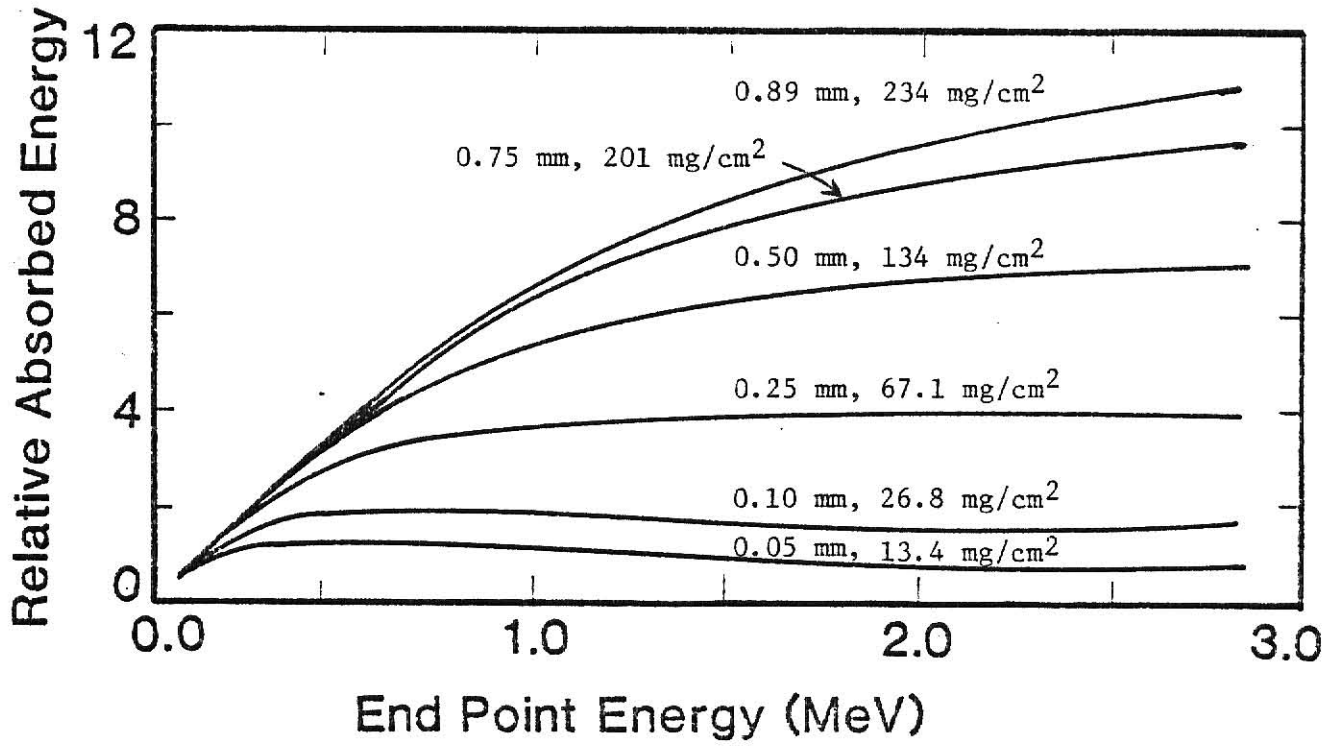

FIG. 2.7. Exponential attenuation model energy response curves for six thicknesses of LiF.

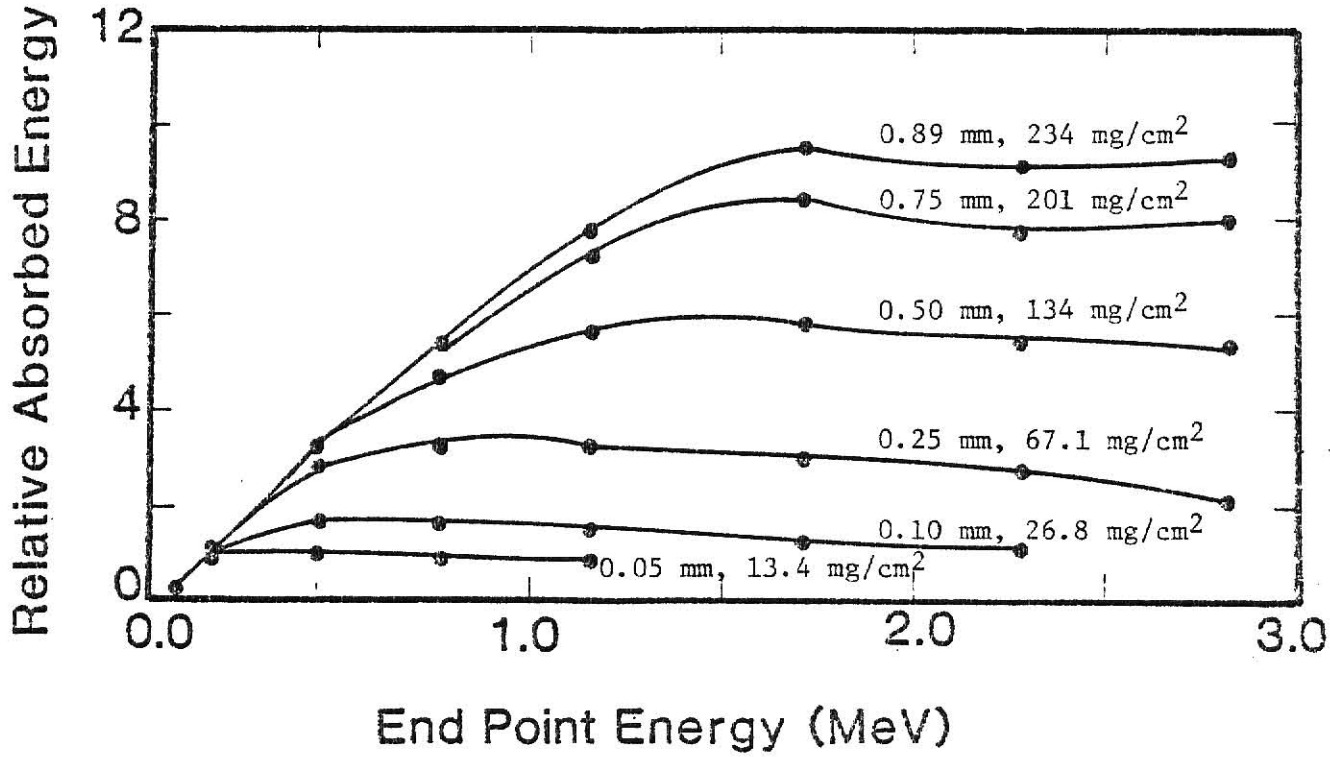

FIG. 2.8. Multiple-scattering model energy response calculations for six thicknesses of LiF. Connecting lines are added for visual clarity.

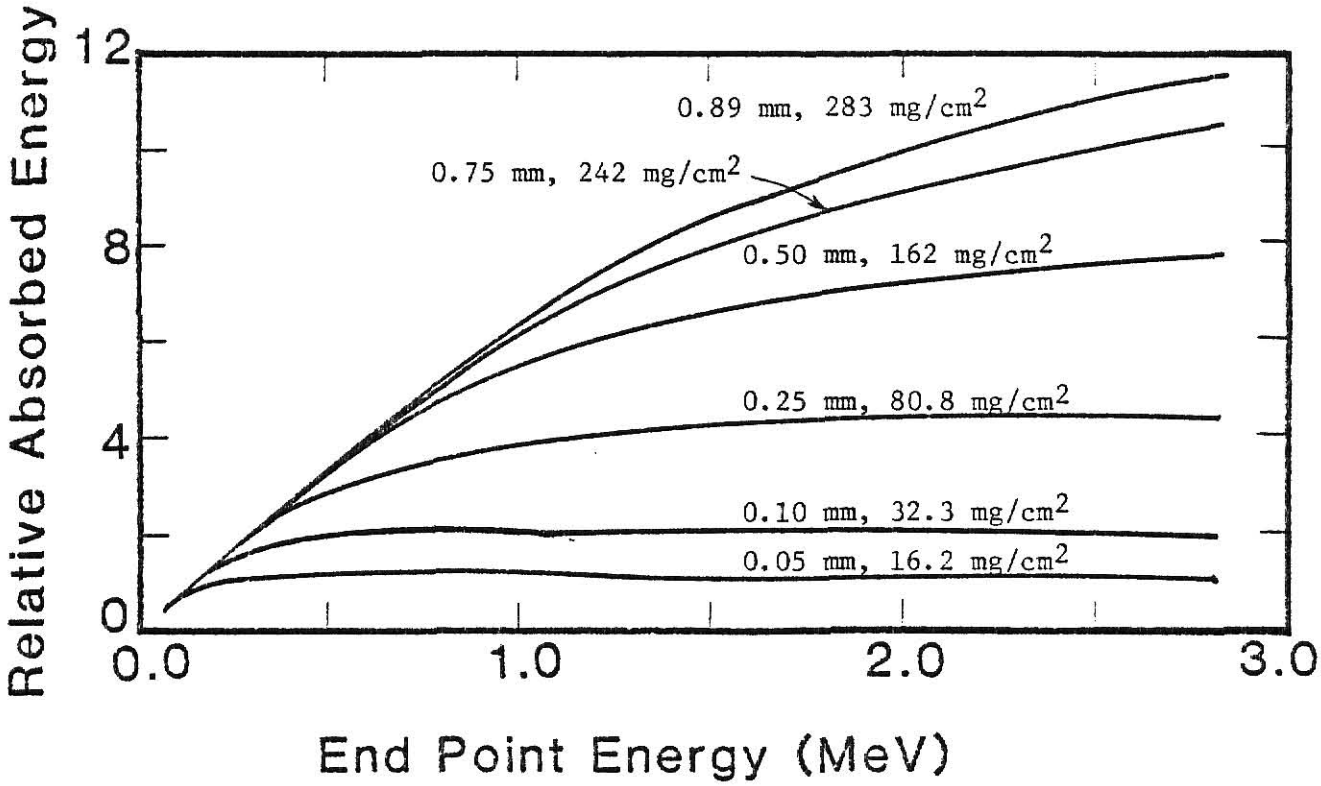

FIG. 2.9. Exponential attenuation model energy response curves for six thicknesses of CaF_2.

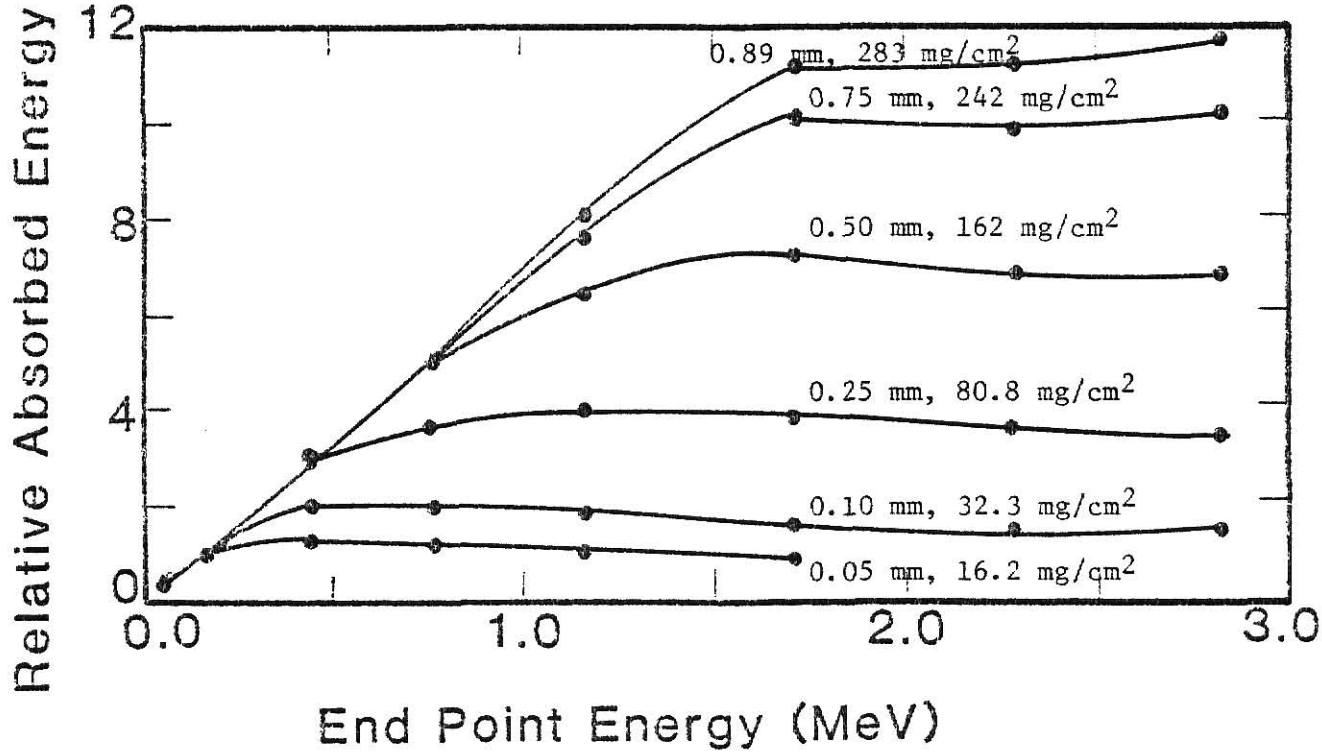

FIG. 2.10. Multiple-scattering model energy response calculations for six thicknesses of CaF_2. Connecting lines are added for visual clarity.

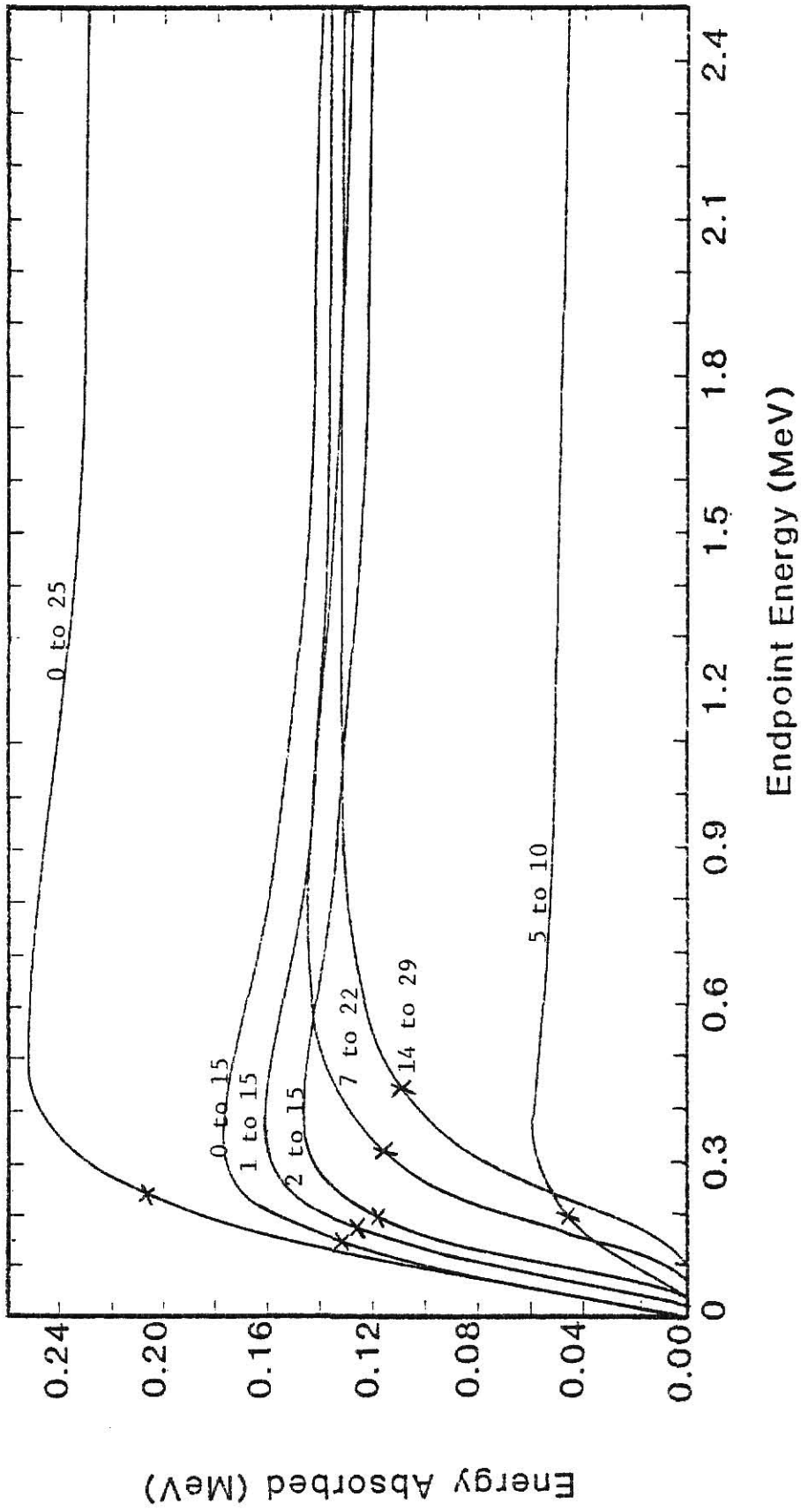

FIG. 2.11 Exponential attenuation model energy response curves for seven thin dosimeters measuring various mass thickness ranges, as indicated in mg/cm^2.

cutoff value can be achieved with a 2 to 15 mg/cm^2 TLD, which could be a 0.05 mm thick LiF wafer with a 2 mg/cm^2 cover.

The theoretical response for the 14 to 29 mg/cm^2 TLD has a -15% low energy cutoff value of 450 keV. This would be the theoretical response for the Panasonic thin dosimeter. Thus a thin TLD and a thin cover are necessary for a good energy response.

III. DOSIMETRY MATERIALS, PROCEDURES AND INSTRUMENTS

A. Beta dosimeters

Six types of TLD materials and five TLD thicknesses were evaluated with respect to their beta-particle dose response. Three TLD types, obtained commercially, were 6.0 mm-dia. disks composed of ^{7}LiF, $CaSO_4$:Dy or CaF_2:Mn in a teflon matrix. These disks had specified thicknesses of 0.02 mm (^{7}LiF and $CaSO_4$:Dy), 0.13 and 0.4 mm (CaF_2:Mn), which corresponds to about 3.7 mg/cm^2 for the ^{7}LiF and $CaSO_4$:Dy disks, and 27 and 82 mg/cm^2 for the CaF_2:Mn disks. When the 0.02 mm-thick disk thicknesses were measured, the actual average thickness was nominally 0.045 mm or about 7.5 mg/cm^2 for the ^{7}LiF and $CaSO_4$:Dy disks. The weight percent of TL phosphor in the teflon TLDs was 30% for the ultrathin ^{7}LiF and $CaSO_4$:Dy disks and 5% for the thicker CaF_2:Mn disks. Three additional types of TL materials obtained commercially were 3.175 x 3.175 mm x 0.89 mm-thick LiF(235 mg/cm^2), CaF_2:Mn (283 mg/cm^2) and CaF_2:Dy solid ribbons. These solid ribbons, as well as the teflon/CaF_2:Mn TLDs, provided dosimeters for use in determining the response of thick TLDs to beta radiation.

In addition to the standard commercial TLDs mentioned above, two general types of locally assembled material composites were prepared. One type of composite consisted of a thick (0.89 mm) LiF TLD ribbon adhered to a thin (approximately 0.05 mm-thick, 16 mg/cm^2) wafer of CaF_2:Mn. The thin TLD wafer provided the skin dose detection. The LiF ribbon provided deep dose detection, a tissue equivalent backing, and structural strength for the thin wafer. When the response of this dosimeter was measured, the skin dose and deep dose were obtained

simultaneously since there was an approximate 65°C separation in the main glow peaks of the phosphors (see Section IV.J). A similar composite technique was tried by Gorbics and Attix to obtain an estimation of effective photon energy.[22] The locally constructed composite has the advantages that it can be annealed at 400°C without being destroyed and the CaF_2 Mn has an efficiency about 10 times that of the LiF, therefore preventing the LiF glow peak from swamping out the thin layer CaF_2:Mn peak. A second, and extensively studied, composite consisted of adhering thin LiF (13 mg/cm^2), CaF_2:Mn (16 mg/cm^2), or CaF_2:Dy (16 mg/cm^2) TLD wafers to a graphite backing.

The overall size of the graphite backed composite was about the same as the TLD/TLD composite, i.e., the graphite was 4 x 4 mm x 0.89 mm-thick (151 mg/cm^2) and the TLD wafers were nominally 3.175 x 3.175 mm x 0.05 mm-thick. In this configuration the TLD wafers provided the skin dose information while the graphite backing was nearly tissue equivalent and supported the fragile TLD wafer. These composites could also be annealed at 400°C due to the high temperature resistant polyimide adhesive which was used. Characteristics of the adhesive material, Kapton XP, are given in Appendix B.

The detailed construction steps for these graphite backed composites are given below.

THIN COMPOSITE TLD PRODUCTION:

1) Use 600 grit (or finer) sandpaper to smooth both faces of the 0.89 mm TLD ribbons. (Wettable sand paper should be used with a small amount of distilled water.)
2) Cut a sufficient number of Kapton XP adhesive squares (∿3.8mm on each side) to make the desired number of dosimeters.

3) Cut graphite into small blocks, ∿3.8mm square and 0.89mm thick. Smooth both faces with sandpaper and soak in acetone or alcohol to clean. Then bake the blocks in the 400°C oven for about 15 minutes. Wipe off any remaining dust. Make enough blocks for the desired number of dosimeters.

4) Glue about 10 thick TLD ribbons from Step 1 to a glass slide with cyanoacrylate glue (Super Glue). Leave a small space between all TLD ribbons and push each ribbon down hard to make a good, flat mounting.

5) Put the glass slide in its holder and wet sand the ribbons until they are approximately 0.05mm thick. This can be measured with a micrometer by comparing the slide plus TLD thickness with the bare slide thickness. Some of the TLD ribbons may be fractured in the sanding process, but this can be minimized by careful sanding.

6) Remove the slide, rinse with water, allow to dry, then put the slide in the 400°C oven for 10 minutes. This vaporizes the glue and frees the TLD wafers. The wafers are extremely fragile in this state and must be handled by sliding them from one position to another. The wafer thickness may be calculated by weighing the wafer on a microbalance and computing the thickness from the known density and side dimensions.

7) Glue the appropriate number of graphite blocks (from Step 3) to a glass slide in the same manner as given in Step 4. Put this slide in the holder and sand lightly to ensure all blocks are the same thickness. Wipe any dust off with an acetone or alcohol dampened cloth.

8) Place a Kapton XP square on top of each graphite block, then place a TLD wafer on top of each Kapton XP square as shown in Figure 3.1. Carefully place another glass slide on top of this assembly and put the entire assembly in the 400°C oven for 5 minutes. Upon removal from the oven, immediately press down hard on the top glass slide to compress the composite dosimeters. Hold for about one minute. Remove the dosimeters from the slide and begin use.

NOTE: These dosimeters are quite rugged, however care should be taken not to get carbon dust on the TL wafer from stacking, sliding in and out of envelopes, etc, since this will reduce the TL output.

B. Beta sources

Five beta sources were used throughout the course of this study. As shown in Table 3.1, their endpoint energies E_o varied from 0.1674 to 2.288 MeV. One of the sources, the $^{90}Sr/^{90}Y$ was purchased. The others were produced in the Kansas State University TRIGA Mk II nuclear reactor.

Dosimetry studies required moderately high activity beta sources. The analysis used to determine a suitable source activity for $^{90}Sr/^{90}Y$ is given in Appendix D. An 8.33 mCi $^{90}Sr/^{90}Y$ source, shown in Fig. 3.2a, encapsulated in stainless steel was one of the sources which satisfied this requirement. It was packaged with a 0.127mm (5 mil) beryllium window of 23.5 mg/cm^2 mass thickness. The source capsule was mounted inside a polyethylene cylinder to minimize beta particle penetration through the sides and back and help reduce bremsstrahlung radiation.

Locally produced sources were mounted in 21.3 mm ID sections of thin cross section (2.54 mm) cylinders of PVC pipe. The source material was contained with a 0.025 mm-thick polyester film on the top and a 0.051 mm-thick film on the bottom. This configuration, shown in Fig.

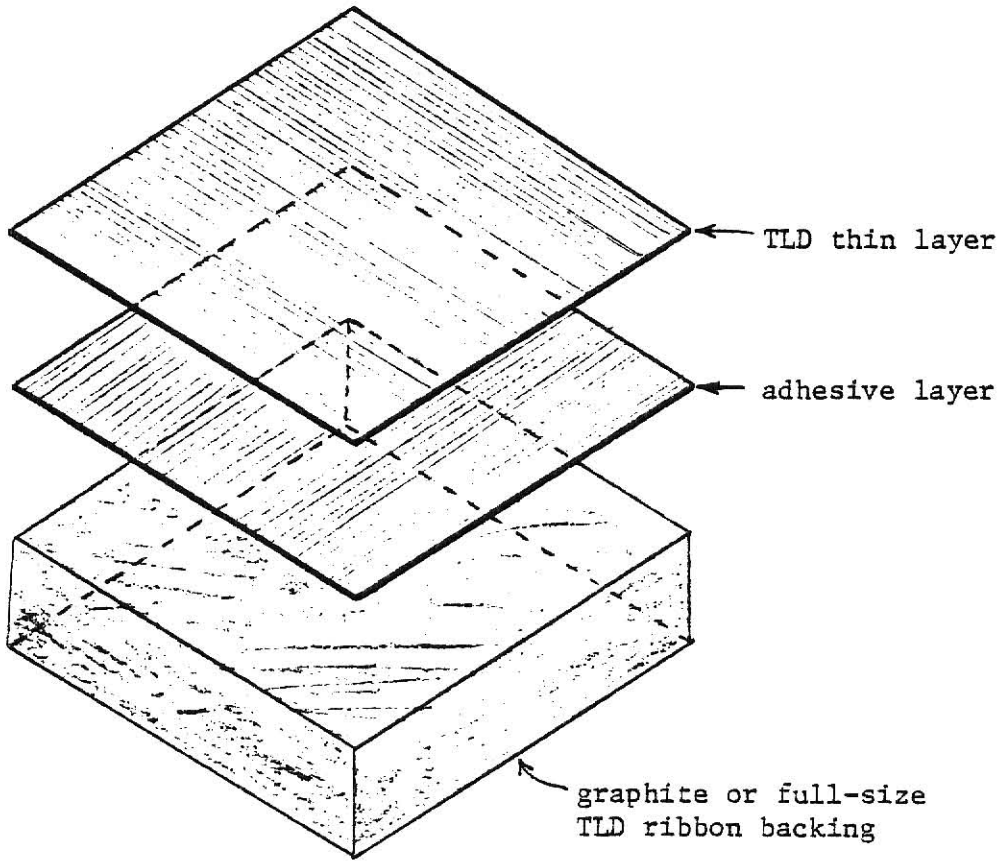

FIG. 3.1 Construction of thin-layer TLD composite dosimeter.

Tabla 3.1. Characterization of the radioisotopes used in the beta dosimetry.

ISOTOPE	HALF-LIFE	ACTIVITY	Eo (MeV)	$\bar{E}$ (MeV)	%YIELD	OTHER EMISSIONS
$^{90}Sr/^{90}Y$	28.5y	8.33mCi	0.5461, 2.288	0.1963, 0.9367	100, 100	γ: 1.761MeV, 3×10^{-3}%, 2.186MeV, 1.4×10^{-6}%
^{35}S	88d	<0.2mCi	0.1674	0.0488	100	None
^{185}W	75d	~3mCi	0.4326	0.144	100	γ: 0.125MeV, 0.021%
^{204}Tl	3.8y	~0.5mCi	0.7635	0.2433	97.7	Hg X-rays, <0.71%
^{32}P	14d	~5mCi	1.711	0.6950	100	None

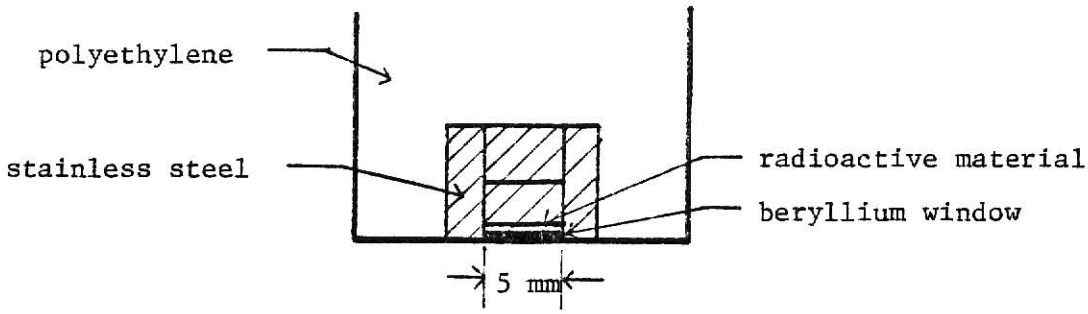

a. Encapsulation of the commercial 8.33 mCi $^{90}Sr/^{90}Y$ beta source.

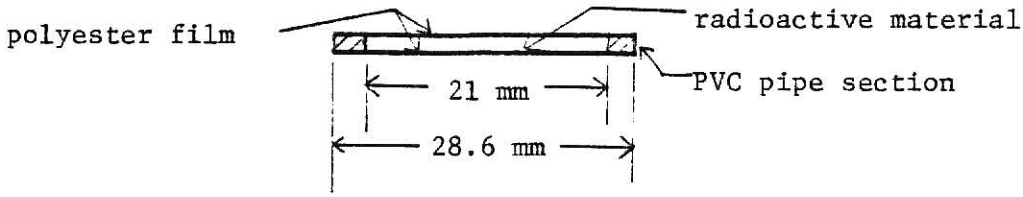

b. Encapsulation used for the KSU produced beta sources.

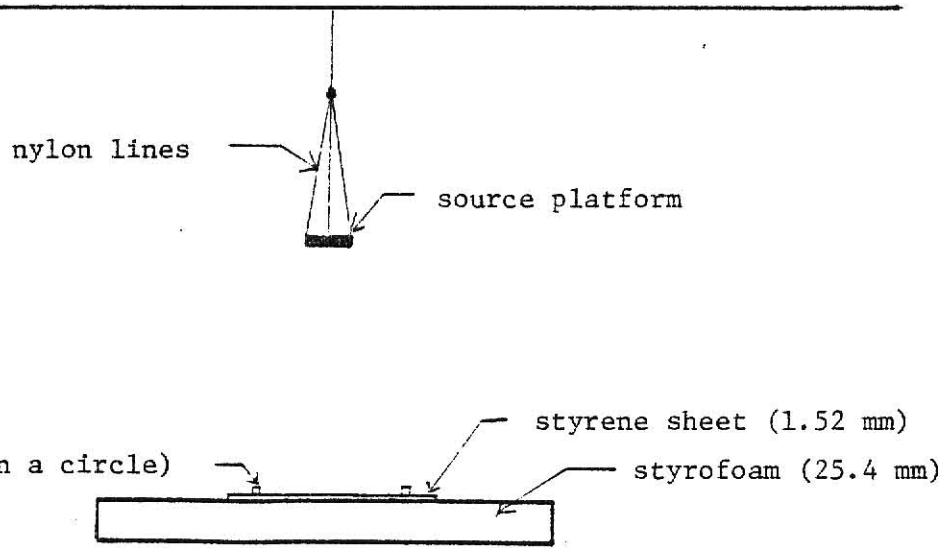

c. Configuration used to perform beta-particle irradiations of TLDs.

FIG. 3.2. Beta source encapsulations and the beta irradiator.

3.2b, provided a low atomic number, thin window source holder which minimized beta attenuation, backscatter and bremsstrahlung production.

The bremsstrahlung produced by the beta sources may be approximated by[16]

$$E_{br}(\text{MeV}) \cong \frac{Z\,E_o^2}{7000} \quad , \tag{3.1}$$

where E_{br} is the average total bremsstrahlung energy emitted per beta disintegration and Z is the atomic number of the source holder. The average fraction of beta energy that is emitted as bremsstrahlung may then be determined by

$$f_\beta = \frac{Z\,E_o^2}{\overline{E}\ 7000} \quad . \tag{3.2}$$

The maximum bremsstrahlung production from the $^{90}Sr/^{90}Y$ source encapsulated in stainless steel will be less than 2.1% of the total beta energy emitted. For the locally produced sources, the maximum bremsstrahlung production will be less than 0.36% of the total beta energy emitted. Due to these low percentages, bremsstrahlung effects were ignored.

C. Beta irradiations

Beta-particle absorbed-dose irradiations were performed by arranging the TLDs in a circle directly below the beta source. Each set of TLDs was always placed on top of a 1.52 mm-thick styrene sheet which was supported by a 25.4 mm-thick styrofoam pad. The beta source was positioned on top of a thin section of PVC pipe suspended from three monofilament nylon lines. The irradiation configuration is shown in

Fig. 3.2c. For experiments designed to investigate the effect of dosimeter covering material, covers of polyester film ranging in thickness from 0.03 mm to 0.71 mm and styrene of 1.52 mm were placed on top of the TLDs to provide the desired cover thickness. As a special precaution, all irradiations were performed in a darkened room. This minimized light induced fading as well as light induced TL which are problems associated with CaF_2 and teflon-based TLDs. All $^{90}Sr/^{90}Y$ irradiations were performed at a source-to-dosimeter distance of 90 cm. This distance provided sufficient air attenuation of the ^{90}Sr beta particles so that only the ^{90}Y betas reached the dosimeters.

D. Gamma irradiations

Gamma irradiations were performed using commercial gamma irradiators with ^{137}Cs and ^{60}Co sources. The TLDs were either held in a plexiglass holder or placed in a glass dish in the irradiator. Gamma irradiations were also performed with various covers in front of the TLDs. The ^{60}Co gamma irradiator was used to provide kilorad-level doses to the TLDs for high dose level investigations.

E. Annealing

Two of the TLD material types received special annealing treatments. All of the LiF ribbon and graphite-backed thin LiF composites were preannealed at 400°C for one hour, followed by 100°C for two hours. In addition, the LiF and CaF_2:Dy ribbons and composites were post-annealed at 100°C for ten minutes. Annealings were performed by placing the dosimeters in pyrex dishes in the oven.

F. TL Analyzers

Four types of TLD reader systems were used to measure TL emissions. Three were commercial readers--a hot finger design for TLDs mounted on

dosimeter cards, a planchet type for individual dosimeter studies and a pulsed-light heating system. Tests were also performed with the KSU designed photon counting analyzer.[17] Additional effort would be required to optimize the procedures for each type of reader. Essentially all of the results presented in this report were obtained from data obtained using either the planchet-type system or the locally designed photon counting system.

The planchet type system was adjusted to measure the response of the dosimeters over a 50 s period with an 8°C/s heating rate and a 290°C maximum limit. Current integration, from the photomultiplier tube (PMT), started at 90°C and continued to the end of the 50 s period. This constant cycle proved adequate and was chosen by considering the wide variation in TL material glow curve peaks and heat transfer characteristics. The reader cycle could be changed to provide for more optimal settings for each type of TLD material if only one type of TLD was to be evaluated. Typical glow curves (PMT output vs temperature) for the planchet system are shown in Appendix A.

The photon counting system was used to evaluate TL emissions from LiF TLDs. This system was designed, constructed, and optimized for LiF evaluation. It was used in this project as recommended by the previous work with two minor modifications. The planchet used in this project was an unstamped (flat) AP permanent type instead of the typical stamped AP permanent type. This was done to allow the evaluation of any size and configuration of TLD without changing planchets in the reader. The second modification was the addition of a band pass filter in addition to the standard Harshaw infrared filter used in the system. The optical characteristics of this filter are shown in Fig. 3.3.[18] This cascading

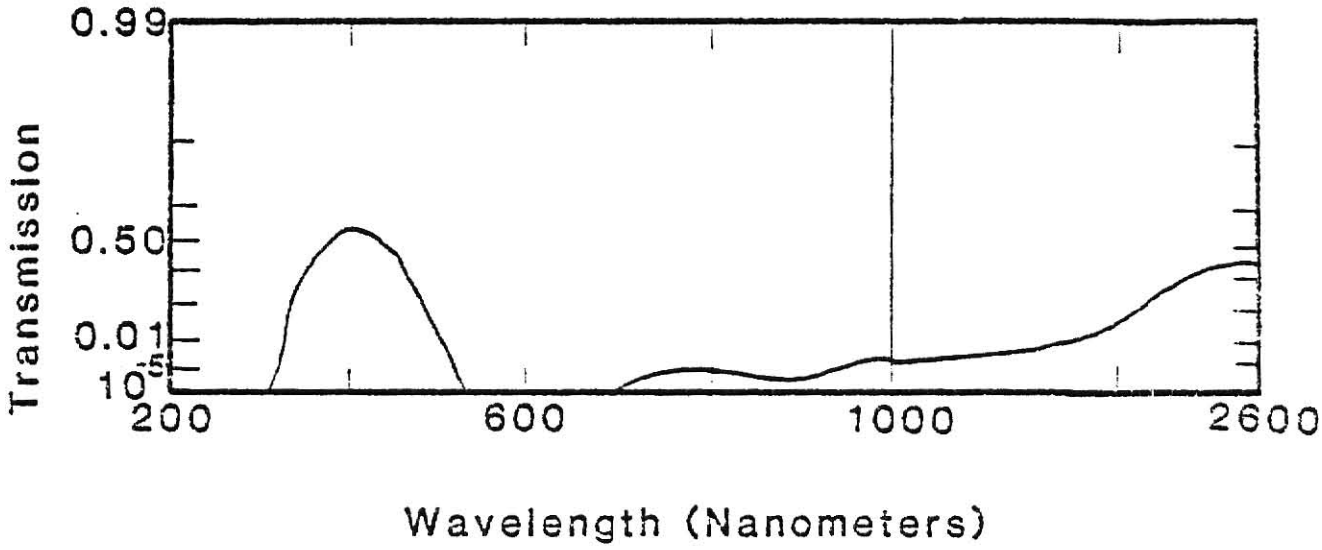

FIG. 3.3. Optical transmission characteristic for bandpass filter used in photon counter analyzer.

of filters helped to significantly reduce the "noise" caused by infrared emissions during the heating cycle, while causing only a slight loss of the 400 nm wavelength TL emitted by the LiF TLDs.

The photon counting system cycle was a heating rate of 10°C/s, an active photon-counting temperature band from 130°C to 200°C, a maximum temperature of 240°C, and a restart temperature of 60°C. This cycle was controlled by a microprocessor based system, which also provided interfacing to a Canberra Series 80 multichannel analyzer (MCA). The MCA was used in the time-scaling mode to provide digital information which could be plotted to show glow curve (number of visible light photons vs temperature) characteristics. Typical glow curves for the photon counter system are also given in Appendix A.

Analysis of thick LiF TLDs with the photon counting system required increasing the upper temperature limit on the photon counting temperature band to 220°C.

IV. DOSIMETRY RESULTS

The TL from a variety of different types of dosimeters was measured following irradiation with beta particles and gamma rays. A range of beta-particle energies was investigated to evaluate the energy and dose range response of the dosimeters.

A. Assumptions

TLD data collected in this investigation are based upon the assumptions that LiF TLDs have a linear energy response from 0.167 MeV to 2.288 MeV and that the 8.33 mCi $^{90}Sr/^{90}Y$ source used gave a dose rate of 0.36 Rad/hr at 90 cm. These assumptions are realistic and were necessary since the absolute activities of the locally produced beta sources were not known. These assumptions should be kept in mind while reviewing the following results.

B. Dosimeter linearity

Beta dose response linearities for the KSU fabricated graphite-backed wafer TLDs and the commercial teflon disks are shown in Figs. 4.1 - 4.7. These results, measured with the commercial planchet analyzer, show that a linear relationship exists between the TL response and the beta dose for the graphite-backed TLDs. This is true for each type of beta source. As expected, from known gamma-ray sensitivities, the LiF TLDs were the least sensitive and the CaF_2:Dy TLDs exhibited the most sensitivity. All of the teflon disks had a larger variance than the graphite-backed dosimeters. Moreover, the ultrathin (0.02 mm) teflon disks were more sensitive to beta radiation than either of the thicker teflon disks. The results also show that the ultrathin LiF/teflon and $CaSO_4$/teflon disks had about the same sensitivities. These relative sensitivities were not expected since the ultrathin $CaSO_4$/teflon disks

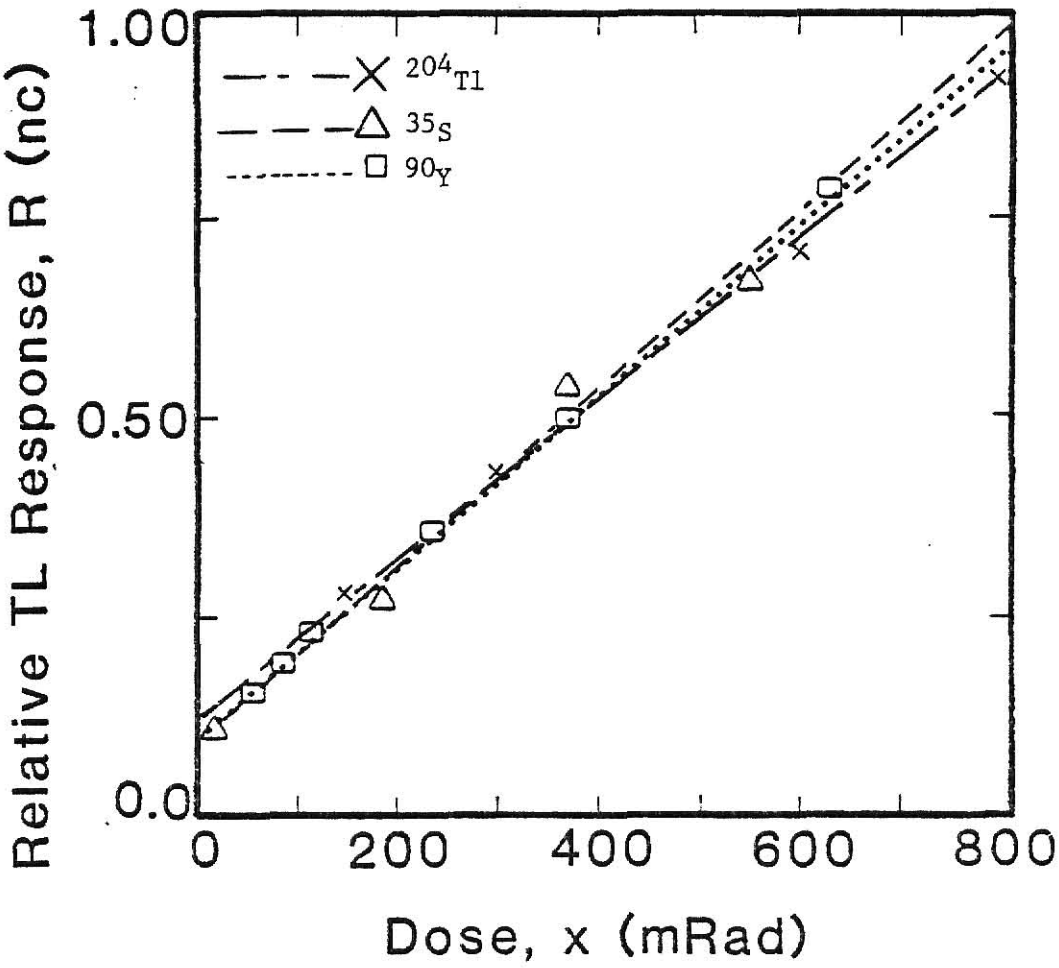

FIG. 4.1. TL response of thin (0.05 mm), graphite-backed LiF TLDs exposed to beta particles and evaluated on the planchet analyzer. Lines show least squares fits.

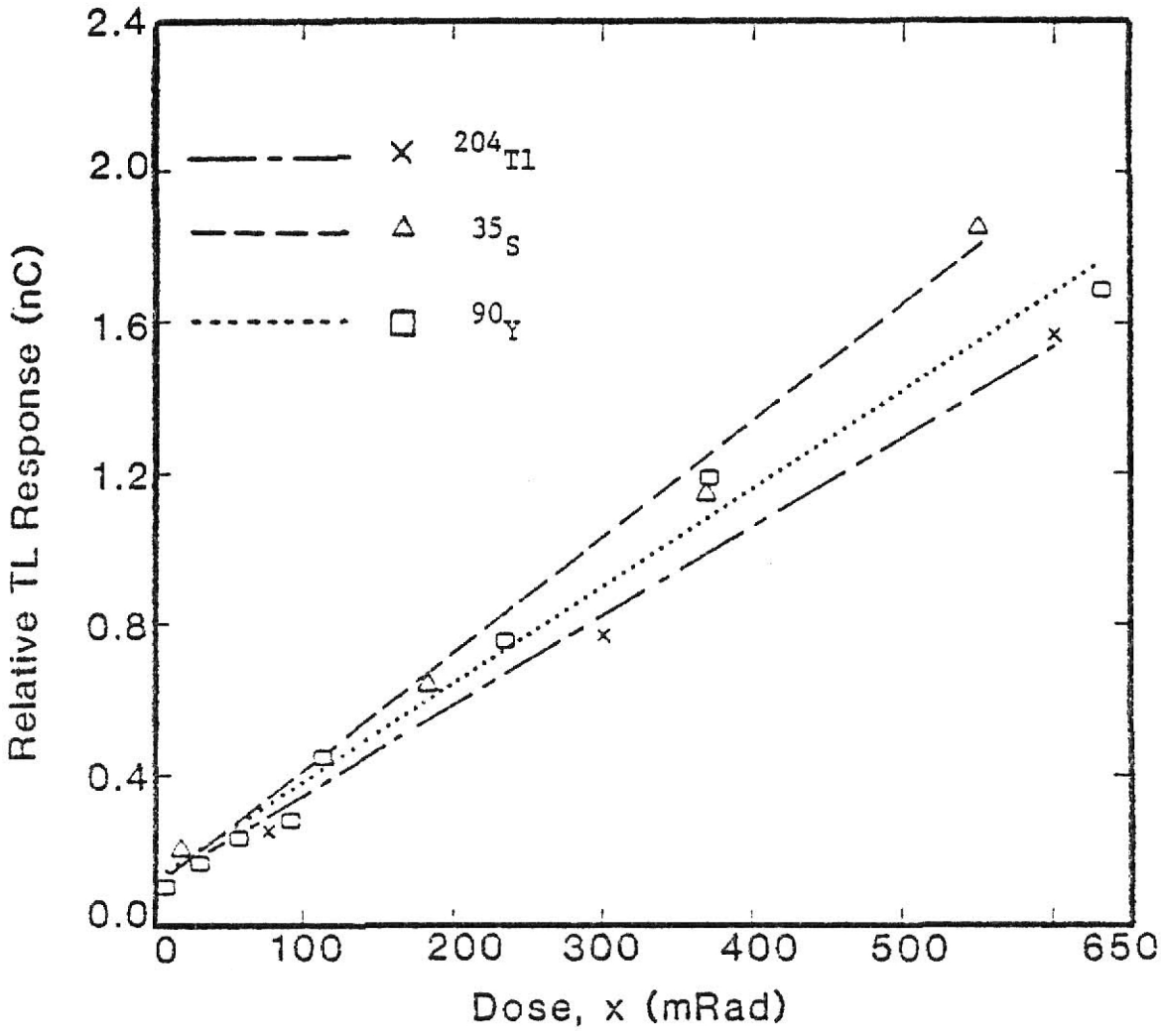

FIG. 4.2. TL response of thin (0.05 mm), graphite-backed CaF_2:Mn TLDs exposed to beta particles and evaluated on the planchet analyzer. Lines show least squares fits.

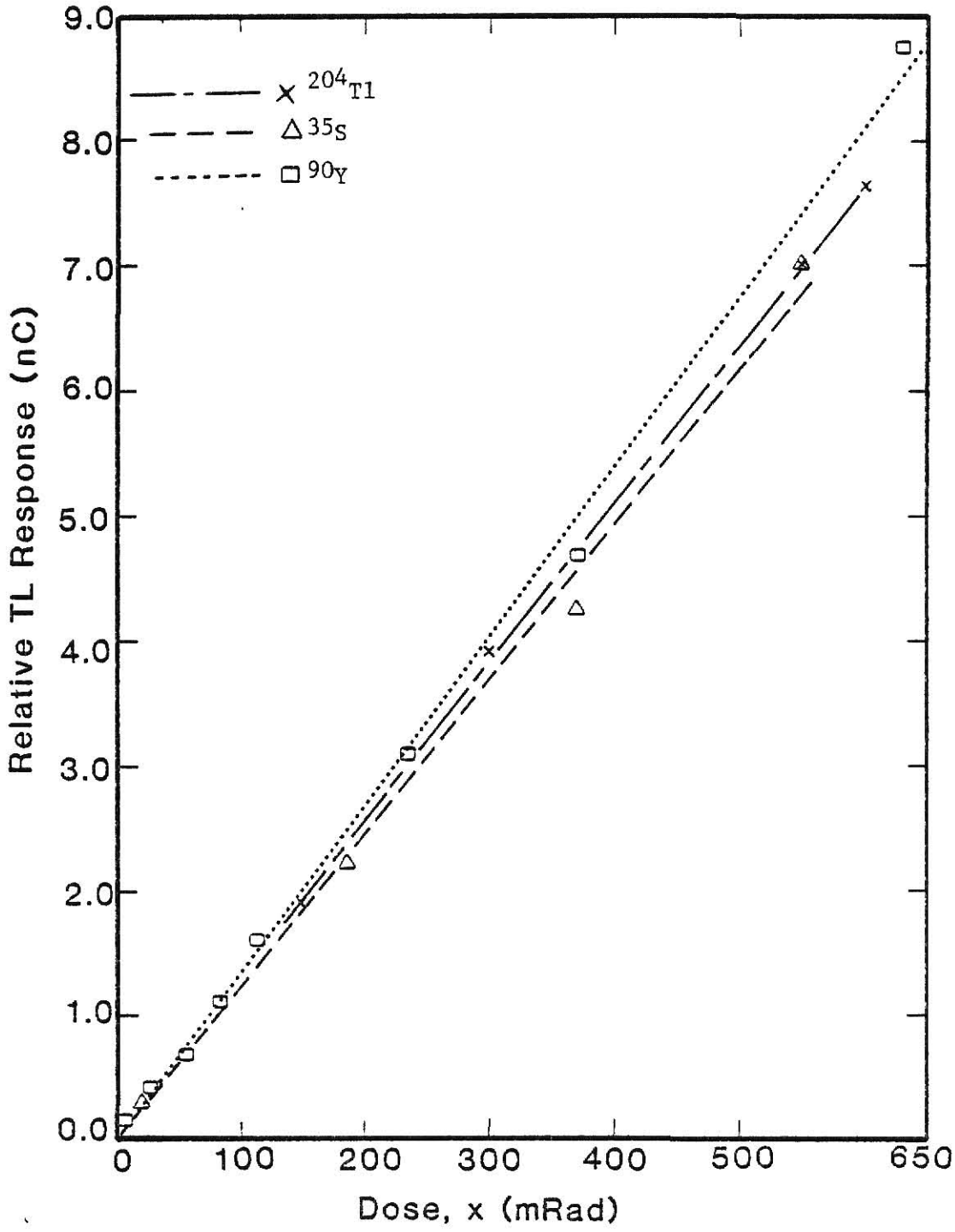

FIG. 4.3. TL response of thin (0.05 mm), graphite-backed CaF_2:Dy TLDs exposed to beta particles and evaluated on the planchet analyzer. Lines show least squares fits.

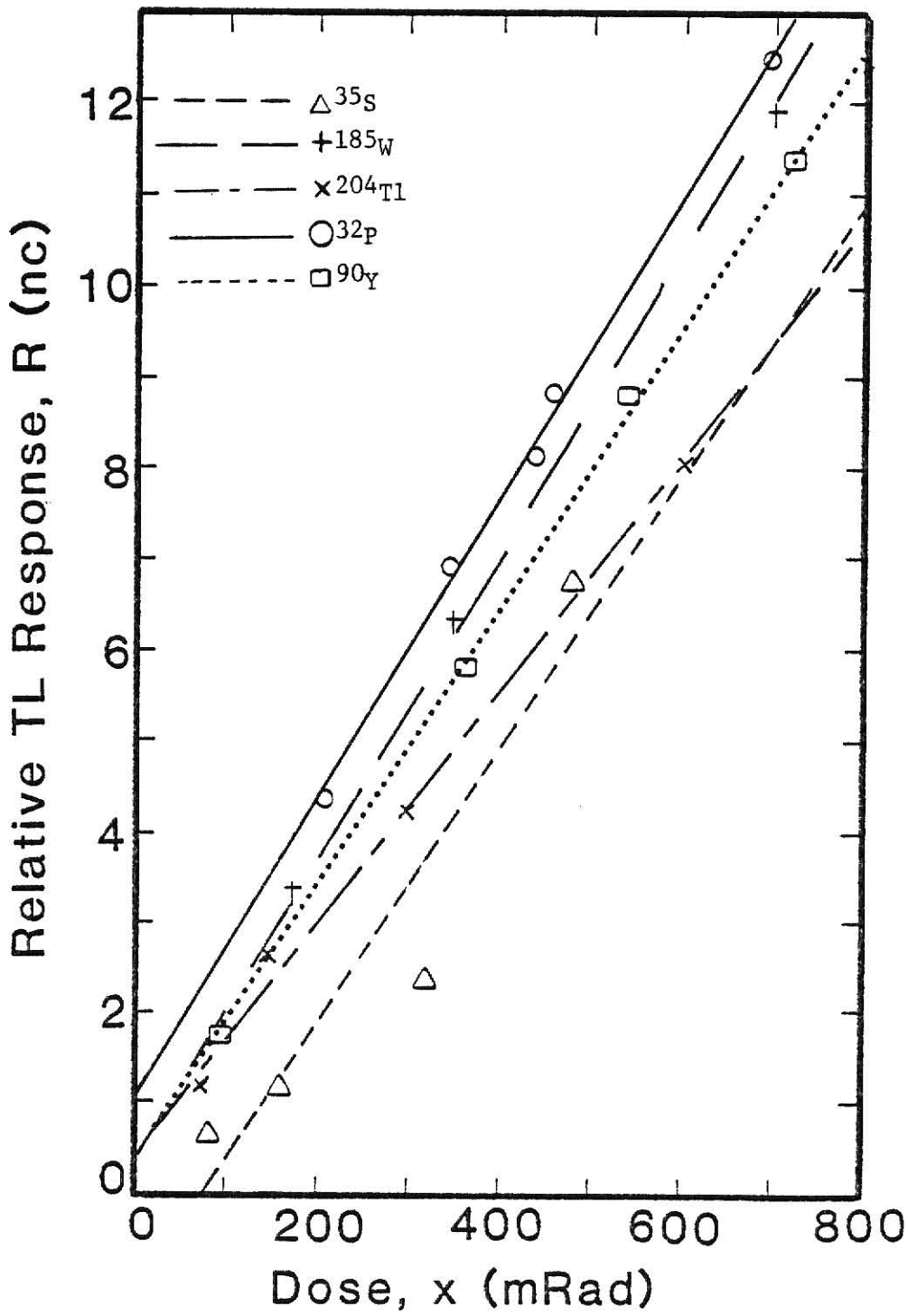

FIG. 4.4. TL response of ultrathin (0.02 mm), ^{7}LiF/teflon TLDs exposed to beta particles and evaluated on the planchet analyzer. Lines show least squares fits.

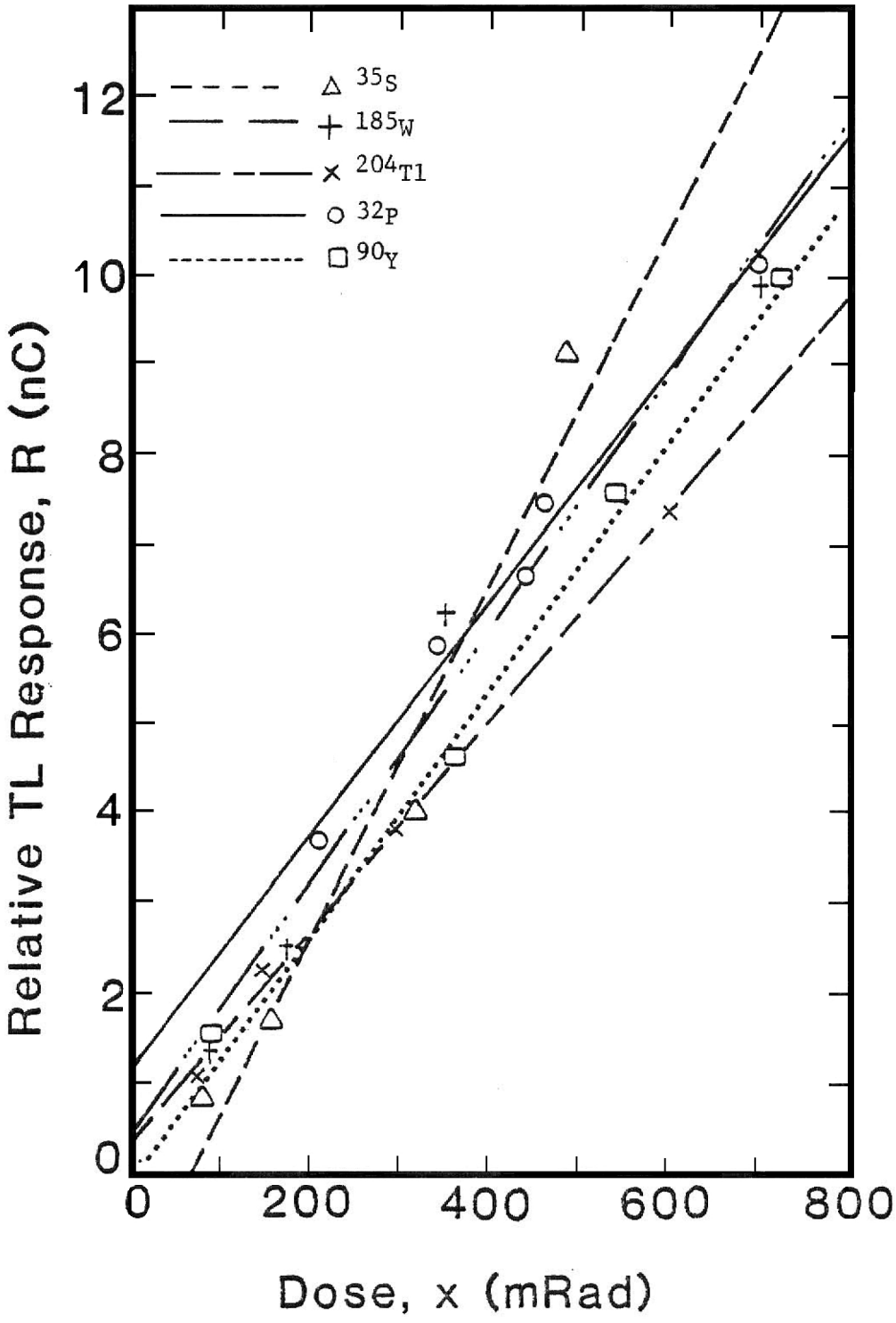

FIG. 4.5. TL response of ultrathin (0.02 mm), $CaSO_4$:Dy/teflon TLDs exposed to beta particles and evaluated on the planchet analyzer. Lines show least squares fits.

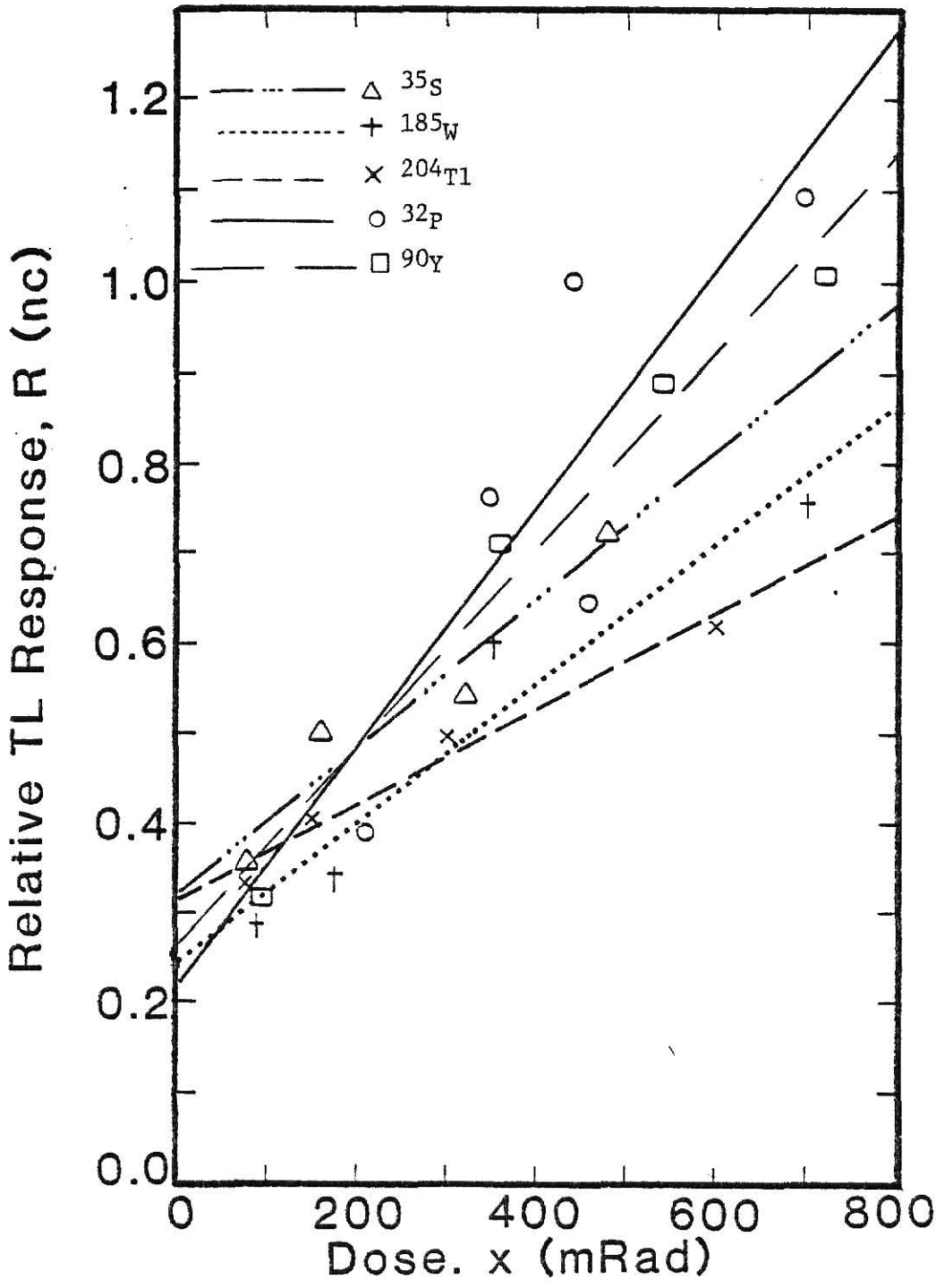

FIG. 4.6. TL response of 0.13 mm-thick CaF_2:Mn/teflon TLDs exposed to beta particles and evaluated on the planchet analyzer. Lines show least squares fits.

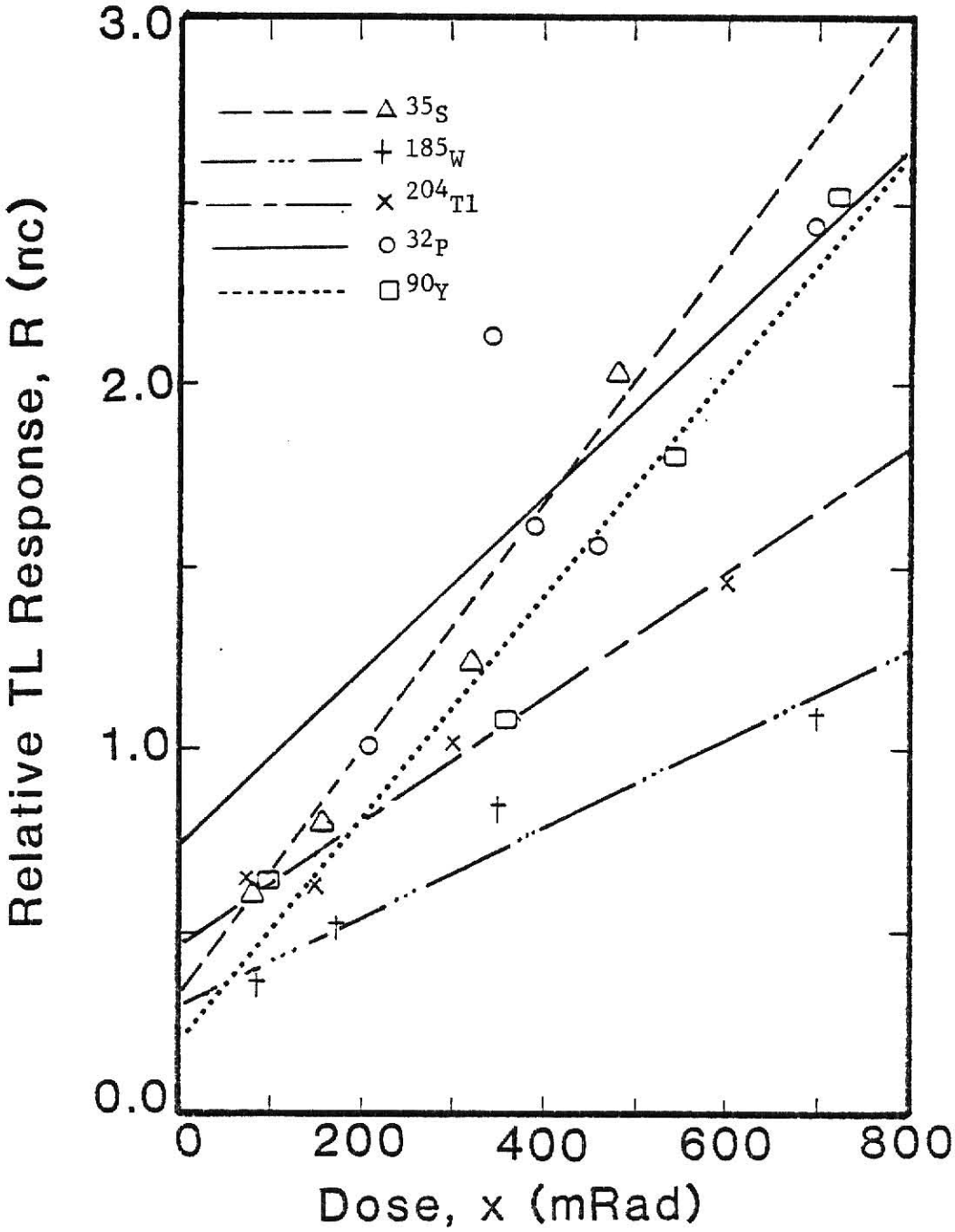

FIG. 4.7. TL response of 0.4 mm-thick CaF_2:Mn/teflon TLDs exposed to beta particles and evaluated on the planchet analyzer. Lines show least squares fits.

should be considerably more sensitive than a similar thickness LiF/teflon disk. Also, the 0.4 mm-thick CaF_2:Mn/teflon disks should be more sensitive than the 0.02 mm LiF disks. The reason for these unexpected results is not known. In addition, the ultrathin teflon disks were very difficult to handle.

C. Precision

The precision of the graphite-backed TLD data was evaluated from the linear least squares lines shown in Figs. 4.1 - 4.3. Results, shown in Table 4.1, were obtained at the 95% confidence level, assuming normally distributed data. The ^{35}S and ^{204}Tl data included four data points and the ^{90}Y had six data points for the LiF TLDs and eight data points for the CaF_2 TLDs. The method used to determine confidence intervals is given in Appendix C.

Precision was also measured, using the commercial planchet system, for graphite-backed CaF_2:Mn and CaF_2:Dy TLDs using a sequence of twenty irradiations (nominally 15 mRad) and TL response measurements. The reproducibility of the absorbed dose for each irradiation was within 0.5%. These trials showed that the individual dosimeters had a standard deviation of between 4.7% and 6.0% while the standard deviation of the mean was between 0.94% and 1.34%.

Many thin, graphite-backed LiF TLD evaluations were made with the photon counting system. Approximately 450 no dose (second read) evaluations were performed. These data were analyzed and plotted as a histogram shown in Figure 4.8. A normal distribution was fitted to these data, as shown by the curve in the figure. A Chi-squared goodness-of-fit test showed the fit was acceptable, within the 10% and 90% confidence levels, with a Chi-squared value of 15.89 and 10 degrees

Table 4.1. Confidence Intervals on the sensitivities of the graphite-backed TLDs.

TL Material	95% Confidence Interval for the Specified Radioisotope		
	^{35}S	^{204}TI	^{90}Sr
LiF	0.00077 to 0.00143	0.00093 to 0.00109	0.00103 to 0.00115
CaF_2:Mn	0.00247 to 0.00371	0.00188 to 0.00298	0.00234 to 0.00282
CaF_2:Dy	0.01024 to 0.01466	0.01230 to 0.01330	0.01294 to 0.01434

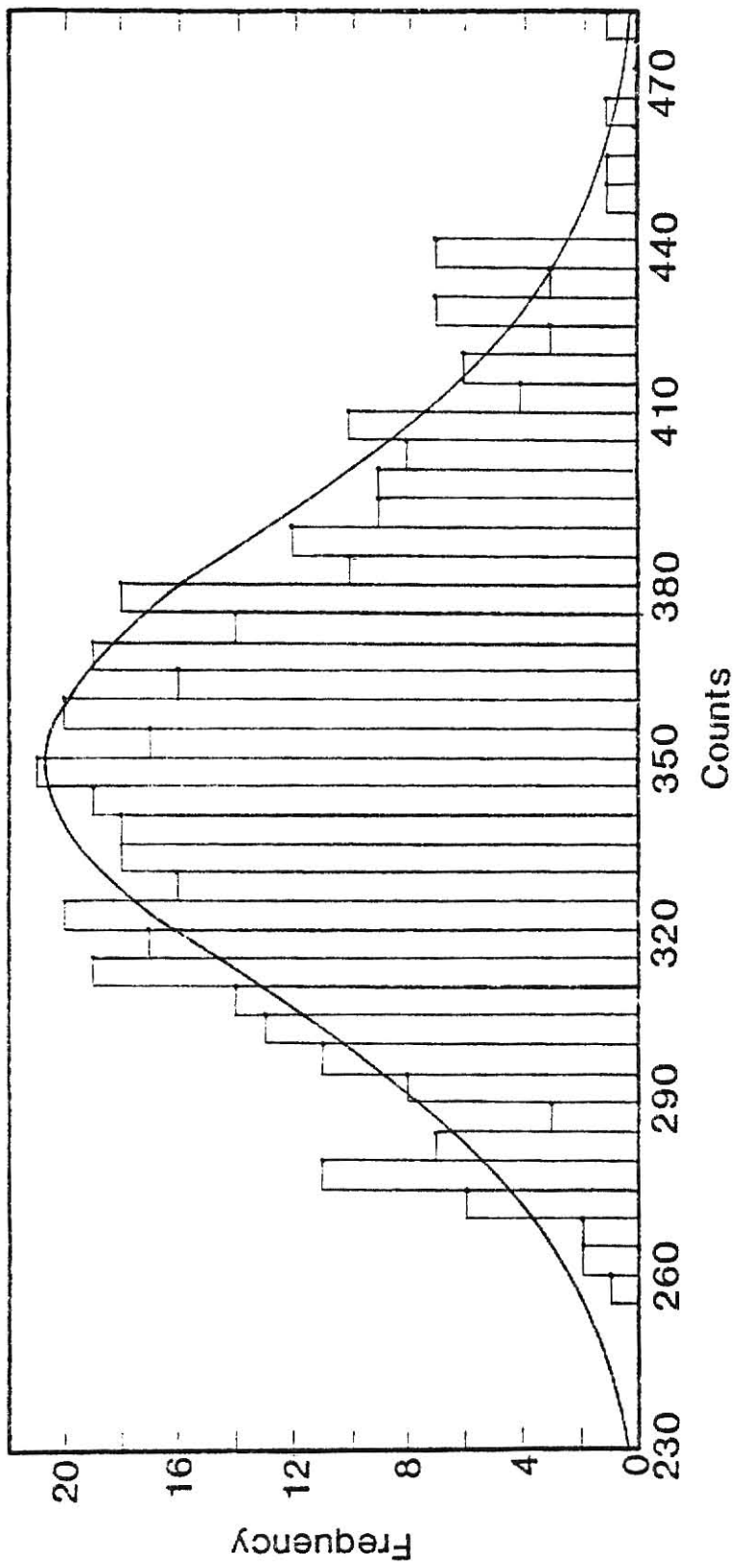

FIG. 4.8. Frequency distribution of over 450 no-dose evaluations of thin, graphite-backed LiF TLDs using the photon counting analyzer. The curve shows the fitted normal distribution.

of freedom. The standard deviation of the no dose distribution was 42.1 counts, which is equal to approximately 1 mR. It should be noted that the second reading of the thin, graphite-backed TLDs appeared to be totally random and did not display any relationship to the magnitude of the prior TLD dose (or first read). This fact was observed with doses up to several hundred rads of gamma exposure. Due to this result, no 400°C pre-annealing of the LiF TLDs was performed during the later part of this project when the photon counting system was used.

D. Minimum detectable beta dose

Minimum detectable dose values were estimated from the TL response linearity data, for the commercial planchet reader. For the graphite-backed wafers, nominal values were: 50 mRad for LiF, 5 mRad for CaF_2:Mn and 2 mRad for CaF_2:Dy. These values are only valid for TL measurements made using a commercial TLD analyzer. Moreover, since fabrication of these graphite-backed dosimeters is still in the development stage, absolute minimum detectable limits and the associated precision for each type of TL material have not been determined.

The minimum detectable beta doses can be inferred in the same manner for the teflon disk dosimeters. However, since these data exhibited large variability, minimum values were not assigned.

Minimum detectable dose evaluation for the photon counting system can be done using the no dose distribution parameters. A commonly accepted definition of minimum detectable dose is the dose equivalent to three standard deviations of the no dose distribution.[19] This would give a minimum detectable dose of approximately 3 mR for the thin, graphite-backed LiF TLDs. This value should be considerably lower for CaF_2 TLDs used with the photon counter.

The photon counting system linearity data, through least squares analysis, also indicates that a dose of 150 mR, evaluated with a single dosimeter, will, at the 95% confidence level, indicate that between 135 mR and 165 mR was received. Figure 4.9 shows the 95% confidence intervals for the individual dosimeter measurements.

E. Beta energy response

Measured energy responses for the thick (0.89 mm) and thin (0.05 mm) graphite-backed dosimeters are shown in Figs. 4.10 - 4.12. Recall that these results were normalized using the assumption that the response of the thin LiF dosimeters was energy independent. It was found that all of the thin, graphite-backed TLD materials -- LiF, CaF_2:Mn and CaF_2:Dy, had an energy independent response. Conversely, the thick dosimeter responses were highly energy dependent. Variations, up to a factor of four, were observed over the beta energy range of 0.433 MeV to 2.288 MeV. These experimental findings show the same trend as the theoretical results discussed in Section II.B.2.

Linearity studies (see Section IV.B) for the teflon disks contained results from five different energy beta sources. These give an indication of the energy response of the teflon disk dosimeters. The considerable variability obtained was not correlated with the beta energy and therefore is considered random.

F. Ratio of thick/thin dosimeter response

Due to the extreme energy dependence of the thick TLDs, the correlation between the ratio of the two responses, i.e., thick over thin dosimeter response, was investigated with respect to the logarithm of the range of the beta particles. As shown, by the results in Figs. 4.13 - 4.15, the relationship is essentially linear. Given a set of

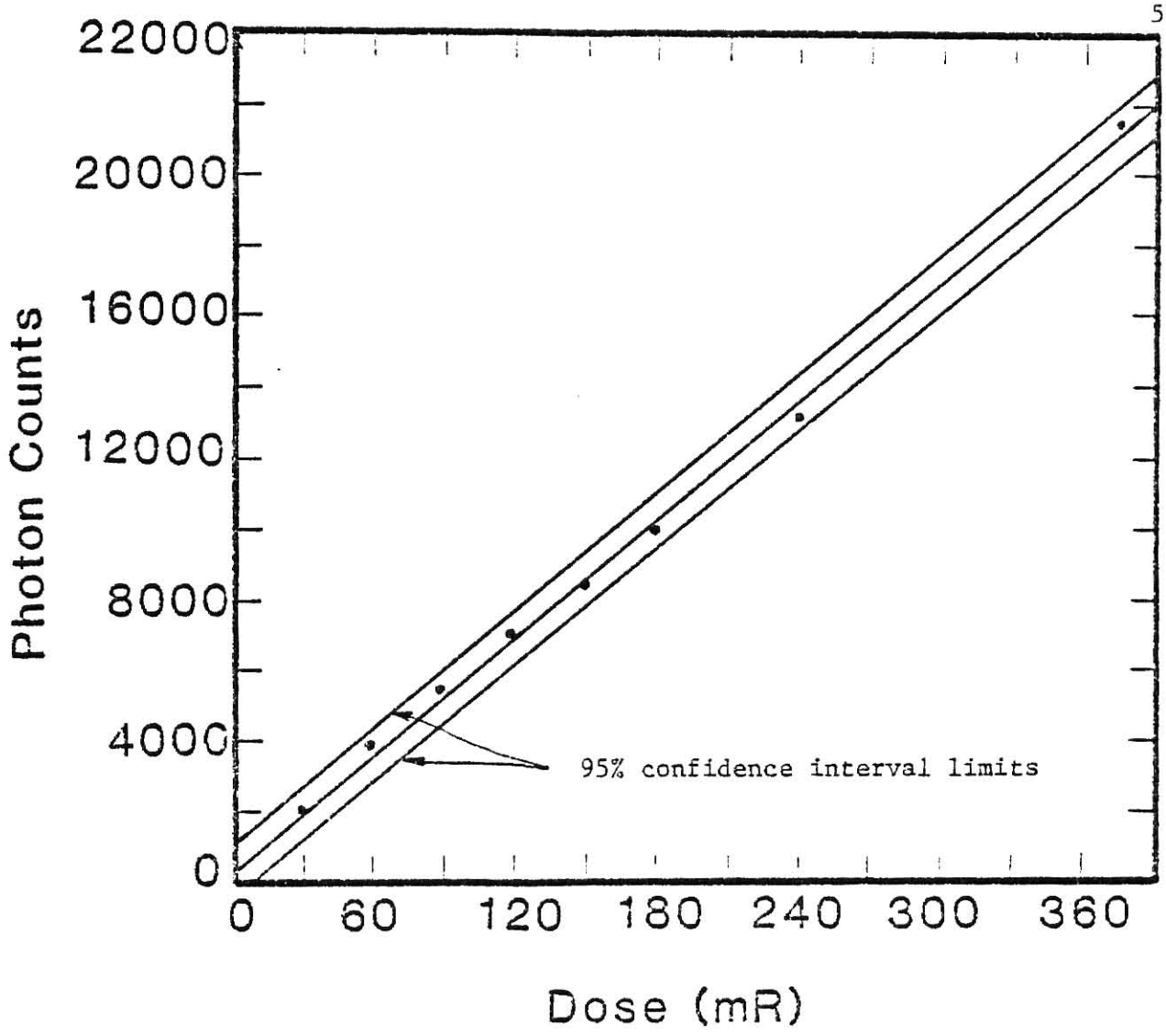

FIG. 4.9. Photon counter linearity data showing least squares fit line and 95% confidence interval limits for a typical thin, graphite-backed LiF TLD.

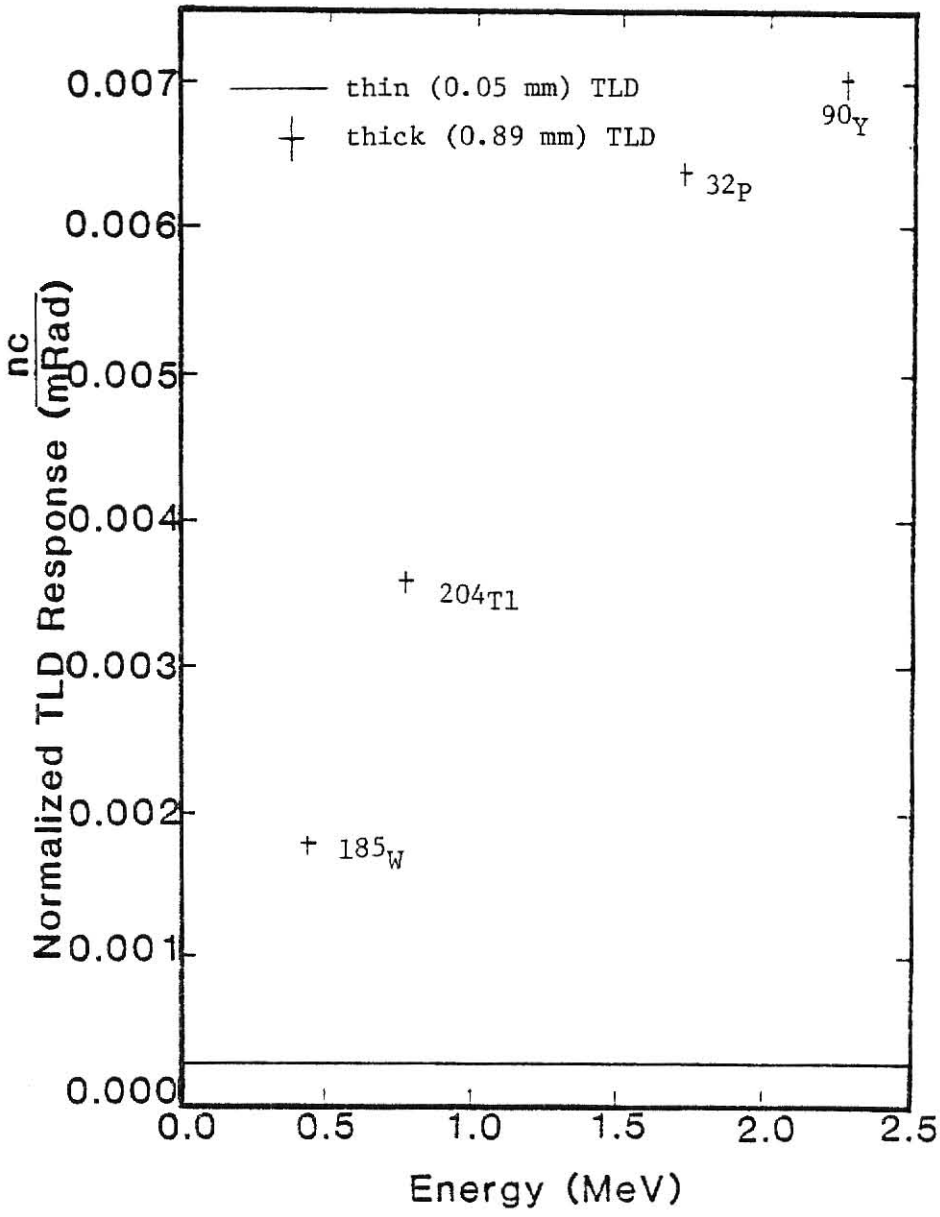

FIG. 4.10. Experimental beta energy response of graphite-backed LiF TLDs evaluated on the planchet analyzer.

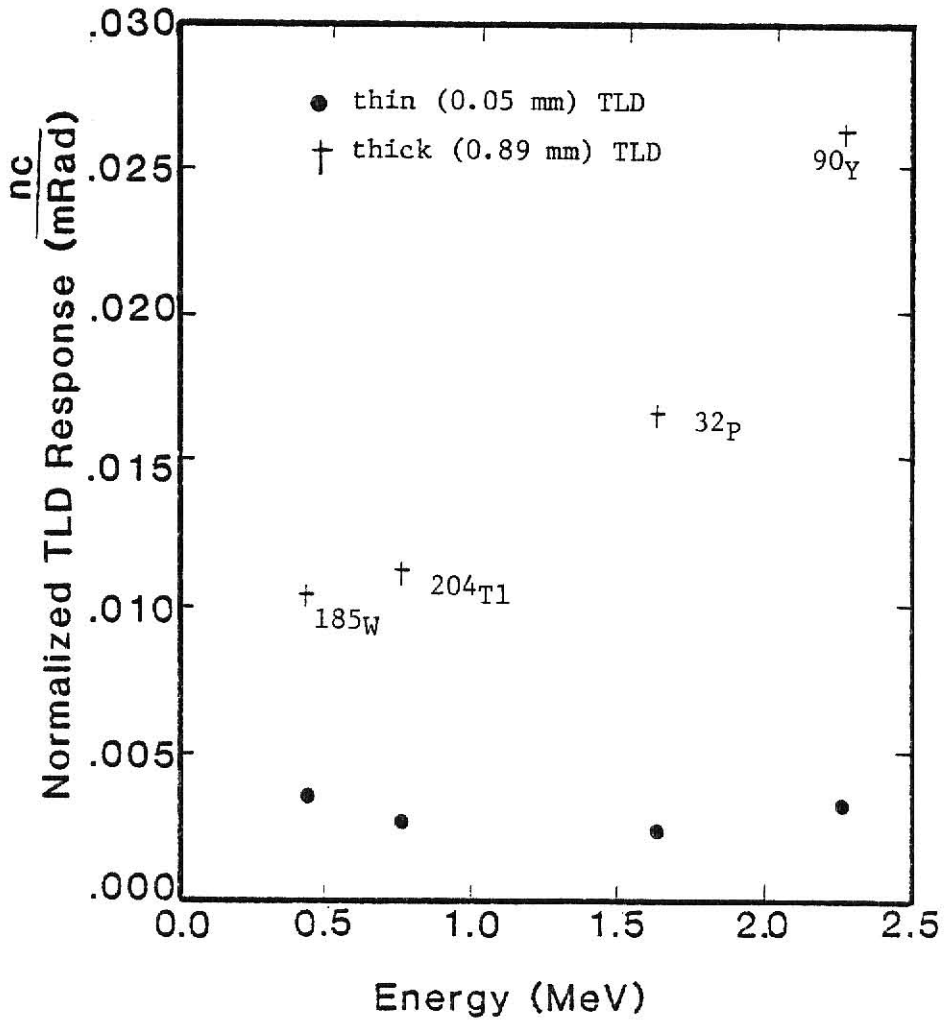

FIG. 4.11. Experimental beta energy response of graphite-backed CaF_2:Mn TLDs evaluated on the planchet analyzer.

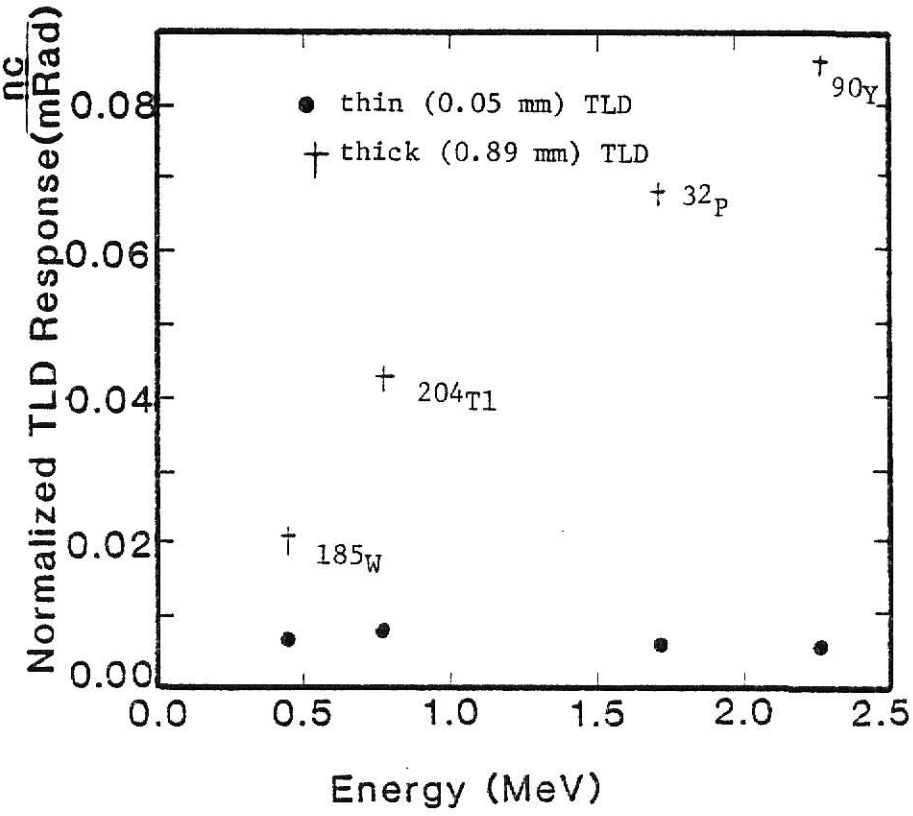

FIG. 4.12. Experimental beta energy response of graphite-backed CaF_2:Dy TLDs evaluated on the planchet analyzer.

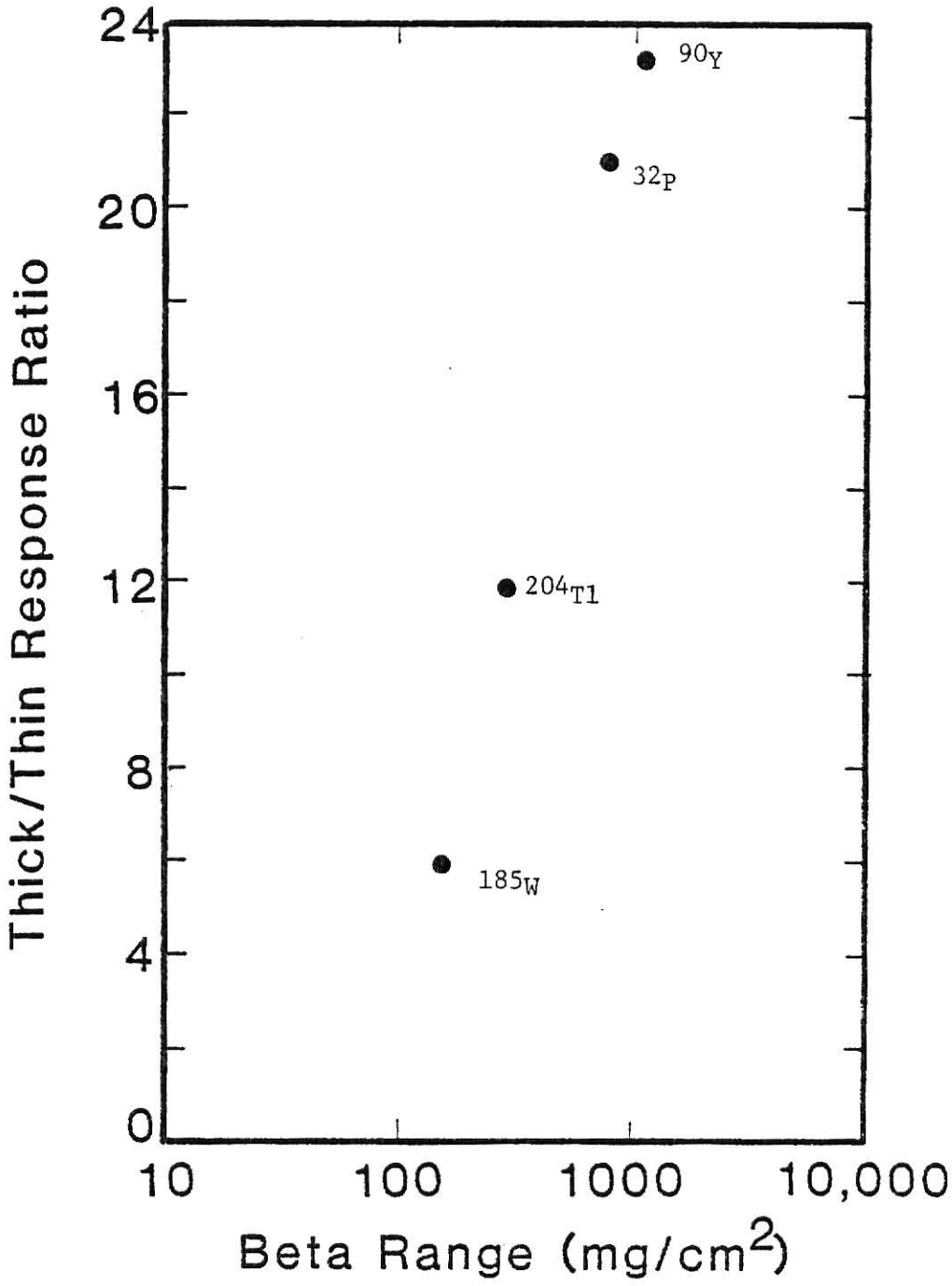

FIG. 4.13. Experimental TL response ratios of 0.89 mm and 0.05 mm graphite-backed LiF TLDs.

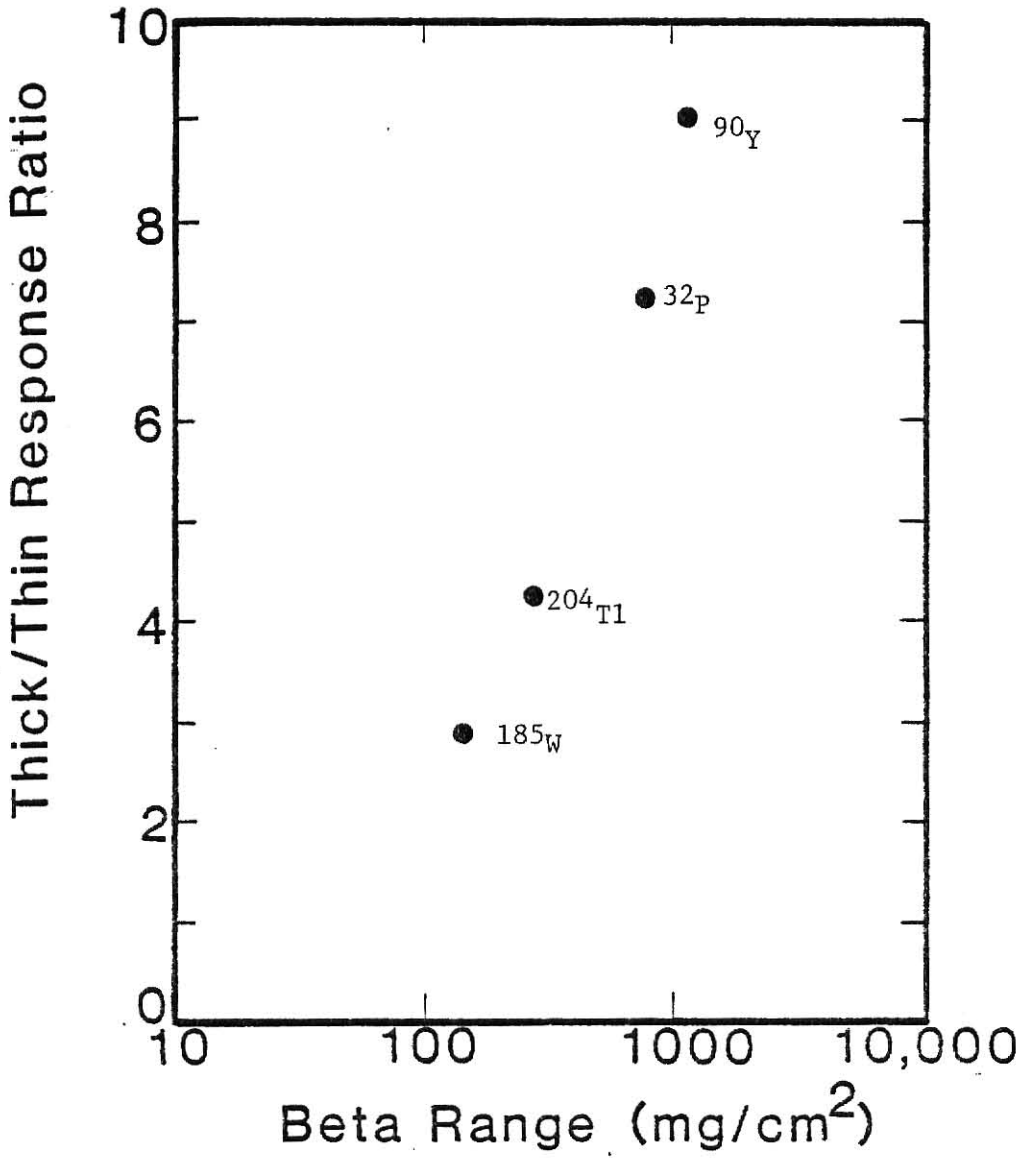

FIG. 4.14. Experimental TL response ratios of 0.89 mm and 0.05 mm graphite-backed CaF_2:Mn TLDs.

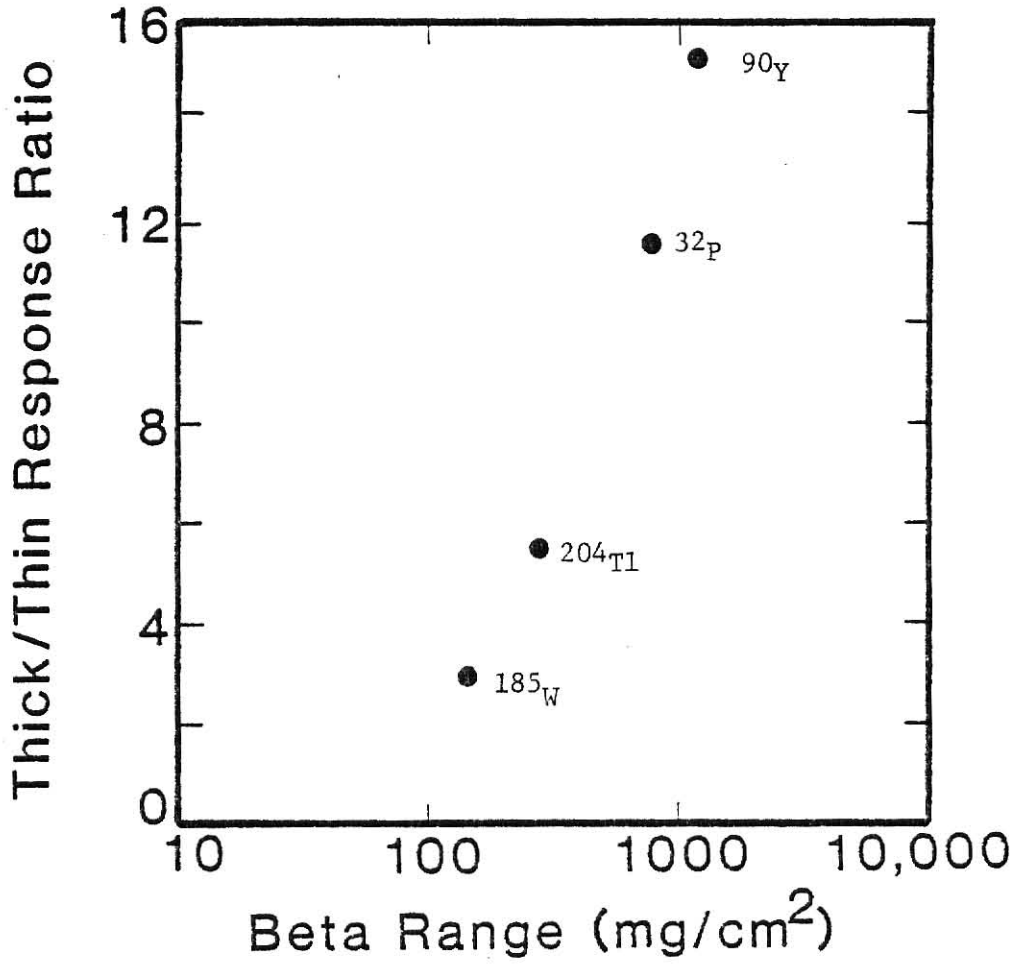

FIG. 4.15. Experimental TL response ratios of 0.89 mm and 0.05 mm graphite-backed CaF_2:Dy TLDs.

calibrated dosimeters, the approximate range of beta particles from a single beta emitter could be measured. This procedure will not provide valid results for very low level beta fields where the absorbed dose is below the detection limit of the thin dosimeters. Additional studies are required if this concept is to be extended to mixed beta fields or beta and gamma-ray fields.

G. TLD cover attenuation

To measure the relative change in TL induced in the graphite-backed CaF_2:Mn wafers when covers were placed directly over the TLDs, bare (no cover) and covered TLDs were irradiated. Experiments performed with two beta sources, ^{185}W and ^{204}Tl with maximum beta energies of 0.4326 and 0.766 MeV, respectively, provided the results shown in Figs. 4.16 and 4.17. Each data point represents the mean and standard deviation of five individual measurements.

Exponential attenuation is evident from the figures. Parameters for the solid lines shown in these two figures were obtained using least squares exponential fitting. It is important to note that the effect of the cover thickness is strongly dependent upon the beta-particle energies -- approximately a factor of two for a 20 mg/cm^2 cover.

H. Gamma-ray response

Gamma-ray response data exists for thick TLD ribbons and teflon disks, therefore, measurements were made only for the new graphite-backed dosimeters. As shown in Fig. 4.18, these new dosimeters exhibited a linear response over the gamma-ray dose range investigated with the commercial TLD analyzer -- from 50 mRad to 770 mRad. Moreover, as expected, the larger slope of the CaF_2:Dy least squares line reflects

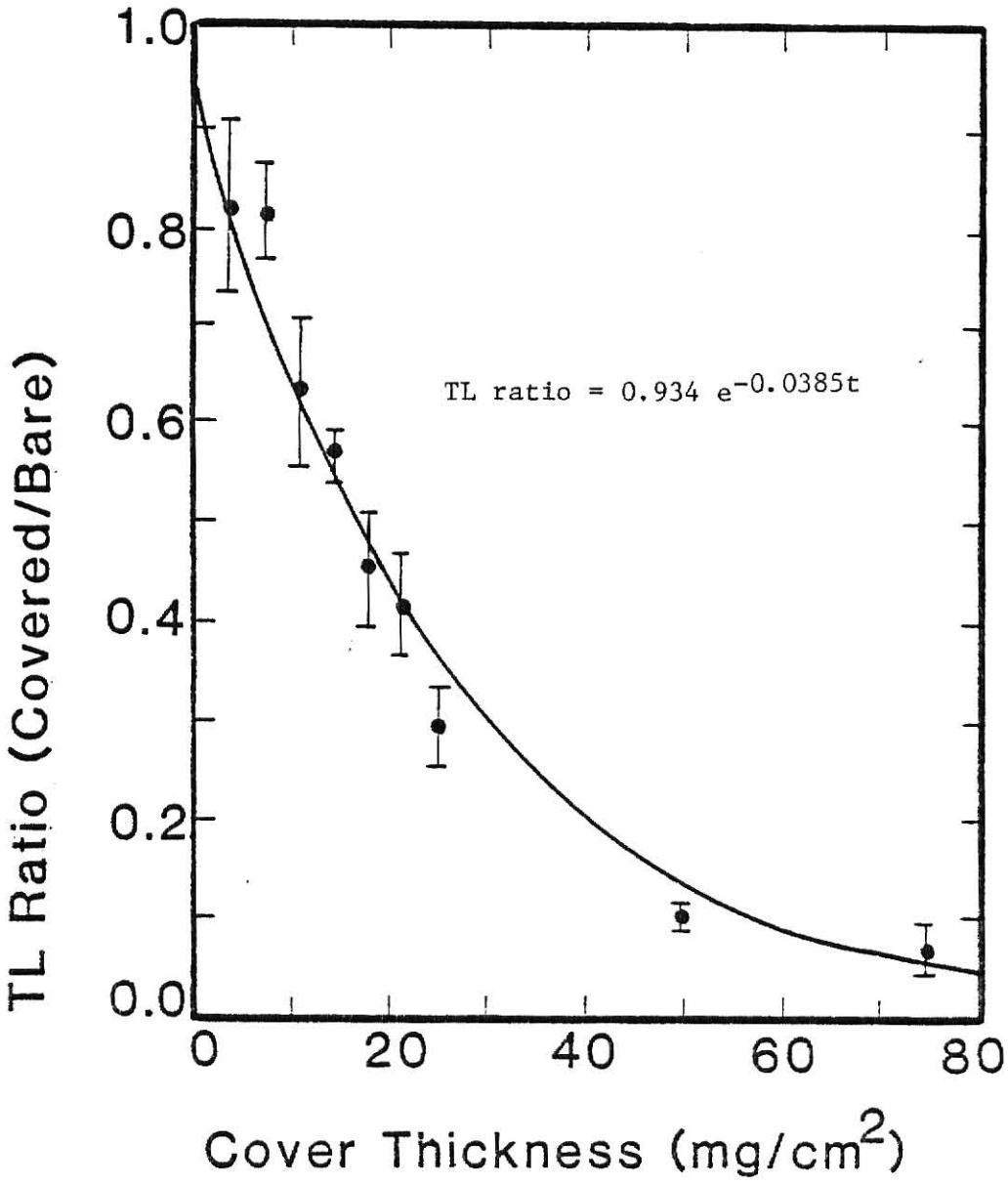

FIG. 4.16. Experimental response of thin, graphite-backed CaF_2:Mn TLDs as a function of polyester cover thickness when exposed to ^{185}W (Eo = 0.4326 MeV) beta particles. The curve shows the least squares fit.

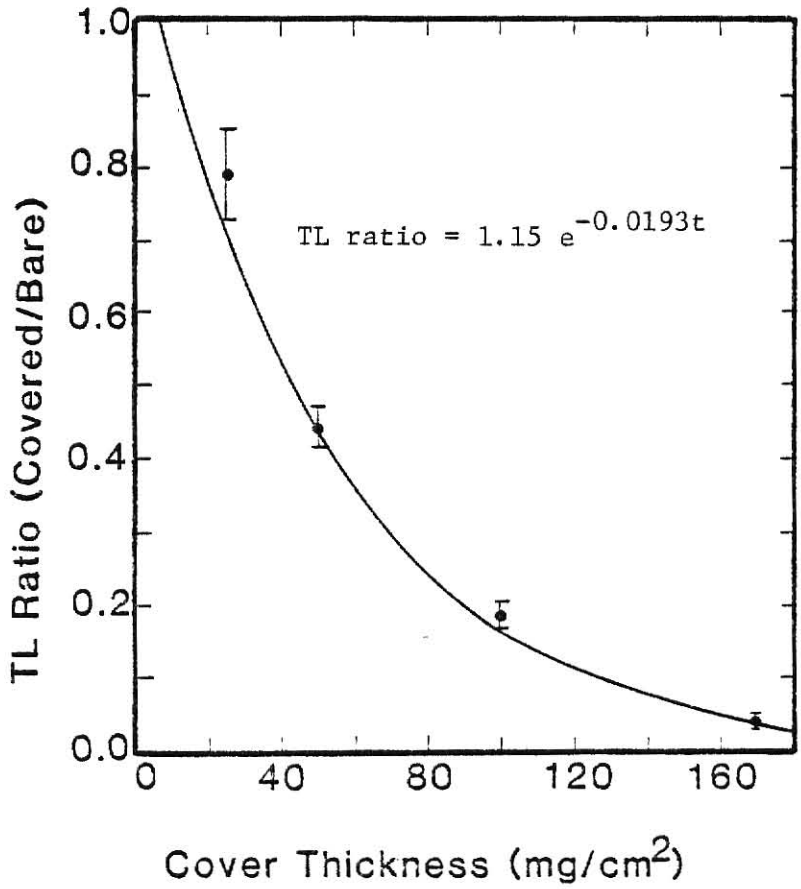

FIG. 4.17. Experimental response of thin, graphite-backed CaF_2:Mn TLDs as a function of polyester cover thickness when exposed to ^{204}Tl (Eo = 0.7635 MeV) beta particles. The curve shows the least squares fit.

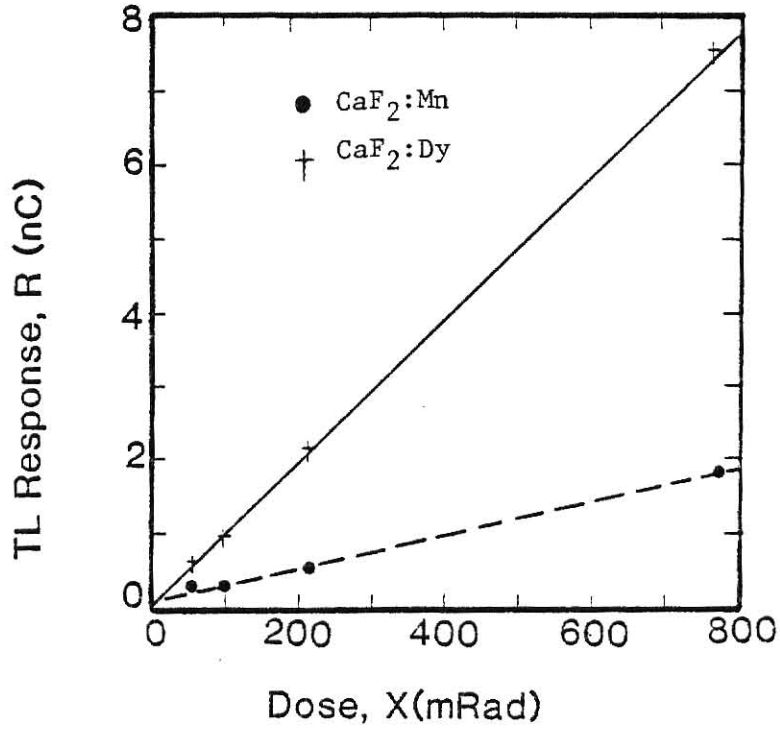

FIG. 4.18. Experimental response of thin (0.05 mm), graphite-backed CaF_2 TLDs to cobalt-60 gamma rays as evaluated on the planchet analyzer. Lines show least squares fits.

the fact that the CaF_2:Dy wafers are more sensitive than the CaF_2:Mn wafers.

Gamma-ray response data were also evaluated for the thin, graphite-backed LiF TLDs using the photon counting system. The dosimeters were irradiated at 90° and 5° to the source. These data also showed a linear dose response and an approximate 15% response change due to the 85° change in radiation incidence angle, as shown in Fig. 4.19. Thick (0.89 mm) LiF TLD ribbons with Kapton on one side were also evaluated for gamma response. These thick TLDs showed a response approximately 24 times greater than the thin TLD response. This can be explained by the factor of 18 difference in TL material and the additional thin TLD light loss due to the graphite backing. More data were obtained with thin covers of aluminum over the TLDs to investigate possible effects of Compton scattered electrons and electronic equilibrium. With thin aluminum covers, which represented a negligible barrier to gamma-rays but a large barrier to scattered electrons, it was found that the energy absorbed in the thin TLDs decreased dramatically, in a typical exponential manner. Only a slight effect was observed when exposing thick TLDs under the same conditions. These results are shown in Fig. 4.20. This indicates that a significant amount of the skin dose from an encapsulated photon source may be from scattered electrons.

High level gamma doses were also investigated using the graphite-backed thin LiF TLDs with the photon counting system. These doses were from a ^{60}Co irradiator which provided an approximate dose rate of 400 Rads/minute, with a minimum dose of approximately 17 Rad.

The data from a single dosimeter is plotted in Fig. 4.21. A linear least squares fit line is shown for the data from 217 to 817 Rads,

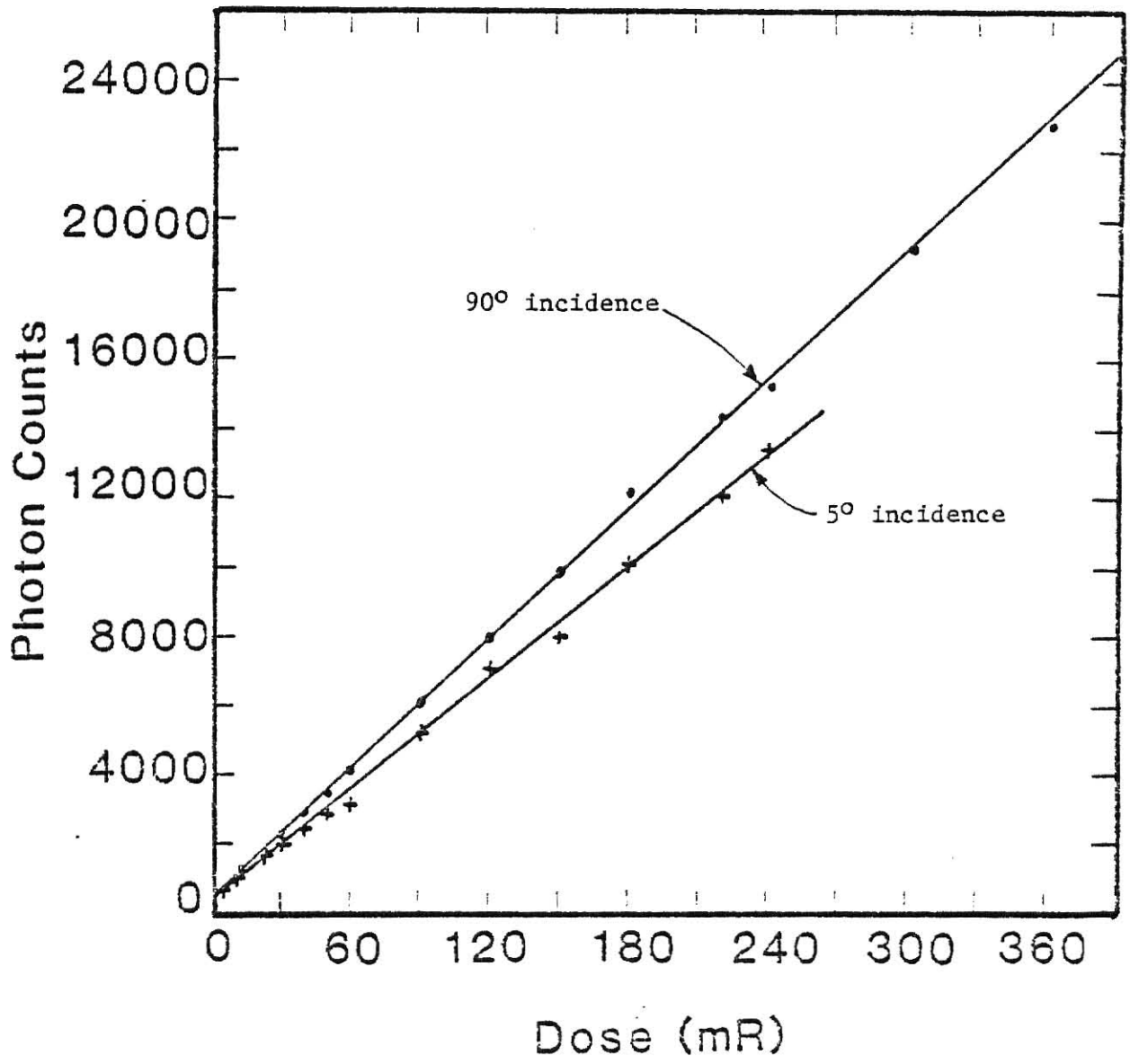

FIG. 4.19. Experimental response of thin (0.05 mm), graphite-backed LiF TLDs to cesium-137 gamma rays at two angles of incidence as evaluated with the photon counter analyzer. Lines show least squares fits.

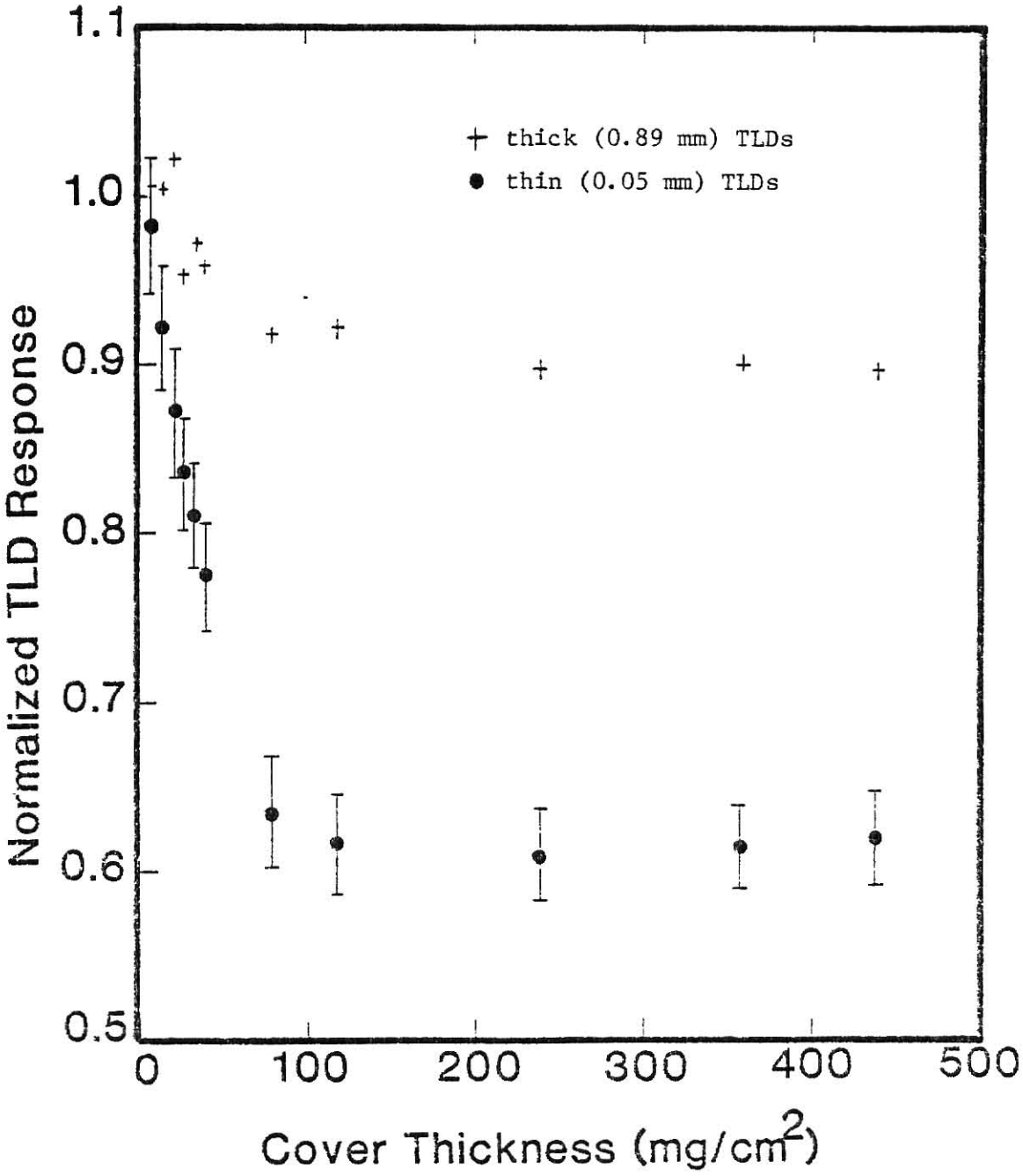

FIG. 4.20. Experimental response of thin and thick graphite-backed LiF TLDs when exposed to cesium-137 gamma rays with varying thickness aluminum covers over the TLDs.

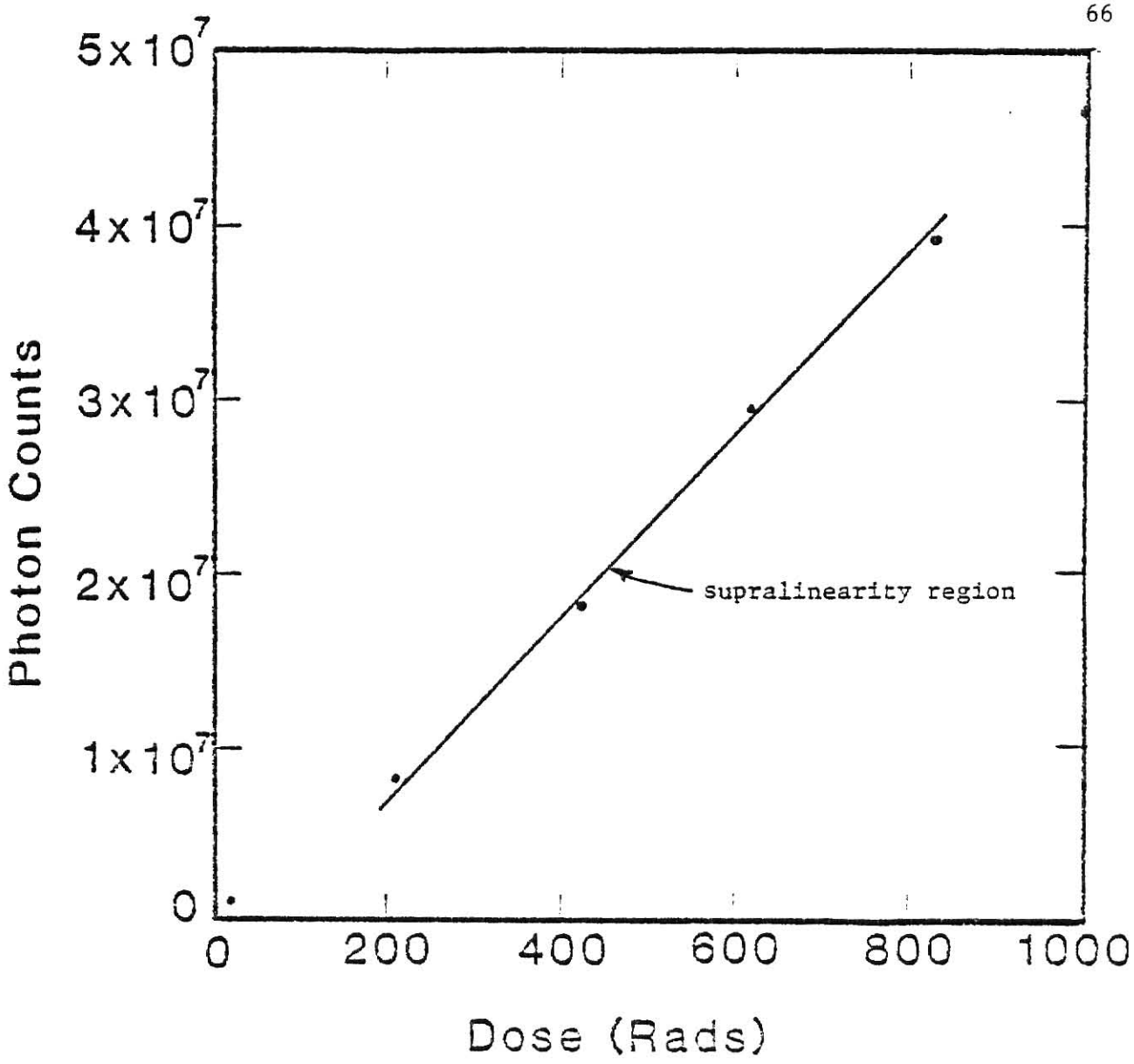

FIG. 4.21. Experimental response from a typical thin (0.05 mm), graphite-backed LiF TLD when exposed to cobalt-60 gamma rays and evaluated on the photon counter analyzer. The line shows the least squares fit to the supralinearity region.

indicating a linear dose response in this region. It should be noted that the dose conversion factor (photon counts per Rad) for this region is approximately twice the factor for doses less than one Rad, indicating that supralinearity exists in the high dose region. The 17 Rad data point is clearly not in the supralinearity region, however the exact transition region is not capable of being determined from the data shown. The 1000 Rad data point is below the value predicted by the least squares fit due to saturation occurring in the photon counting system. This saturation limit occurred with standard LiF TLD rods (1mm x 1mm x 6mm) at approximately 50 Rad, so the thin TLD layer has resulted in an approximate factor of 20 increase in the upper limit of the linear response region. This increase in linear response region upper limit should be even greater when compared to the 0.89 mm thick TLD response; up to approximately a factor of 30.

The second read data for the high gamma doses are shown in Fig. 4.22. It can be seen that for doses above approximately 100 Rads, the second read value is above its typical "no dose" value ($\sim$350). This means that the dosimeter will require 400°C annealing after receiving a dose above 100 Rads. The higher second read value should not require any correction be applied to the first read, however, since the second read value is very insignificant when compared to the first read value. For example, at 1000 Rads the first read was 4.64×10^7 counts and the second read was 3380 counts, making the second read only about 0.0073% of the first read.

Also investigated at the high level gamma doses was the response of the graphite backing layer. A graphite backing block, with a Kapton layer attached, was irradiated, post-annealed, and read. The 1000 Rad

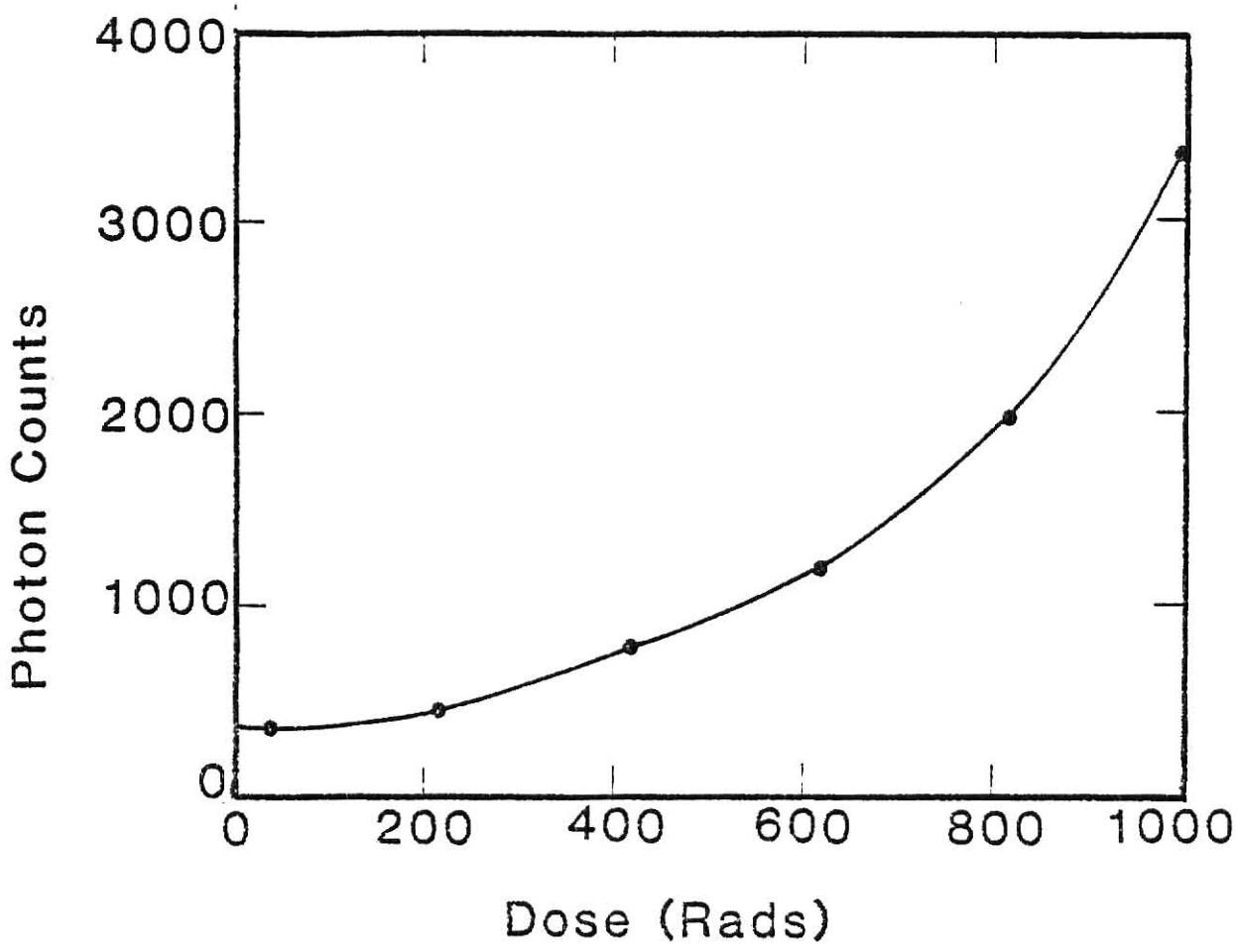

FIG. 4.22. Experimental second read data from a thin (0.05 mm), graphite-backed LiF TLD after exposure to cobalt-60 gamma rays and evaluation on the photon counter analyzer. The connecting lines are added for visual clarity.

dose gave a first read of 20,190 counts, which is still insignificant compared to the 4.64×10^7 counts from a TLD given an equivalent dose. The second read of the graphite plus Kapton gave 690 counts, thus indicating the potential of using graphite blocks as kilorad-level dosimeters. A layer of Kapton was irradiated and read but it emitted essentially no TL, confirming the potential usability of the graphite as a high-dose TLD. Additional work would need to be done to determine the response characteristics of the graphite.

Although electronic equilibrium is not achieved in the thin dosimeters with thin covers, this condition closely approximates the condition of the 5 to 10 mg/cm^2 region of skin. The thick graphite backing also provides backscattering of radiation which approximates the backscattering from underlying skin and therefore the thin graphite-backed dosimeter with a thin cover should provide a very good estimation of actual skin dose from both beta and gamma radiation.

I. Relationship of β,γ responses

The ratio of the beta response (counts/mR) to the gamma response (counts/mR) for the thin graphite-backed dosimeters is of considerable interest. This response ratio is often called the beta factor and it is energy dependent. Actually, a more meaningful ratio would be the ratio of electron response to photon response since beta sources may produce photons and gamma sources will produce free electrons. These values were evaluated with the photon counting system.

The beta factor for one typical thin layer dosimeter was 0.95 with a beta response of 55 counts/mR and a gamma response of 58 counts/mR. This beta factor is only accurate within approximately $\pm$ 0.15 due to the inaccuracies in the doses from the sources and therefore could be assumed

to be approximately equal to unity. This value was determined with no cover on the dosimeter, but if a cover is used to shield the electrons that were produced by the gamma source, the photon response is 32 counts/mR. This gives an electron/photon response of about 1.7.

Since a detailed gamma response evaluation of the thin layer dosimeters was not performed, the energy dependence of the beta factor is not known. The beta energy response of the dosimeters was found to be quite flat above 167 keV and the gamma energy response should also be quite flat, so the beta factor should be essentially energy independent above 167 keV for thin LiF dosimeters. It is believed that much of the photon response is due to backscattered Compton electrons and therefore it would decrease if the graphite backing was thinner. No experimental data are available at this time to indicate the effects of backing thickness changes.

J. Composite TL dosimeters

Temperature dependent TL emissions (glow curves) were evaluated for CaF_2:Mn wafer/LiF ribbon composite dosimeters following exposures to beta sources with maximum energies from 0.433 to 1.711 MeV. Typical glow curve results, after 10 minute 100°C post-anneals, are shown in Fig. 4.23. Interpretation of these composite glow curves follows directly from the fact that the thick LiF ribbon has its main glow peak at about 180°C and the thin CaF_2:Mn wafer's maximum emission occurs at 240°C. It can be seen that the relative peak heights vary dramatically as a function of source type. The most prominent peak stems from TL emission from the thin CaF_2:Mn wafer when the dosimeter is exposed to low energy beta particles. Conversely, the most prominent peak is associated with

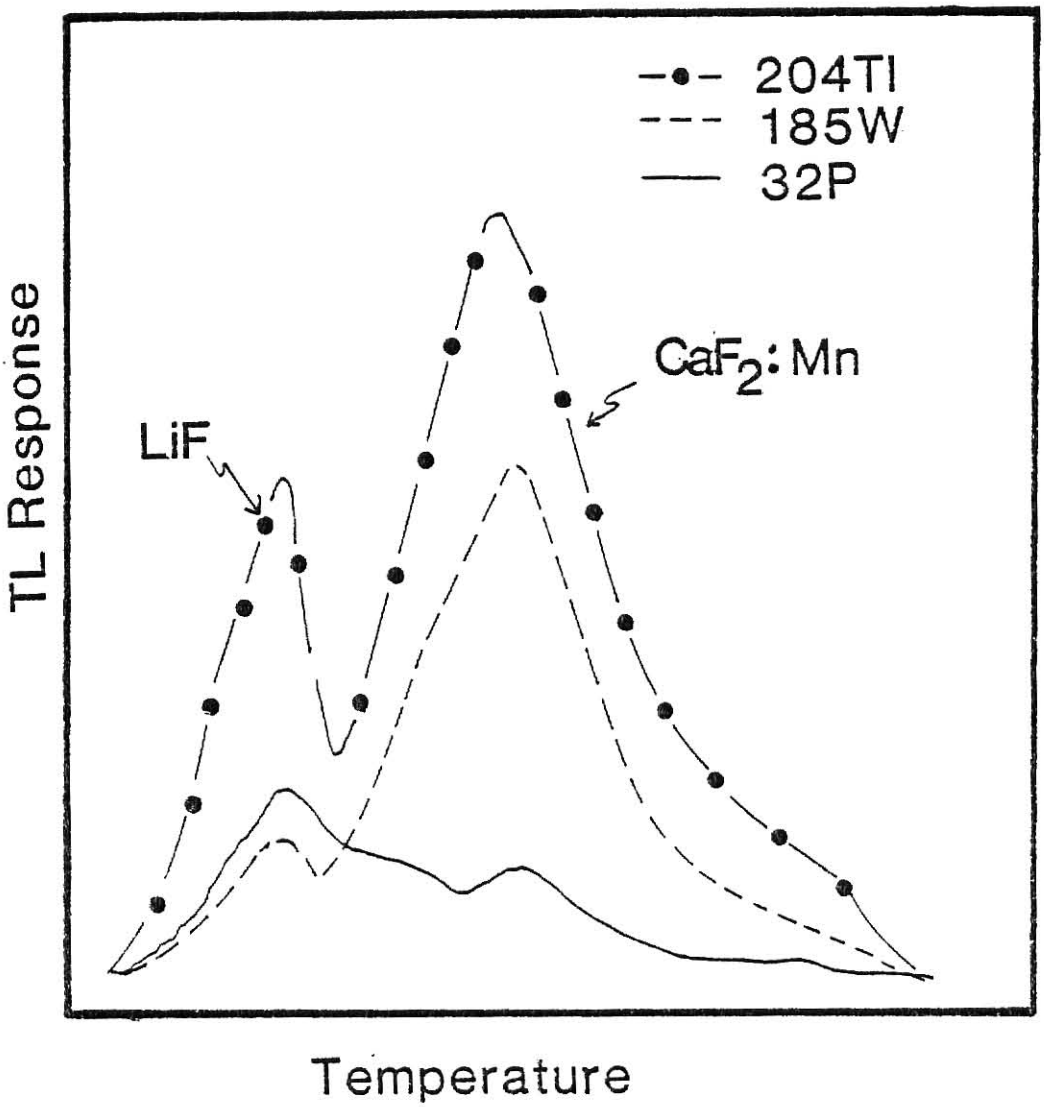

FIG. 4.23. Glow curves for composite TLDs (0.05 mm CaF_2:Mn wafer on top of a 0.89 mm LiF ribbon) exposed to three beta sources--W-185 (Eo = 0.433 MeV), Tl-204 (Eo = 0.766 MeV), and P-32 (Eo = 1.711 MeV). The absorbed doses were not the same for each source, therefore only the relative shapes are important to note.

the TL from the thick LiF ribbon for high energy beta particles. This information is similar to the thick/thin ratios discussed in Section IV.F. However, it is now derived from a single composite dosimeter.

V. CONCLUSIONS

Several types of TL radiation dosimeters were studied by performing irradiation experiments with beta and gamma sources. Results of these studies have clarified several ideas of beta dosimetry. Teflon-matrix ultrathin TLDs were difficult to handle and had a large variance. Popular commercial TLDs with a thickness of 0.89 mm (0.035-in.) proved to exhibit an energy-dependent response for beta particles with endpoint energies below 2.3 MeV regardless of the type of TLD material. Conversely, thin composite TLDs, fabricated from a variety of TL materials, showed some outstanding properties as discussed below.

Thin TLDs of thickness 0.05 mm (0.002-in.) coupled to either a thick graphite or TL material backing had an energy-independent response for beta particles above approximately 200 keV, a linear dose response, precision within approximately 10%, and a usable range from 3 mRad to 800 Rad which is more than adequate for personnel dosimetry. These thin TL dosimeters appear well suited for the measurement of skin dose since, in addition to their good response characteristics, they are small, rugged and capable of withstanding annealing at 400°C. Prolonged periods (more than 20 hours) of annealing at 400°C should, however, be avoided because this could lead to fracturing of the thin TL wafer and peeling of the bonding material. The composite dosimeters are also compatible with commercial Harshaw analyzers since their size is approximately the same as a standard Harshaw TL ribbon.

It was also shown that the covering material had a significant effect on the response of the TLDs, depending upon the beta energy, such that the endpoint energy could be estimated through analysis of the

attenuation caused by several thicknesses of covers. In addition the range of the beta emitter could be estimated by simultaneously exposing thick and thin TLDs, and these two thicknesses could be incorporated into a single composite dosimeter. An additional result for the TLD/TLD composite dosimeter was that, with additional study, beta and gamma (or surface and deep dose) measurements appear possible through analysis of the resultant glow curve from a single dosimeter.

VI. SUGGESTIONS FOR FURTHER STUDY

Continued research should be performed to optimize and characterize the thin layer dosimeters.

The photon counter system should be used to further investigate the electron fields from gamma sources. Varying energy sources, source-to-dosimeter distances, and scattering conditions should be investigated. This investigation should lead to possible methods for separating the electron (beta) field from a mixed beta-gamma field.

A calculation of the theoretical TLD response for specific beta emitters should be performed with the simple exponential formulas by integrating over the theoretical beta energy spectra.[20] This could also be extended into theoretical predictions of TLD angular response for specific beta emitters.

The effect of changing the graphite backing thickness upon the beta and gamma responses of the thin dosimeter should also be investigated. This could lead to a larger beta factor with little loss in dosimeter ruggedness.

A dosimeter badge design should be attempted, with the goal to make a dosimeter system which would be commercially viable and compatible with current TLD reader systems. The effect of the badge upon the dosimeter angular response, especially the beta angular response, should be investigated and compared to the bare dosimeter angular response. A comparison of this new dosimeter system with current dosimeter systems should also be performed.

Additional studies should be performed on CaF_2 thin layer dosimeters and the composite TL dosimeters to characterize fully their responses.

These studies will require altering the photon counter system to allow evaluation of CaF_2 materials.

The effects of sanding the solid TL materials should also be investigated. The reduced non-radiation induced TL effect from sanding should be compared to similar effects observed from washing TLDs, and the long-term effects of sanding should also be investigated. Also, it seems that a highly-matched set of dosimeters could be constructed with the sanding used to match sensitivities and so this warrants further research.

Finally, further work on optimizing reader systems for all TL materials should be performed.

VII. ACKNOWLEDGEMENTS

I would like to express my sincere appreciation to Dr. G. G. Simons for his assistance and guidance during this research project and during the preparation of this thesis. I am also grateful to Dr. G. R. Clark and B. K. Harms for their technical assistance and many helpful suggestions.

I also wish to express my gratitude to the Battelle Pacific Northwest Laboratories for sponsoring this research and providing the necessary financial support.

VIII. REFERENCES

1. International Commission on Radiological Protection, "Recommendations of the International Commission on Radiological Protection," ICRP Publication 26, (Pergamon Press, Oxford, 1977).

2. Division of Rules and Records - United States Nuclear Regulatory Commission, "Standards for Protection Against Radiation," Title 10, Chapter 1, Part 20, Code of Federal Regulations, (U.S. Government Printing Office, Washington, D.C., 1978).

3. M.S.H. Di Fiore, Atlas of Human Histology, 4th edition, Lea & Febigen, Philadelphia (1974), pp. 100-101.

4. W.S. Snyder, Chairman, "Report of the Task Group on Reference Man," ICRP Publication 23, (Pergamon Press, Oxford, 1975).

5. Commission of the European Communities, "Technical Recommendations for Monitoring the Exposure of Individuals to External Radiation," EUR 5358, Luxembourg (1975).

6. T.F. Gesell, D.E. Jones, V.P. Gupta, F.L. Kalbeitzer, J.P. Cusimano, "A Personnel β-Dosimetry Method for Reducing Energy Dependence," IDO-12090, March 1979.

7. American National Standards Institute, Criteria for Testing Personnel Dosimetry Performance, ANSI N13.11, (1982).

8. T.D. Marshall, R.J. Pattison, A. Twyman, "The Performance of the NRPB Thermoluminescent Dosimeter," Nucl. Instr. and Meth., 175, 147 (1980).

9. K.B. Shaw, B.F. Wall, "Performance Tests on the NRPB Thermoluminescent Dosimeter," NRPB-R65, (Her Majesty's Stationery Office, England, 1977).

10. O. Yamamoto, Y. Yasuno, S. Minamide, S. Hasegawa, H. Tsutsui, M. Takenaga, T. Yamashita, "Construction of a Composite Thin-Element TLD Using an Optical-Heating Method," Health Physics, 43, 383 (1982).

11. L. Katz and A. Penfold, "Range-Energy Relations for Electrons and the Determination of Beta-Ray End-Point Energies by Absorption," Rev. Mod. Phys., 24, 28 (1952).

12. M.J. Berger, "Distribution of Absorbed Dose Around Point Sources of Electrons and Beta Particles in Water and other Media," nm/mird Phamphlet No. 7, J. Nucl. Med., 12, Supplement No. 5 (1971).

13. K.Z. Morgan and J.E. Turner, Principles of Radiation Protection, Robert E. Krieger Publishing Co., Huntington, New York (1973), pp. 253-265.

14. M.J. Berger and S.M. Seltzer, "Tables of Energy Losses and Ranges of Electrons and Positrons," NASA SP-3012, Washington, D.C. (1964).

15. S.G. Gorbics and F.H. Attix, "LiF and CaF_2:Mn Thermoluminescence Dosimeters in Tandem," Int. J. Appl. Radiat. Isotopes, 19, 81 (1968).

16. A.B. Chilton, J.K. Shultis, R.E. Faw, Principles of Radiation Shielding, Prentice-Hall, Englewood Cliffs, N.J. (1984), pp. 109-111.

17. B.K. Harms, "The Optimization and Use of a Photon Counting System for Thermoluminescent Dosimetry," Master's Thesis, Kansas State University (1982).

18. ORIEL Corporation Catalog of Optical Systems and Components, Oriel Corporation, Stamford, Conn. (1979), pp. H10-H11.

19. "Finger and Hand Dosimetry", T17820, Teledyne Isotopes, Westwood, N.J.

20. R.B. Stuewe, "Evaluation of Plastic Scintillator and High-Purity Germanium Detectors for use in Beta Spectroscopy," Master's Thesis, Kansas State University (1982).

Appendix A: Typical Glow Curves

All thermoluminescent materials have characteristic glow curves - light emission as a function of temperature. Although these curves are not needed for the evaluation of radiation doses from TLDs, they do provide valuable information, including the temperature of peak emission rate and characteristics of any residual TL that is emitted during the second reading of the TLD.

It should be kept in mind that glow curves will change with changes in the TLD heating rates, generally becoming more peaked and featureless.

Figures A.1 and A.2 are from the commercial planchet reader and the remaining figures are from the photon counting system. The figures show glow curves from CaF_2:Mn, CaF_2:Dy, LiF, and graphite. Only the high dose glow curves show the second read curves since low dose second read glow curves provide no information. Even the high dose second read glow curves are quite insignificant when compared to the high dose first read glow curves, however it can be seen that high doses cause a second peak to be seen at a higher temperature than the main glow peak.

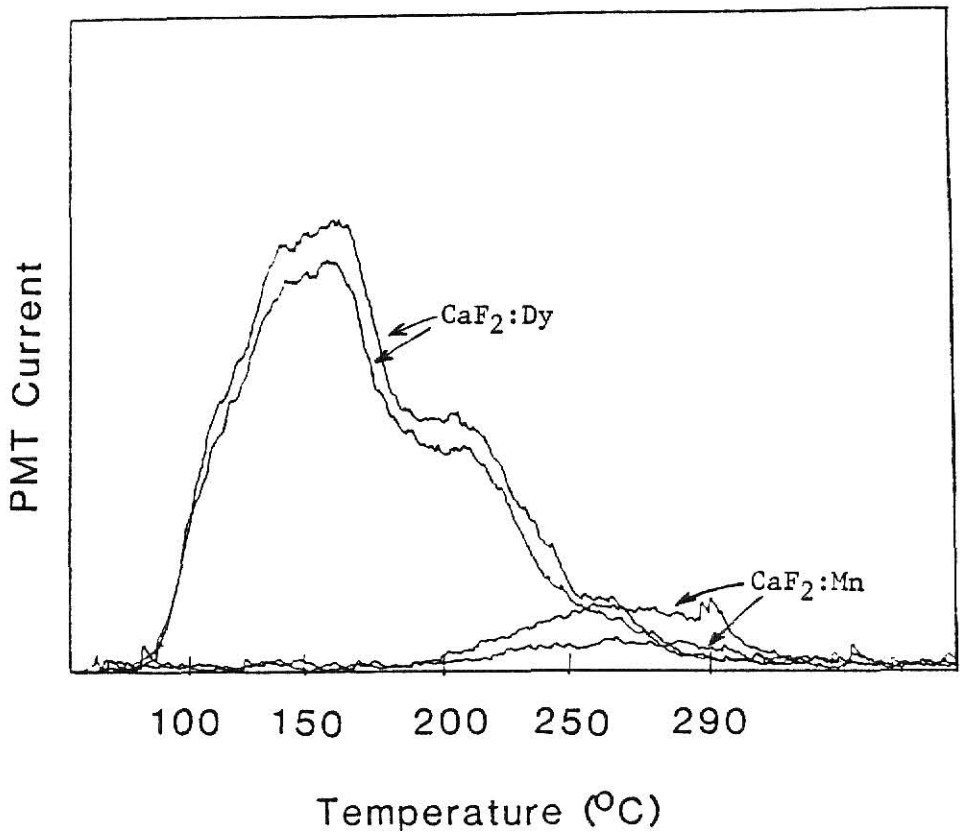

FIG. A.1. Typical glow curves from thin (0.05 mm), graphite-backed TLDs after 23 mRad doses from sulphur-35 beta particles, as evaluated on the commercial planchet reader.

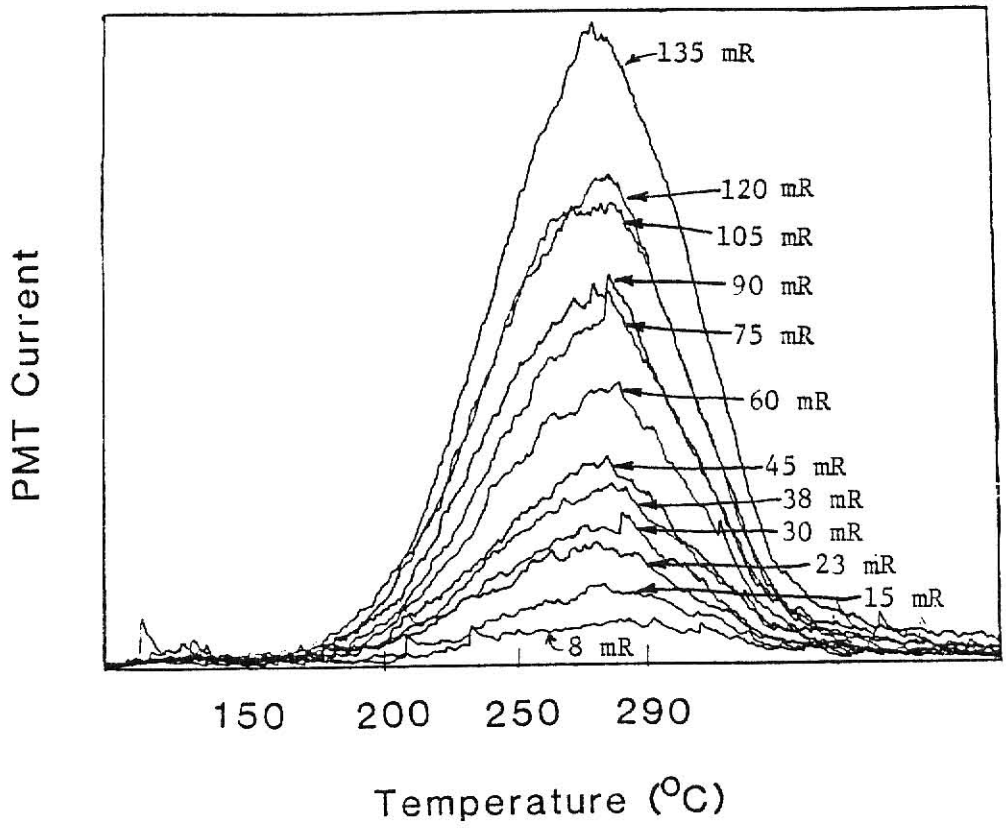

FIG. A.2. Typical glow curves from thin (0.05 mm), graphite-backed CaF_2:Mn TLDs after doses from sulphur-35 beta particles, as evaluated on the commercial planchet reader.

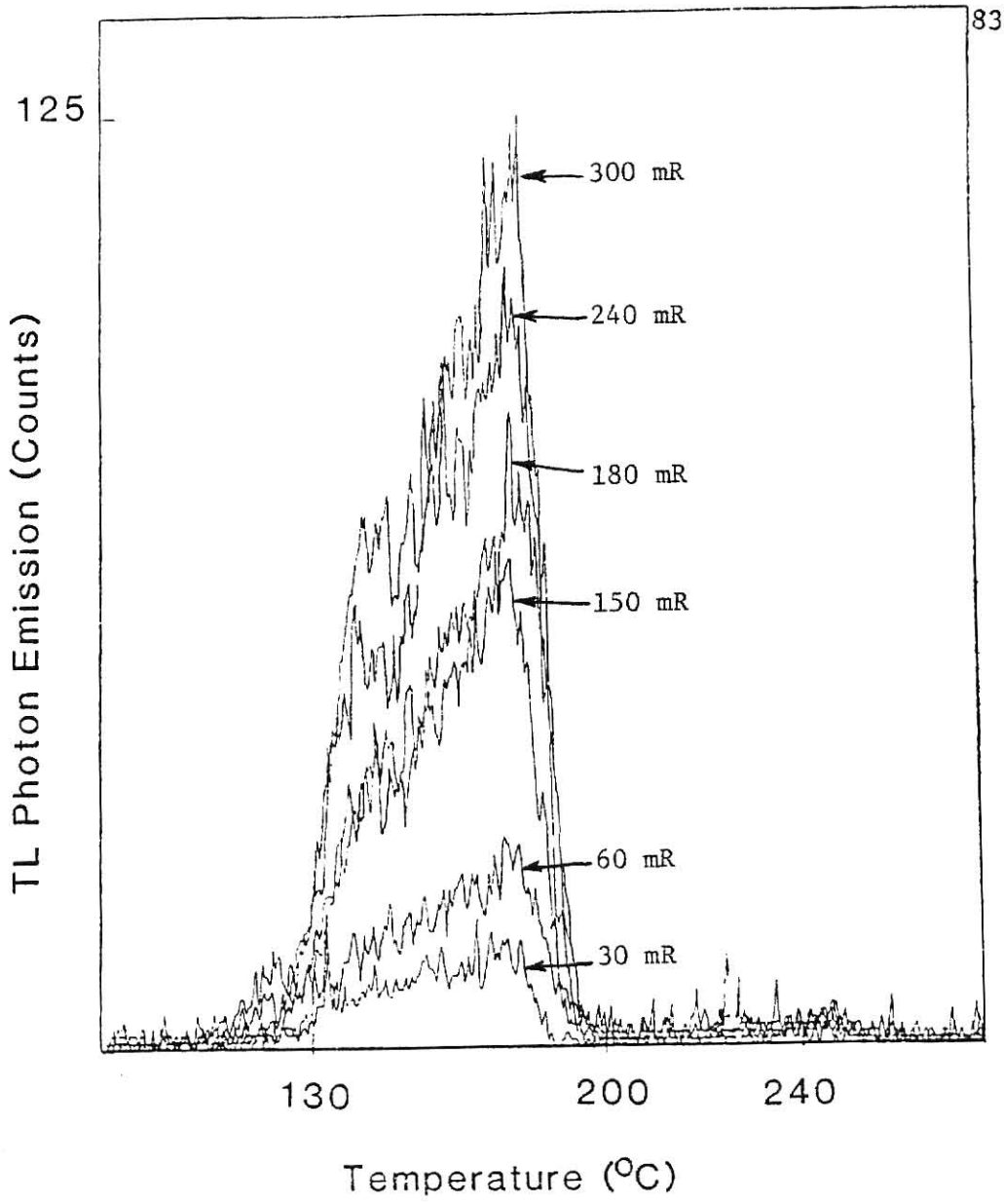

FIG. A.3. Typical glow curves from thin (0.05 mm), graphite-backed LiF TLDs after doses from ^{90}Y beta particles, as evaluated on the photon counter system.

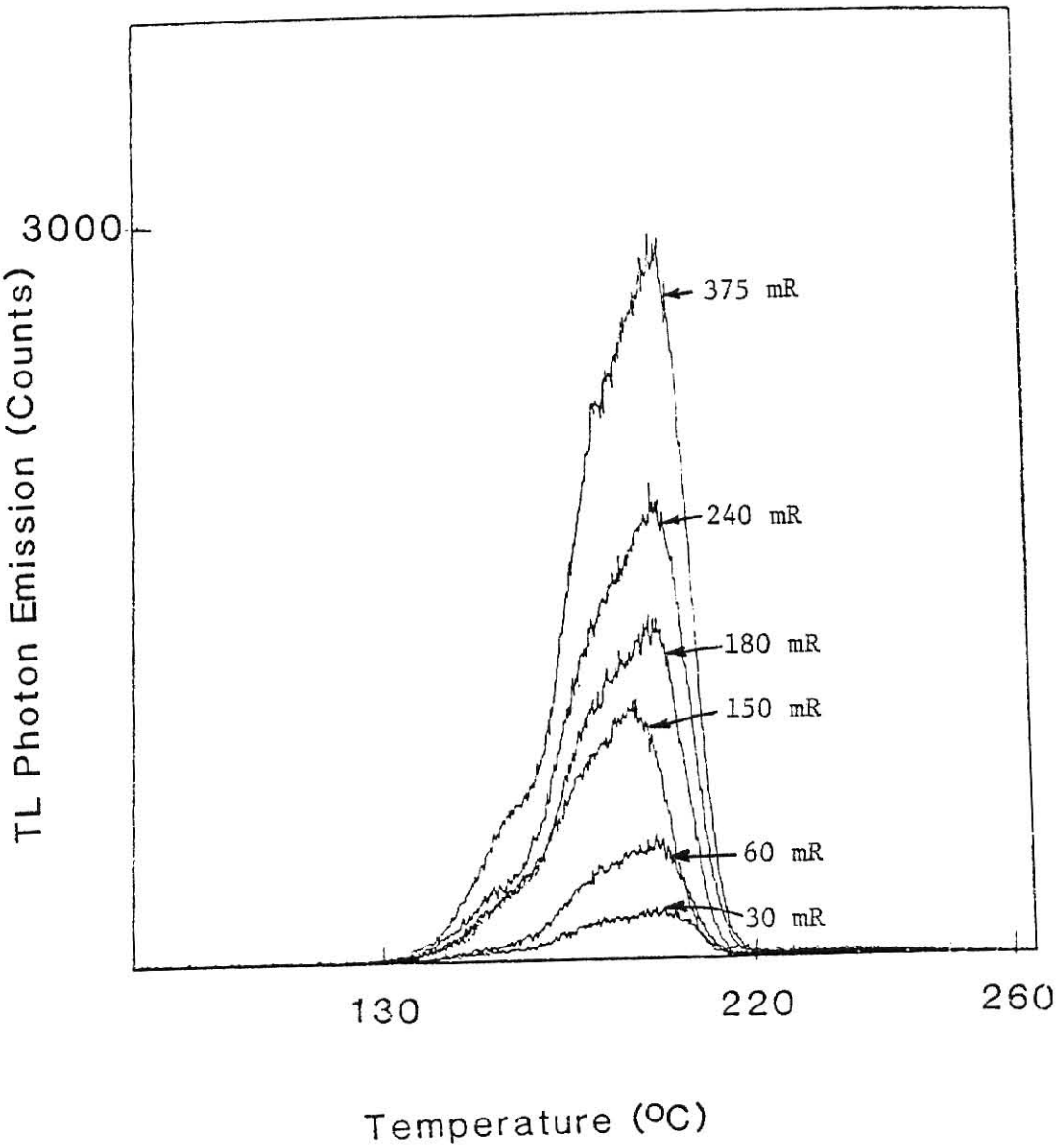

FIG. A.4. Typical glow curves from thick (0.89 mm), graphite-backed LiF TLDs after doses from ^{90}Y beta particles, as evaluated on the photon counter system.

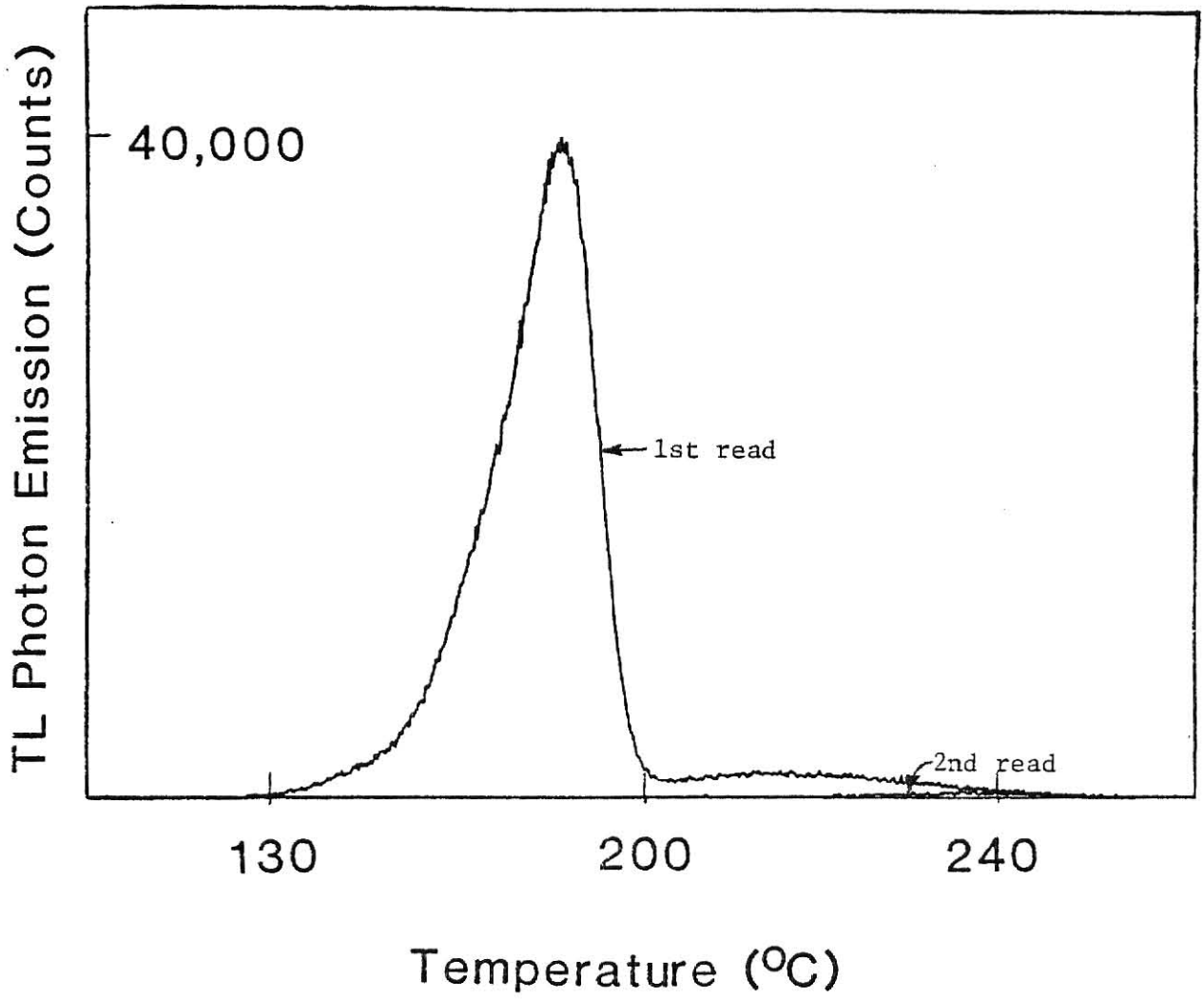

FIG. A.5. Typical glow curves from a thin (0.05 mm), graphite-backed LiF TLD after a 1000 Rad dose from ^{60}Co gamma rays, as evaluated on the photon counter system.

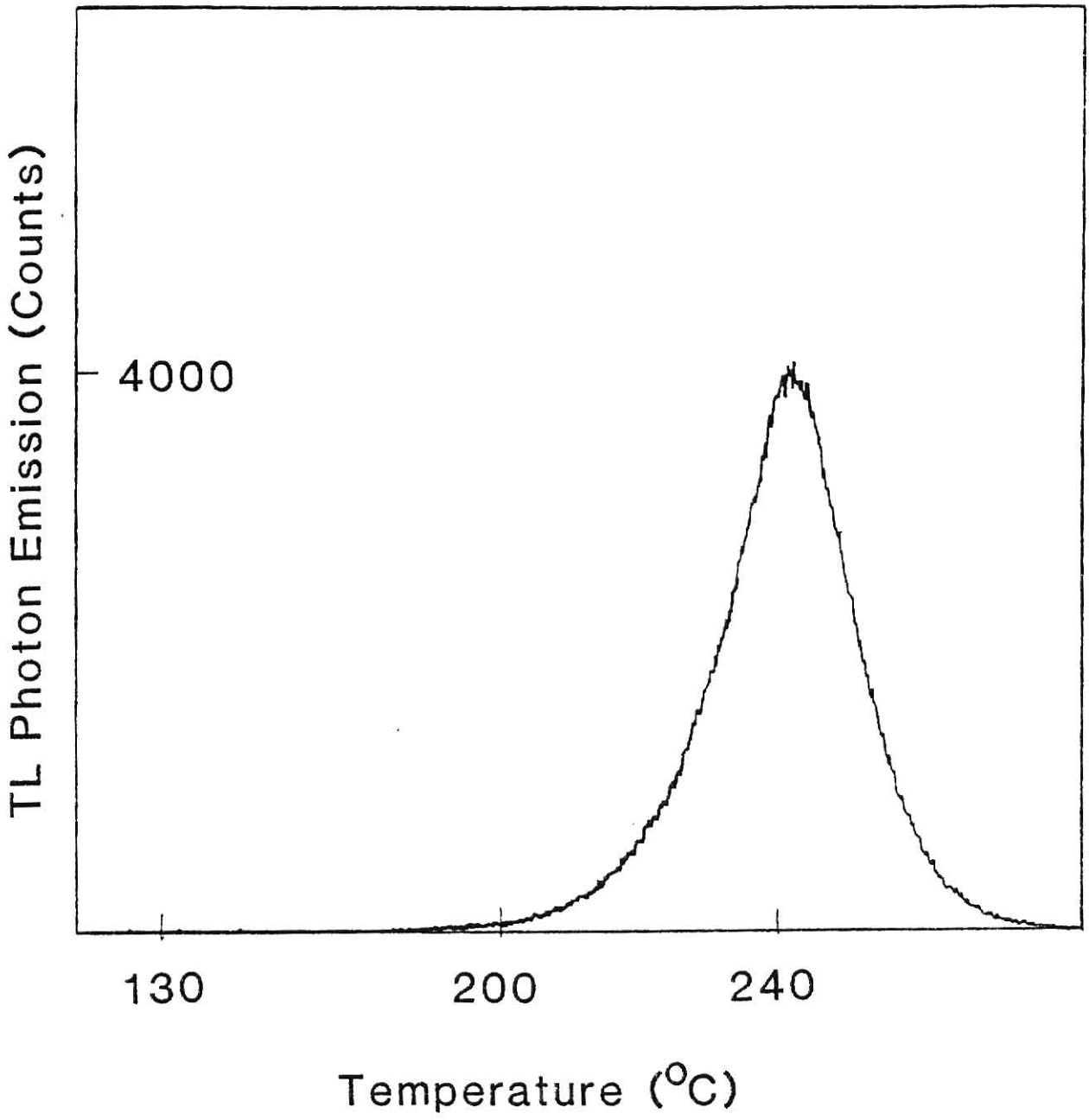

FIG. A.6. A typical second read glow curve from a thin (0.05 mm), graphite-backed LiF TLD after a 1000 Rad dose of ^{60}Co gamma rays, as evaluated on the photon counter system. This is a magnified look at the second read of Fig. A.5.

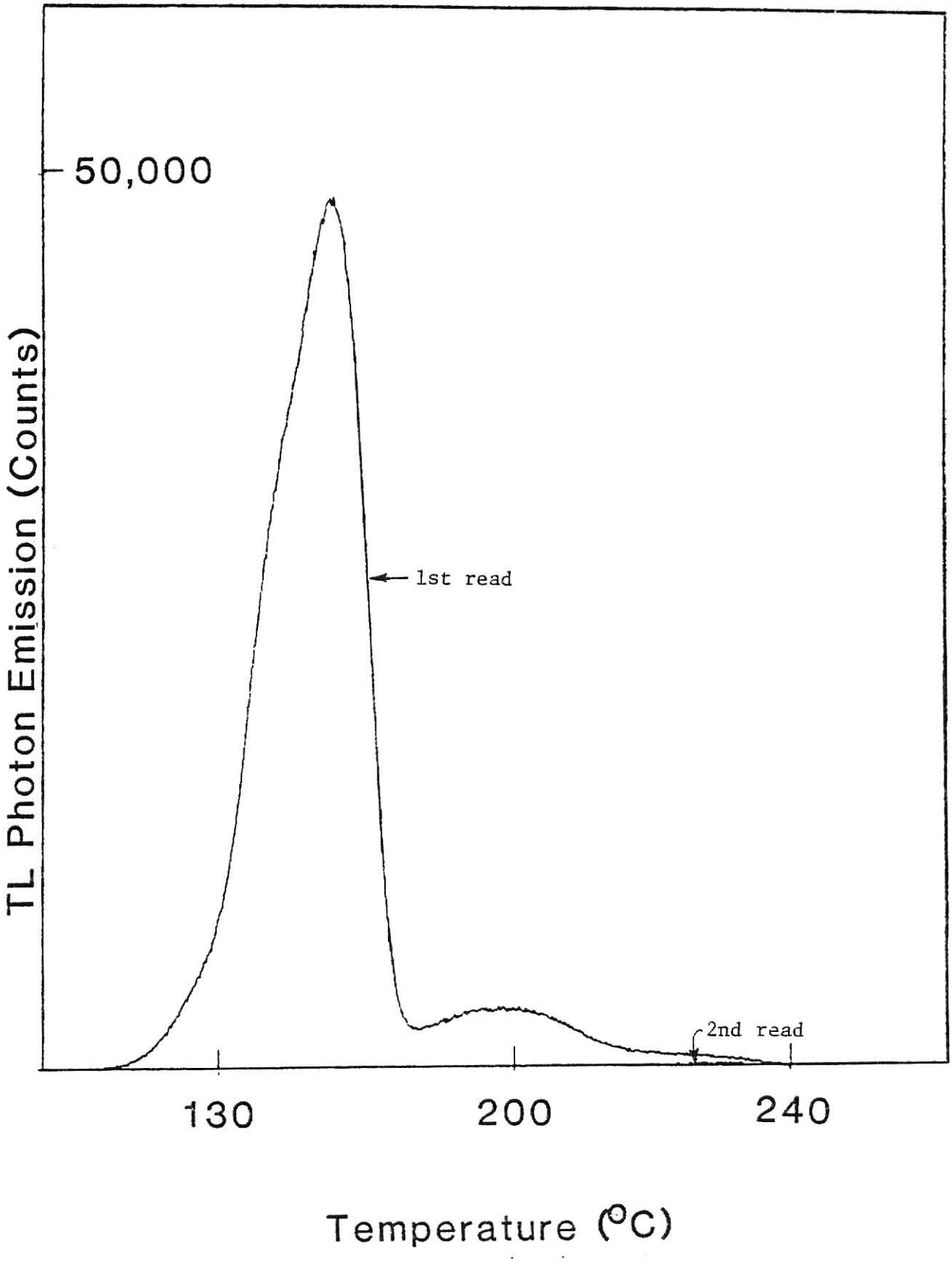

FIG. A.7. Typical glow curves from a thin (0.05 mm), LiF TLD (no backing) after a 1000 Rad dose from ^{60}Co gamma rays, as evaluated on the photon counter system.

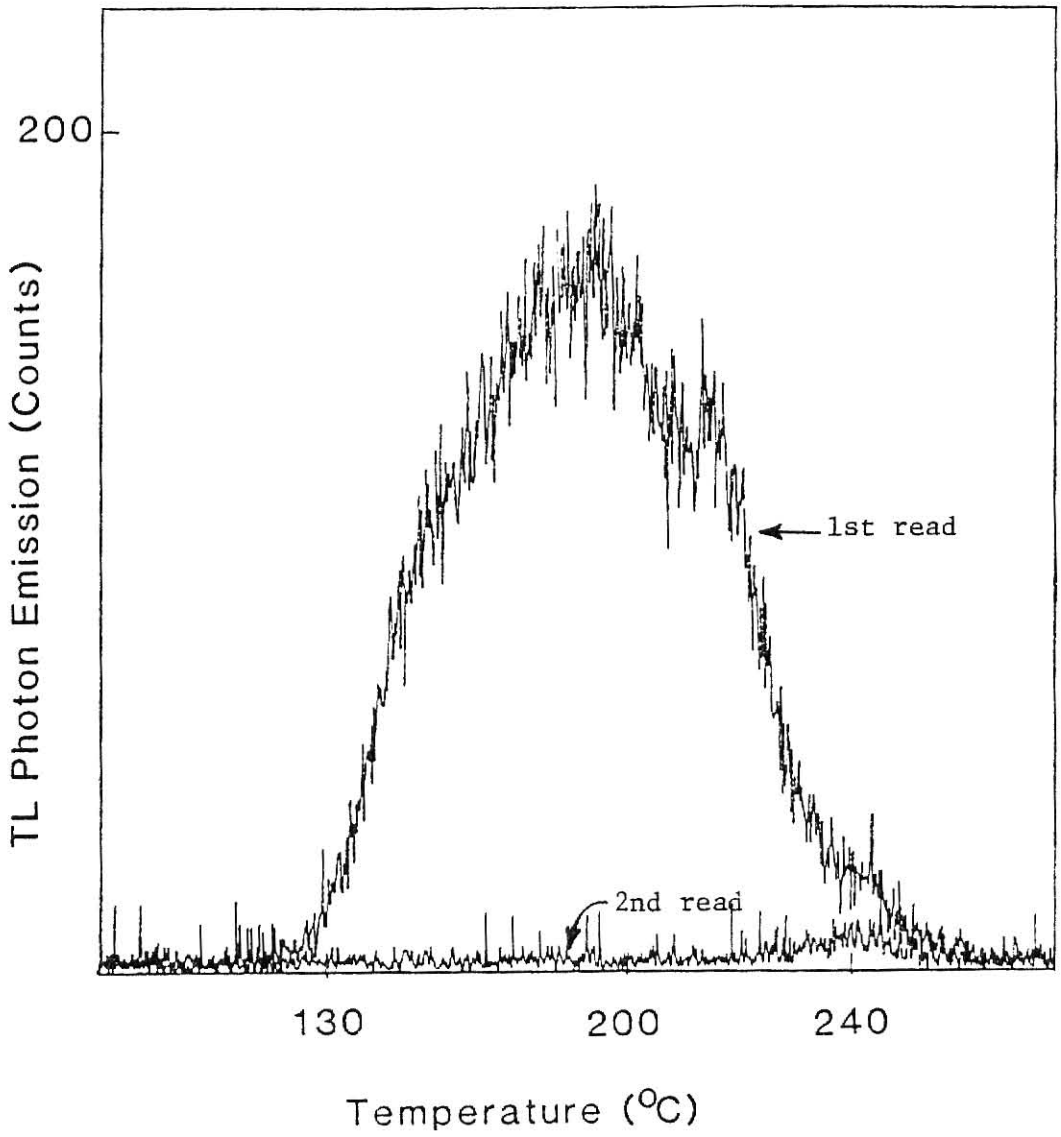

FIG. A.8. Typical glow curves from a thick (0.89 mm), graphite block after a 1000 Rad dose from ^{60}Co gamma rays, as evaluated on the photon counter system.

Appendix B. Kapton Film Characteristics

Kapton XP (registered trademark) is a recently developed product of E.I. duPont de Nemours and Co., Inc. It is a thin polyimide film based on pyromellitic dianhydride and 4,4, diaminodiphenyl ether. The molecular formula of Kapton is $(C_{22}\ H_{10}\ O_5\ N_2)_n$. This film was developed primarily to be used as an electrical insulator in high temperature environments such as for motor and generator windings. The Kapton XP film has a coating of Teflon PFA (a copolymer of tetrafluoroethylene with a fully fluorinated alkoxy side chain) on one or both sides to act as a high temperature adhesive and allow heat sealing of the Kapton to many materials.(a)

The Kapton XP used in this project to make the TLD composites was 0.025 mm thick with a 0.013 mm layer of Teflon PFA adhesive on each side. Since the Kapton XP is a recently developed product, limited information on its characteristics was available. Testing by DuPont showed that the weakest point in a Kapton laminate was the bond of the Teflon PFA to the polyimide film, which had a value of approximately 1.1 lb./in. at 200°C. No information is available for values above 200°C. See Fig. B.1 for a plot of this bond testing data.

The polyimide film (with no adhesive) was tested for elongation after aging at 400°C for two hours, with a maximum allowed elongation of 10%. The film has a typical tensile strength of 20,000 psi at room temperature and thickness tolerances of 0.020 mm and 0.030 mm for film of 0.025 mm nominal thickness.

Slight amounts of moisture may be absorbed by the polyimide film and DuPont recommends drying the film prior to using it in a laminate. This

would eliminate the potential for blistering in the laminate upon rapid heating. Experience in making the TLD composites showed that this was not a problem and therefore this pre-drying of the Kapton was not performed.

Since the Kapton XP film was used to make composite dosimeters which would potentially be exposed to a 400°C environment for extended period of time, its stability at 400°C was of great interest. No quantitative data were gathered, however experiments showed that the Kapton XP could withstand the 400°C temperature for approximately 10 hours with no observable changes. Beyond 10 hours at 400°C, the Kapton XP began to discolor to the point of being a dark bronze color after approximately 20 hours. Continued exposure to 400°C beyond this caused gradual peeling and buckling of the film until, after approximately 50 hours, the film was reduced to a small piece of "ash". During the buckling and peeling of the Kapton XP film, the thin TLD layer would usually be broken. The gradual darkening of the film did not produce any observable change in the radiation dose response of the thin TLD layer. It is believed that the black graphite backing of the dosimeter made its response insensitive to the color of the Kapton film.

Reference

[a] "Kapton Type XP New Product Information", E42732, Industrial Films Division, E.I. duPont de Nemours & Co., Inc., Wilmington Delaware.

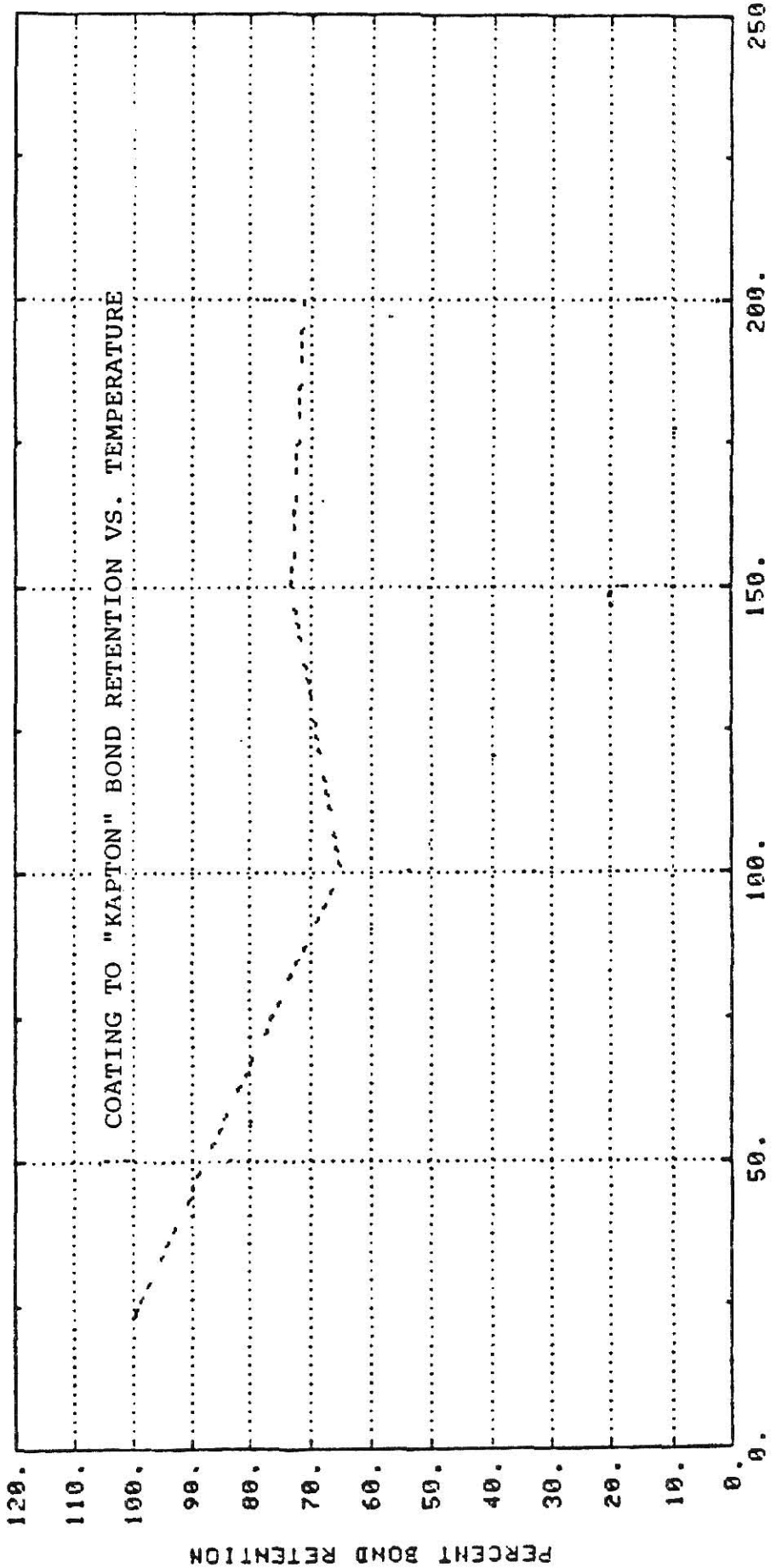

FIG. B.1. The Kapton polyimide film - to - PFA adhesive coating bond retention as a function of temperature.

Appendix C. Confidence Interval Analysis

The relationship between two parameters may be investigated through regression analysis to determine if a significant relationship exists. In the case of radiation dose and dosimeter response, a linear relationship should exist and may be written as

$$y_i' = a + bx_i,$$

where y_i' = the predicted dosimeter response for the ith point,

a = the predicted dosimeter response for no dose,

b = the slope of the line relating dose to response,

x_i = the radiation dose for the ith point.

From a set of n dose and response data (x_i and y_i), the a and b values can be determined using least squares analysis where

$$b = \frac{n \sum_i x_i y_i - \sum_i x_i \sum y_i}{n \sum_i x_i^2 - \left(\sum_i x_i\right)^2} \quad , \tag{C.1}$$

and

$$a = \frac{\sum_i y_i - b \sum_i x_i}{n} \quad . \tag{C.2}$$

If the dosimeter response to a given radiation dose can be characterized by a normal distribution, then confidence intervals can be determined for the response of the dosimeter. Given the following definitions,

$$\overline{X} = \frac{\sum_i x_i}{n} \quad , \tag{C.3}$$

$$SS_x = \Sigma(x_i - \overline{X})^2 \quad , \tag{C.4}$$

$$SS_{y/x} = \Sigma(y_i - y_i')^2 \quad , \tag{C.5}$$

$$\text{and} \qquad S_e^2 = \frac{SS_{y/x}}{n-2} \quad , \tag{C.6}$$

confidence intervals may be determined at the (1-α) 100% confidence level using the Student's t distribution with n-2 degrees of freedom as follows:

1) Confidence interval (C.I.) on zero dose response (a):

$$(1-\alpha)\ 100\%\ \text{C.I.} = a \pm t_{\frac{\alpha}{2},n-2} \sqrt{S_e^2 \left(\frac{SS_x + n\bar{X}^2}{n\ SS_x}\right)} \quad , \tag{C.7}$$

2) Confidence interval on slope (b) of line relating dose to dosimeter response:

$$(1-\alpha)\ 100\%\ \text{C.I.} = b \pm t_{\frac{\alpha}{2},n-2} \sqrt{S_e^2/SS_x} \quad , \tag{C.8}$$

3) Confidence interval on the response (y) of a single dosimeter at dose X_o:

$$(1-\alpha)\ 100\%\ \text{C.I.} = a + bX_o \pm t_{\frac{\alpha}{2},n-2} \sqrt{\left(1 + \frac{1}{n} + \frac{(X_o-\bar{X})^2}{SS_x}\right) S_e^2} \quad . \tag{C.9}$$

The above equations were used to calculate confidence intervals of various dosimeter responses. It should be noted that the confidence intervals are sensitive to the number of data included in the analysis such that a small number of data will result in large confidence intervals. This effect comes both from direct use of n in the equations and from the Students t value which increases as n decreases.

Appendix D: Beta Dose Rate Calculations Using the Loevinger Empirical Formula

Calculation of the beta dose rate as a function of source-to-dosimeter distance can be accomplished by applying the Loevinger empirical formula.[c] Several limitations must be considered before applying this technique. Basically, the model is valid for a point beta source located in a homogeneous infinite absorbing medium of low atomic number materials. The formula is, therefore, suitable for characterizating beta dose rates in air or tissue media provided the range of the most energetic beta particle does not exceed the dimensions of the media. For a beta dosimetry project, such as the one under investigation, the absolute dose rate in air can be estimated at the dosimeter position as long as the source approximates a point emitter of beta particles, the source encapsulation is ignored, the source strength is known, and the air region is large.

The beta particle dose rate J(x), in Grays per disintegration, at a distance x, in g/cm^2, for an absorbing medium is given by the Loevinger formula:

$$J(x) = \frac{k}{(\nu x)^2}\{c[1-(\nu x/c)e^{1-(\nu x/c)}] + \nu x e^{1-\nu x}\} \text{ for } x \leq \frac{c}{\nu} \qquad (D.1)$$

and

$$J(x) = \frac{k}{(\nu x)^2}(\nu x e^{1-\nu x}) \qquad \text{for } x \geq \frac{c}{\nu} \ ,$$

where

$\nu \equiv$ the apparent absorption coefficient (cm^2/g),
$c \equiv$ a parameter which depends upon the maximum beta-particle energy E_o,

and $k \equiv$ a normalization parameter dependent upon the medium and beta energy.

The k parameter is equal to

$$k = 1.28 \times 10^{-11} \rho^2 \nu^3 \bar{E}_\beta \alpha \ (\text{Gy/dis}) \quad , \tag{D.2}$$

where

$$\alpha = [3c^2 - (c^2 - 1)e]^{-1} \tag{D.3}$$

ρ = the density of the medium (g/cm^3),

and e = the base of the natural logarithm.

If the absorbing medium is air, then

$$c = 3.11e^{-0.55E_o} \tag{D.4}$$

and

$$\nu = \frac{16.0}{(E_o - 0.036)^{1.4}} \ (2 - \bar{E}/\bar{E}^*_\beta) \ , \tag{D.5}$$

where

$\bar{E}$ = average beta-particle energy,

and $\bar{E}^*_\beta$ = hypothetical average beta energy per disintegration for a hypothetical allowed spectrum having the maximum energy E_o, i.e., for allowed transitions, $\bar{E} = \bar{E}^*_\beta$.

Loevinger's empirical formula was used to calculate beta dose rates in air for a 10 mCi $^{90}Sr/^{90}Y$ source. The distance parameter x included only the air thickness. Backscatter of the primary beta particles from structural material located directly behind the source material and attenuation in the window were not accounted for in these calculations. Dose rates for each radionuclide were calculated separately and then summed to obtain the net source dose rate.

Since both ^{90}Sr and ^{90}Y decay by 1st forbidden transitions, the $\bar{E}/\bar{E}^*_\beta$ ratios were unequal to unity. To determine appropriate ratios, $\bar{E}^*_\beta$ was first calculated for each radionuclide from $\bar{E}$ and $\bar{E}/\bar{E}^*_\beta$ values given in ref (c). New ratios, based upon mean beta energies of 0.1963 and

0.9367 MeV, for ^{90}Sr and ^{90}Y, were then calculated to be 1.16 and 1.03, respectively. Based upon maximum beta energies of 0.546 and 2.288 MeV $c = 2.303$ and $\nu = 34.499$ cm^2/g in air for ^{90}Sr, while $c = 0.884$ and $\nu = 4.996$ cm^2/g in air for ^{90}Y.

The results of these calculations, shown in Table D.1, provided a method of estimating beta dose rates. This information was required in order to estimate the dose rate prior to purchasing a point source. Since the model used did not account for beta particle attenuation or scattering in the source holder, these dose rate values are only estimates of the absolute dose rates.

Reference

[c] R. Loevinger, E.M. Japha, G.L. Brownell, Discrete Radioisotope Sources, in Radiation Dosimetry, G.J. Hine and G.L. Brownell, eds. (Academic Press, New York, 1956), p.p. 693-740.

Table D.1. Beta-particle dose rates in air from a 10 mCi $^{90}Sr/^{90}Y$ source.

Distance in air from the source (cm)	x[a] (mg/cm^2)	Dose rates in air (mGy/h)[b]		
		^{90}Sr	^{90}Y	$^{90}Sr/^{90}Y$
10	12.9	570.2	240.3	810.5
20	25.9	113.1	60.3	173.4
30	38.8	37.2	27.0	64.2
40	51.7	15.1	15.3	30.4
50	64.7	7.2	9.9	17.1
60	77.6	3.8	6.9	10.7
70	90.5	2.1	5.2	7.3
80	103.4	1.2	4.0	5.2
90	116.4	0.7	3.2	3.9
100	129.3	0.4	2.6	3.0

[a] x equals the air thickness. The density of air (STP) was 1.293×10^{-3} g/cm^3.

[b] mGy = 0.1 rads

SKIN DOSIMETRY USING THERMOLUMINESCENT DOSIMETERS

by

Timothy Miles DeBey

B.S., Kansas State University, 1981

AN ABSTRACT OF

A MASTER'S THESIS

submitted in partial fulfillment of the
requirements for the degree

MASTER OF SCIENCE

Department of Nuclear Engineering

KANSAS STATE UNIVERSITY

Manhattan, Kansas

1983

ABSTRACT

Measuring the radiation dose to skin has proven to be difficult to do in practice, although the criteria have been specified for many years by the regulatory agencies. This project's goal was to develop a thermoluminescent dosimeter (TLD) which would meet all of the requirements for skin dosimetry.

Theoretical calculations showed that most current methods of measuring skin dose have a very poor beta-particle energy response. A thin, graphite-backed TLD was developed which, theoretically, had a good beta-particle energy response. Beta sources were used to acquire experimental data with the newly developed dosimeters and several commercially produced dosimeters. These data verified the superior beta energy response of the thin, graphite-backed TLDs.

Tests also indicated that the newly developed TLDs have a linear gamma response, a beta energy response that is highly sensitive to cover thickness, and a minimum detectable dose of approximately 3mR for LiF when evaluated with a photon counting system.

Additional tests indicated that a composite dosimeter with a thin water TLD adhered to a thick ribbon TLD could be used to determine the penetrating ability of an uncharacterized radiation field.

Data in this project were taken from commercial TLD analyzer systems and from a photon counter system designed and constructed at Kansas State University. These data indicated that the thin, graphite-backed TLD will meet the regulatory agency requirements for measuring skin radiation dose and have sufficiently good material properties to withstand routine use without being damaged.